Supplemental Material

For

The utilization of the cycloaddition and oxidation dehydrogenation chemistry of $SNSMF_6$ (M = As, Sb) salts in the preparation of the 1,4-naphthoquinone fused 1,3,2-dithiazolylium salts and the full characterization of the corresponding prototype hybrid 7π 1,3,2-dithiazolyl radical

Andreas Decken,[a] Aaron Mailman,[a] Jack Passmore*[a], J. Mikko Rautiainen[a], Wolfgang Scherer[b] and Ernst-Wilhelm Scheidt[b]

Table of Contents

1. List of Tables

2. List of Figures

3. List of Charts and Schemes

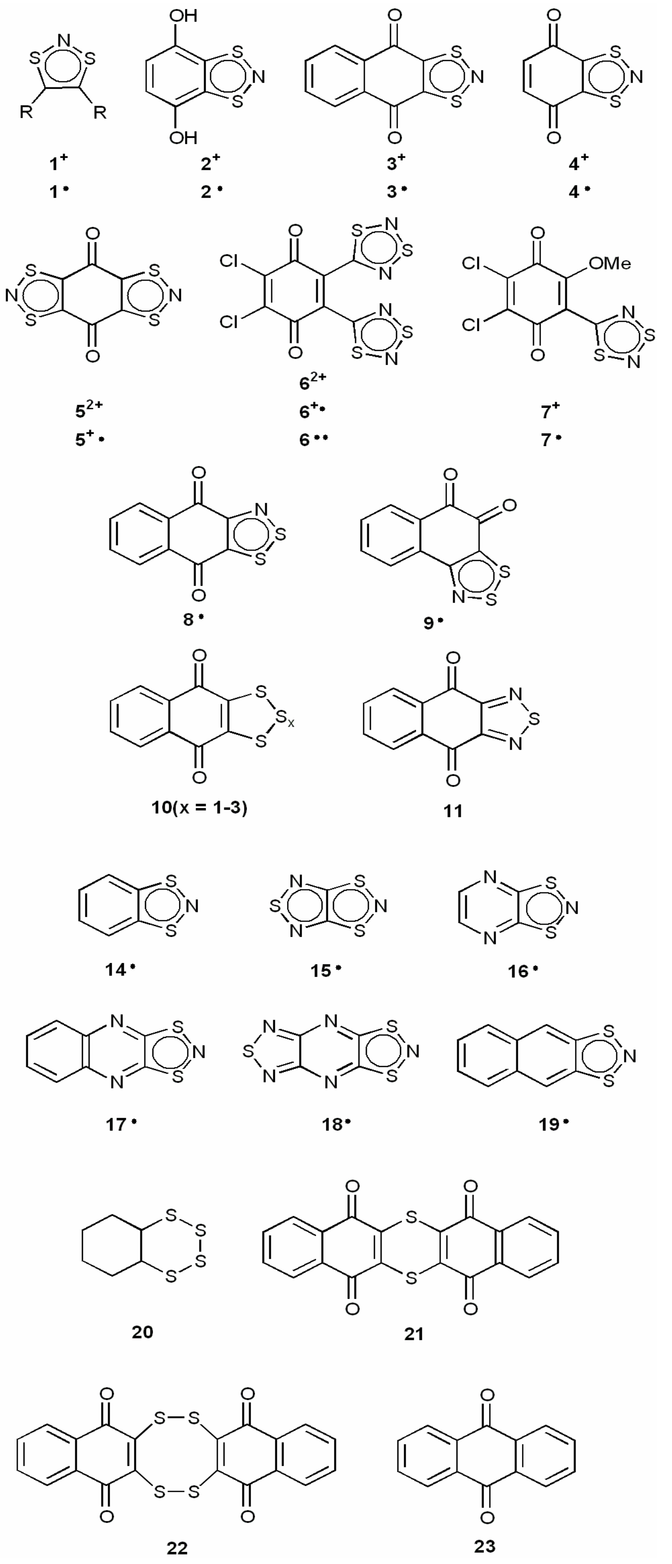

4. Chart S1 (Collection of Relevant Molecules from Chart 1 and Scheme 1 in main text): Molecules of interest (**12**$^+$ and **13**$^+$ are in Scheme S1)

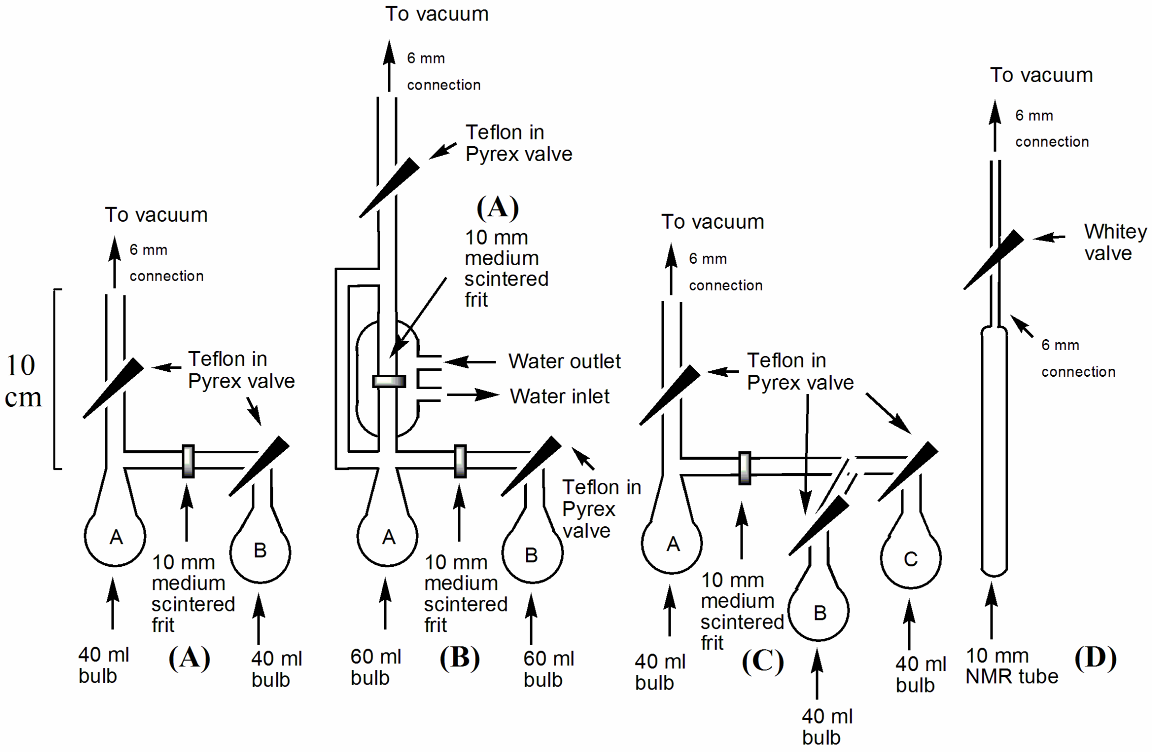

5. Figure S1: One piece Pyrex vessels. Unless otherwise stated, all Pyrex tubing was standard 12 mm O.D. and the valves were J. Young (POR/10/RA) Teflon in glass valves.

6. Materials and General Procedures:

A. Materials. SNSMF$_6$ (M = As, Sb) were prepared and purified according to literature procedures[1]. Ferrocene ($C_{10}H_{10}Fe$; Aldrich, 98%) and 1,4-Naphthoquinone ($C_{10}H_6O_2$; Aldrich, 98%) was purified by vacuum sublimation prior to use. Sodium Dithionite ($Na_2S_2O_4$; Aldrich, technical grade ~ 85 %), Triphenyl antimony ($C_{18}H_{15}Sb$; Aldrich, 99 %), 18-benzocrown-6 ($C_{16}H_{24}O_6$; Aldrich, 99 %), Tetrabutylammonium chloride ($C_{16}H_{36}NCl$; Fluka, purum ≥ 97 %) was used as received. Sulfur dioxide (SO_2; Liquid Air, 99.9998%) was stored over CaH_2 for at least 24 hrs and freshly distilled prior to use (*Caution!* SO_2 is a condensable gas with a high vapour pressure (~3.25 atm at 20^{o}C) which should be handled in well ventilated fumehood, leather gloves, face shield, blast shield, carefully built pyrex vessel). Acetonitrile (CH_3CN; Fisher, HPLC grade) and dichloromethane (CH_2Cl_2; Fisher, HPLC grade) were dried over refluxing CaH_2 for 24 hrs and distilled onto fresh CaH_2 under nitrogen atmosphere. CH_3CN and CH_2Cl_2 were degassed by three freeze-pump-thaw cycles and freshly distilled *in vacuo* prior to use.

B. General Procedures. Pyrex vessels of three types (Figure S1a-c on pg. 8) were employed throughout unless otherwise stated: Type A, incorporating two bulbs (40 ml) separated by a 10 mm medium scintered glass frit and closed by two J. Young (POR/10/RA) Teflon in glass valves (See Figure S1a on pg. 8 with a Teflon coated stir bar in one bulb. Type B, incorporating a 10 mm medium scintered glass frit centered in a water cooled condenser with a pressure equilizing side-arm with two 60 ml bulbs separated by a second 10 mm medium scintered glass frit and two Rotoflo (6 HK) Teflon in glass valves (See Figure S1b on pg. 8). Type C, incorporating three bulbs (40 ml) where one bulb is separated from the remaining two bulbs by a 10 mm medium scintered frit and closed by three J.Young (POR/10/RA) Teflon in glass valves (See Figure S1c on pg. 8) with a Teflon coated stir bar in bulb C. One piece 10 mm (o.d.) NMR tubes with ¼ inch (6 mm, o.d.) Pyrex tube were connected to stainless steel Whitey® valves (1KS4) by Swagelok® compression fittings, using Teflon back and front ferrules. The Whitey® valve was attached directly to the vacuum line by ¼ inch Monel tubing (See Figure S1d on pg. 8). The NMR tubes were cooled with liquid N_2 and flame sealed at the ¼ inch (6 mm) Pyrex tube.

7. Computational Details and Volume Based Thermodynamic (VBT) Estimates Lattice Enthalpies

A. Calculated gas phase energetics. Geometry optimizations and vibrational frequencies of all molecules were carried out using the PBE0 method [3] and the 6-311G(d) basis set as implemented in Gaussian 03W.[2] All structures were found to be minima as indicated by the absence of imaginary frequencies.

B. Calculated NMR tensors (See Table S1 on pg. 13). The geometries of **3**$^+$ (C_2v), **3**$^{\bullet}$ (C_2), **12**$^+$ (C_2v), **13**$^+$ (C_2v), **10** (x = 1, C_2v; x = 2, C_2; x = 3, C_2), **11** (C_1), **21** (D_2h), **22** (C_2) and 1,4-naphthoquinone ($C_{10}H_6O_2$, D_2h) in Chart S1 were used to calculate the NMR tensors using the GIAO method as implemented in Gaussian 03W [2] at the same level of theory (PBE0/6-311G(d)) and referenced to benzene for ^{13}C (49.8 ppm, D_6h), TMS for ^{1}H (31.981, T_d) and HCSNSCH (-193.6, C_2v) for ^{14}N-NMR as a standard according to [1]:

δ | Calc. Compound | - δ Calc. Reference (benzene, TMS, $\mathrm{H\overline{CSNSC}H}$)
= δ Chemical shift (calculated) [1]

Given the experimental ^{13}C chemical shift of benzene in SO_2 relative to TMS (129.2 ppm), correlation of the calculated ^{13}C-NMR chemical shifts with the experimental values provided very good agreement according to:

δ Benzene Experimental – δ Chemical shift (calculated)
= δ Predict experimental [2]

The correlation of the calculated ^{1}H and ^{14}N-NMR chemical shifts relative to TMS (0 ppm) and HCSNSCH (-5 ppm), respectively according to [2] provides qualitative agreement with respect to the experimental chemical shifts (See Table S1 on pg. 13).

C. Volume based thermodynamic (VBT) lattice enthalpies for the preparation of $3MF_6$ (M = As, Sb) according to Scheme 1 (Main Text).

The lattice potential energy (U_{pot}) of salts were estimated using the volume based thermodynamic (VBT) approach[3] according to Eqn. (A),

$U_{pot} = 2I(\alpha V_m^{-1/3} + \beta)$ [A]

For 1:1 salts (monocation and monoanion), α / kJ mol^{-1} nm = 117.3, β / kJ mol^{-1} = 51.9, I = 1. The lattice energies, on incorporation into the traditional Born–Fajans–Haber enthalpy cycle requires correction to an enthalpy term by the inclusion of the appropriate number of RT terms to account for the rotational and translational degrees of freedom of the gaseous ions as described by Jenkins.[4] The lattice enthalpies of $SNSMF_6$ (M = As, Sb) and **3**MF_6 were estimated using this approach. The Born-Fajan-Haber cycle is shown in Scheme S2.

Volume estimates (Hofmann estimates given for comparison)[5]**:**

$V[SNS^+] = 0.060$ nm^3; 0.062 nm^3, Hofmann estimate
$V[SbF_6^-] = 0.121$ nm^3; 0.115 nm^3, Hofmann estimate
$V[AsF_6^-] = 0.110$ nm^3; 0.103 nm^3, Hofmann estimate
$V[NH_4^+] = 0.036$ nm^3; 0.034 nm^3, Hofmann estimate
$V[SO_2] = 0.047$ nm^3, Hofmann estimate

V[**3**$^+$] = 0.224 nm^3 [from X-ray data of **3**SbF_6, Table 1 (main text)]; 0.231 nm^3 [from X-ray data of (**3**$AsF_6)_2$•SO_2, Table 1 (main text)]; Based on X-ray structural determinations, an estimate of a formula unit volume, V_m (i.e., $V_m = V_{cell}/Z$) can be determined. Hence, for a given formula unit volume, V_m, of a given salt, M_pX_q, the individual ion volume components can be calculated (i.e., $V_m(M_pX_q)$ – $p(V(M_q^+) + q(V(X_p-))$).[4] Here we obtain the formula unit volume of **3**(SbF_6) as V_m = 1.3808/4 = 0.345 nm^3 from the X-ray crystal structure (Table 1; main text). The volume of the SbF_6^- anion is $V(SbF_6^-) = 0.121$ nm^3, therefore since: V(**3**$^+$) ≈ $V_m - V(SbF_6^-)$ = 0.345 - 0.121 = 0.224 nm^3. However, we obtain the formula unit of (**3**$(AsF_6))_2$•SO_2 as V_m = 2.9179/4 = 0.729 nm^3 from the X-ray crystal structure (Table 1; main text). The volume of the AsF_6^- anion is $V(AsF_6^-) = 0.110$ nm^3 [4] and $V(SO_2) = 0.047$ nm^3,[5] therefore since V(**3**$^+$) ≈ ($V_m - 2V(AsF_6^-) - V(SO_2)$)/2 = (0.729 – 2(0.110) – 0.047)/2 = 0.231 nm^3.
Alternatively, using Hofmann's approach we can estimate the volume of **3**$^+$ as 0.244 nm^3.[5]

Calculated lattice potential energies (U_{pot}):
$U_{pot}(SNSSbF_6)$ = 519 kJ mol^{-1} (V = 0.181 nm^3, I = 1)
$U_{pot}(SNSAsF_6)$ = 527 kJ mol^{-1} (V = 0.170 nm^3, I = 1)
$U_{pot}(NH_4SbF_6)$ = 539 kJ mol^{-1} (V = 0.157 nm^3, I = 1)
$U_{pot}(NH_4AsF_6)$ = 549 kJ mol^{-1} (V = 0.146 nm^3, I = 1)
U_{pot}(**3**SbF_6) = 438 kJ mol^{-1} (V = 0.345 nm^3, I = 1)
U_{pot}(**3**AsF_6) = 442 kJ mol^{-1} (V = 0.334 nm^3, I = 1)

Enthalpy of sublimation:
ΔH_{sub}(1,4-Np) = 91 kJ mol^{-1} [6]
$\Delta H_{sub}(\alpha\text{-}S_8)$ = 100 kJ mol^{-1} [7]

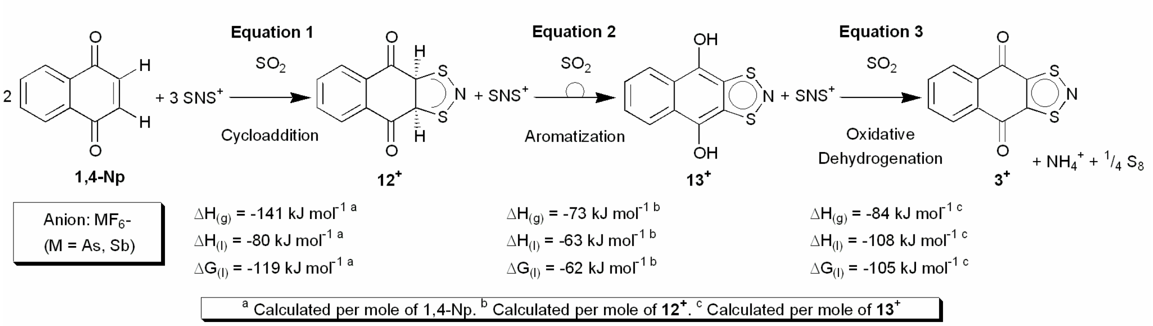

i) Scheme S1: Proposed Reaction of 1,4-naphthoquinone and SNS^+ leading to 3^+ and calculated (PBE0/6-311G(d)) gas phase enthalpies (ΔH).

$$\begin{tikzcd}
2\ 1{,}4\text{-Np}_{(g)} + 3\ SNS^+_{(g)} + 3\ MF_6^-{}_{(g)} \arrow[r, "\Delta H_g\ = -298\ \text{kJ mol}^{-1}"] & 2\ \mathbf{3}^+_{(g)} + NH_4^+{}_{(g)} + \frac{1}{4}\ S_{8(g)} + 3\ MF_6^-{}_{(g)} \arrow[d, "\begin{array}{l}\frac{1}{4}\ \Delta H_{sub}(S_8)\\ + U_{pot}(NH_4MF_6)\\ + 2U_{pot}(\mathbf{3}MF_6)\\ + 8\ RT\end{array}"] \\
2\ 1{,}4\text{-Np}_{(s)} + 3\ SNSMF_{6\ (s)} \arrow[u, "\begin{array}{l}\Delta H_{sub}(1{,}4\text{-Np})\\ + 3\ U_{pot}(SNSMF_6)\\ + 4\ RT\end{array}"'] \arrow[r] & 2\ \mathbf{3}MF_{6(s)} + NH_4MF_{6(s)} + \frac{1}{4}\ S_{8(s)}
\end{tikzcd}$$

Where
M = As, Sb

$$\Delta H_{rxn}^{298}\ (AsF_6) = -94\ \text{KJ mol}^{-1}$$
$$\Delta H_{rxn}^{298}\ (SbF_6) = -100\ \text{KJ mol}^{-1}$$

$$\Delta H_g = \Delta H_{Eq1} + \Delta H_{Eq2} + \Delta H_{Eq3}\ \text{(See Scheme S1)}$$

$$\Delta H_{rxn} = \Delta H_{sub}(1{,}4\text{-Np}) + 3\ U_{pot}(SNSMF_6) + \Delta H_g - \frac{1}{4}\ \Delta H_{sub}(S_8) - U_{pot}(NH_4MF_6) - 2\ U_{pot}(\mathbf{3}MF_6) - 4\ RT$$

ii) Scheme S2: Born-Fajan-Haber cycle for the reaction of 1,4-naphthoquinone $SNSMF_6$ (M = As, Sb) leading to $\mathbf{3}MF_6$ and the by-products NH_4MF_6 and S_8.

8. Experimental and Discussion:

A. Reaction of 1,4-naphthoquinone with excess $SNSSbF_6$ in liquid SO_2 according to Equation S1 and Purification of $\mathbf{3}SbF_6$

See main text for experimental procedures for preparation of $\mathbf{3}SbF_6$.

Purification. SO_2 (14.221 g, ~10 ml) was condensed onto crude $\mathbf{3}SbF_6$ (7.283 g) in bulb A of reaction vessel of Type A (Figure S1a). A yellow-brown solution over a white solid of sparingly soluble NH_4SbF_6 and S_8 was obtained on warming to ambient temperature. The more soluble yellow-brown solution was filtered to bulb B. The volume of the volatiles were reduced to 6.889 g (~5 ml) giving a yellow-brown solution over a yellow solid ($\mathbf{3}SbF_6$). The solution was cooled to -78 ^oC to facilitate deposition of $\mathbf{3}SbF_6$ and the more soluble yellow-brown fraction filtered to bulb A. The volatiles were condensed back to bulb B and then CH_2Cl_2 (27.217 g, ~ 21 ml). A yellow-brown solution over yellow $\mathbf{3}SbF_6$ was obtained upon warming to ambient temperature. The more soluble yellow-brown fraction was filtered to bulb A. The volatiles were condensed back to bulb B and the more soluble fraction filtered to bulb A. The washing was repeated (x 5) until the more soluble fraction was yellow and solid $\mathbf{3}SbF_6$ in bulb B was bright yellow. The volatiles were removed under dynamic vacuum. The bright yellow $\mathbf{3}SbF_6$ in bulb B (4.943 g, 87% isolated yield based on 1,4-naphthoquinone and Equation 1-3 in Scheme S1) and 2.135 g of a brown solid mixture of $\mathbf{3}SbF_6$, NH_4SbF_6 and S_8 in bulb A were collected in the drybox. The FT-IR, FT-Raman and Raman microscopy spectra of the bright yellow solid in bulb B were consistent with $\mathbf{3}SbF_6$. See Figure S8-S10a and the experimental vibrational assignments based on the calculated IR and Raman frequencies and intensities given in Table S2.

Equation S1 (A summary of Equations 1-3 in Scheme 1 in main text):

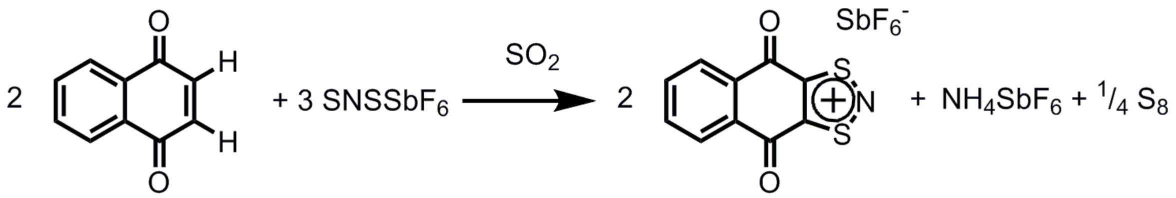

Table S1: Comparison of calculated (PBE0/6-311G(d)) and experimental ^{1}H, ^{13}C and ^{14}N-NMR tensors of **12**$^{+}$, **13**$^{+}$, **3**$^{+}$ and 1,4-naphthoquinone ($C_{10}H_6O_2$); See pg. 14-16, 59-61 and 67-69:

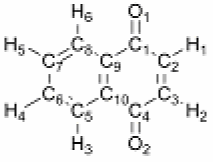

1,4-Np
($C_{10}H_6O_2$)

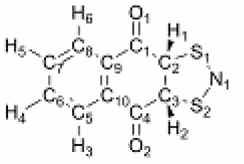

12^{+}

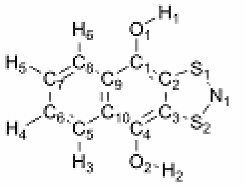

13^{+}

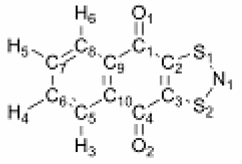

3^{+}

Molecule	1,4-Np ($C_{10}H_6O_2$)		**12**$^{+}$		**13**$^{+}$		**3**$^{+}$		**3**$^{\bullet}$	
Symmetry	C_2v		C_1		C_2		C_2v		C_2v	
	Calc.	Exp.[a]	Calc.	Exp.[c]	Calc.	Exp.[a]	Calc.	Exp.[a, d]	Calc.	Exp.[a, e]
^{13}C-NMR										
C1	184.9	186.2	175.4	186.3	143.1	143.4	171.4	173.6	174.4	NA
C2	139.8	140.0	78.5	75.3	140.3	139.2	181.4	179.2	157.0	NA
C3	139.8	140.0	72.1	75.3	140.4	139.2	181.4	179.2	157.0	NA
C4	184.9	186.2	184.7	186.3	143.0	143.4	171.4	173.6	174.4	NA
C5	127.9	128.2	132.3	132.2	120.1	119.9	134.1	130.1	128.6	NA
C6	134.5	135.5	142.5	139.3	135.9	134.9	143.5	138.5	135.2	NA
C7	134.5	135.5	143.0	139.3	135.8	134.9	143.5	138.5	135.2	NA
C8	127.9	128.2	133.7	132.2	120.1	119.9	134.1	130.1	128.6	NA
C9	131.2	-[b]	128.2	128.5	120.3	-[b]	129.4	129.0	131.8	NA
C10	131.2	-[b]	131.4	128.5	120.4	-[b]	129.4	129.0	131.8	NA
^{1}H-NMR										
H1	6.84	7.59	5.30	7.05	6.33	7.39	NA	NA	NA	NA
H2	6.84	7.59	5.81	7.05	6.34	7.39	NA	NA	NA	NA
H3	8.26	8.16	8.62	8.06	8.21	8.29	8.94	8.96	8.30	NA
H4	7.86	7.93	8.53	7.90	8.71	8.42	8.64	8.68	7.87	NA
H5	7.86	7.93	8.59	7.90	8.72	8.42	8.64	8.68	7.87	NA
H6	8.26	8.16	8.77	8.06	8.21	8.29	8.94	8.96	8.30	NA
^{14}N-NMR										
N1	NA	NA	149.5	127	7.2	-[b]	1.1	-6	-171.9	NA

[a] The experimental assignments are based on the reaction of 1,4-naphthoquinone and excess $SNSSbF_6$ and the multinuclear NMR spectra given in Figure S2-S5 on pg. 14-16. Assignments for ^{13}C and ^{14}N-NMR are consistent with related reactions (See experimental and discussion section 8.D-F on pg. 55-66) but tentative unless otherwise stated. [b] Due to the low concentration of a species or similarity in chemical shift, the individual chemical shifts were not observed or resolved under these conditions in liquid SO_2 solution and therefore can not be unambiguously assigned.[c] The experimental assignments are based on the 1:1 molar ratio reaction of 1,4-naphthoquinone and $SNSAsF_6$. See Figure S31-S33 on pg. 59-61. [d] The assignments are based on a pure sample of **3**SbF_6 and are unambiguously assigned (See Figure S2c-S5c on pg. 14-16). [e] The radical species **3**$^{\bullet}$ was not observed by NMR and the calculated ^{1}H, ^{13}C and ^{14}N-NMR tensors are only shown for comparison.

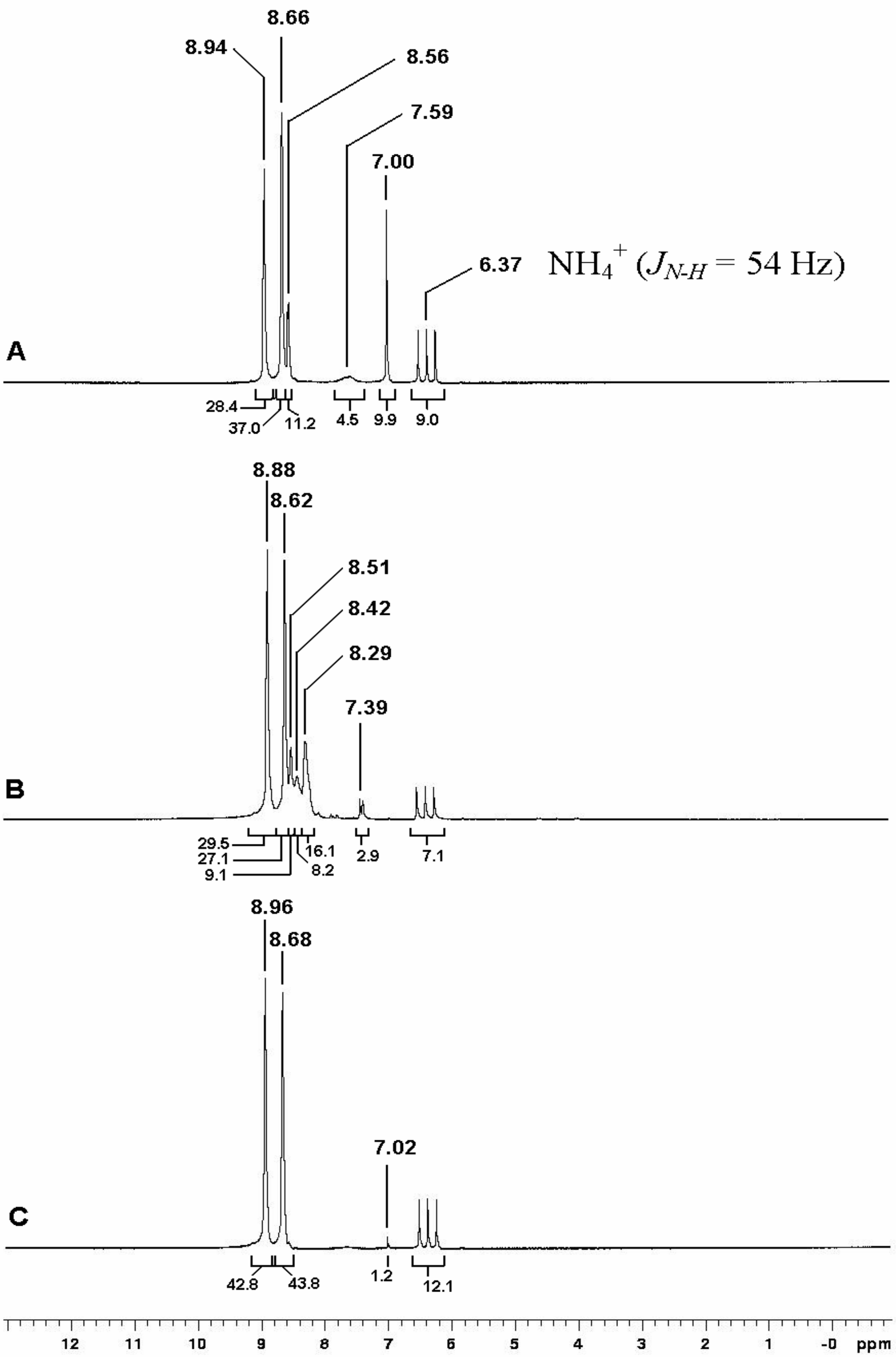

Figure S2: ^{1}H-NMR spectra of reaction of 1,4-naphthoquinone and $SNSSbF_6$ in 1:2 molar ratio in liquid SO_2 after a) ~ 15 min. (initial), b) after 24 hours and c) after 1 week at RT according to Equation 1-3 in Scheme S1 on pg. 11.

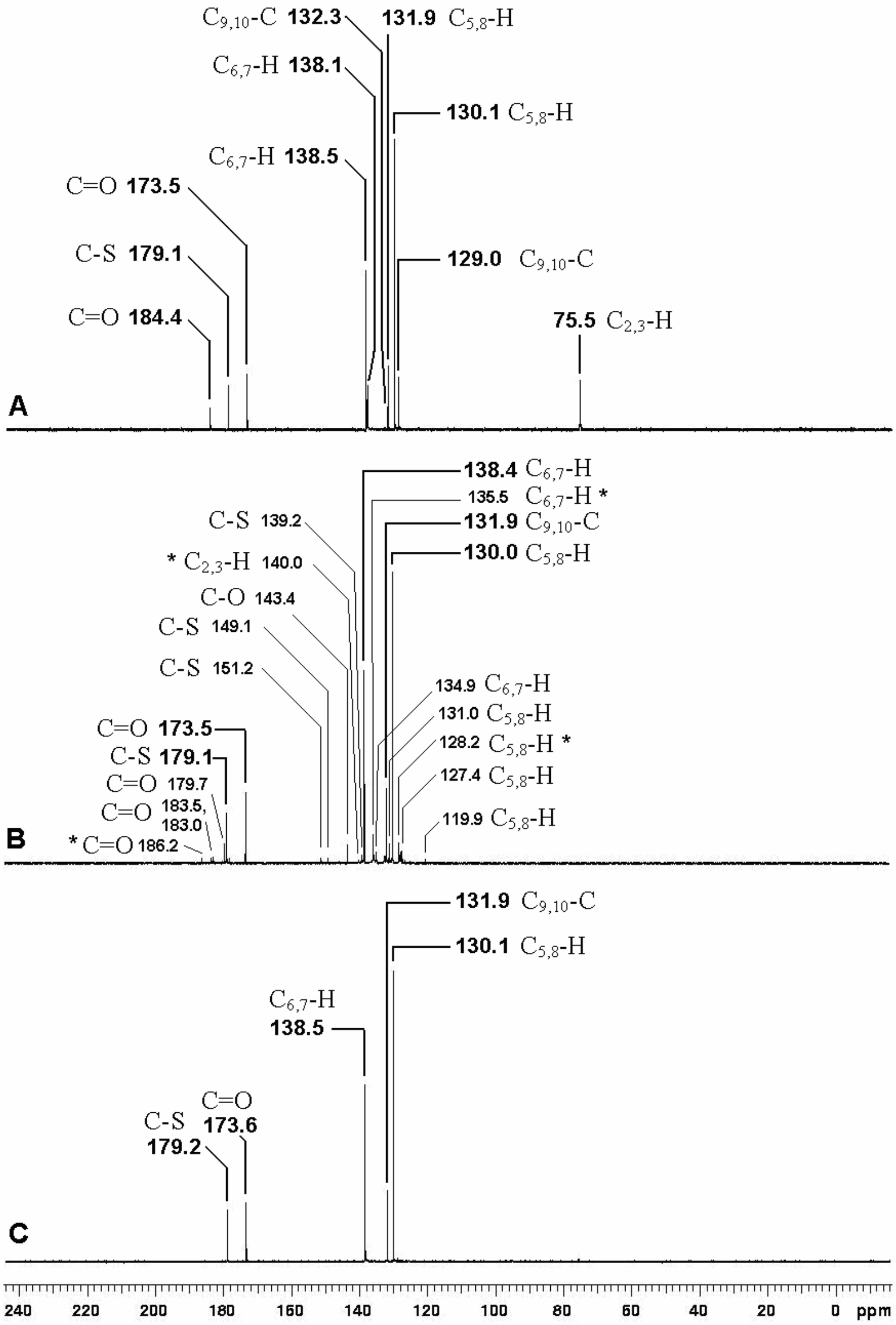

Figure S3: ^{13}C-NMR spectra of reaction of 1,4-naphthoquinone and $SNSSbF_6$ in 1:2 molar ratio in liquid SO_2 after a) ~ 15 min. (initial), b) after 24 hours and c) after 1 week at RT according to Equation 1-3 in Scheme S1 on pg. 11.

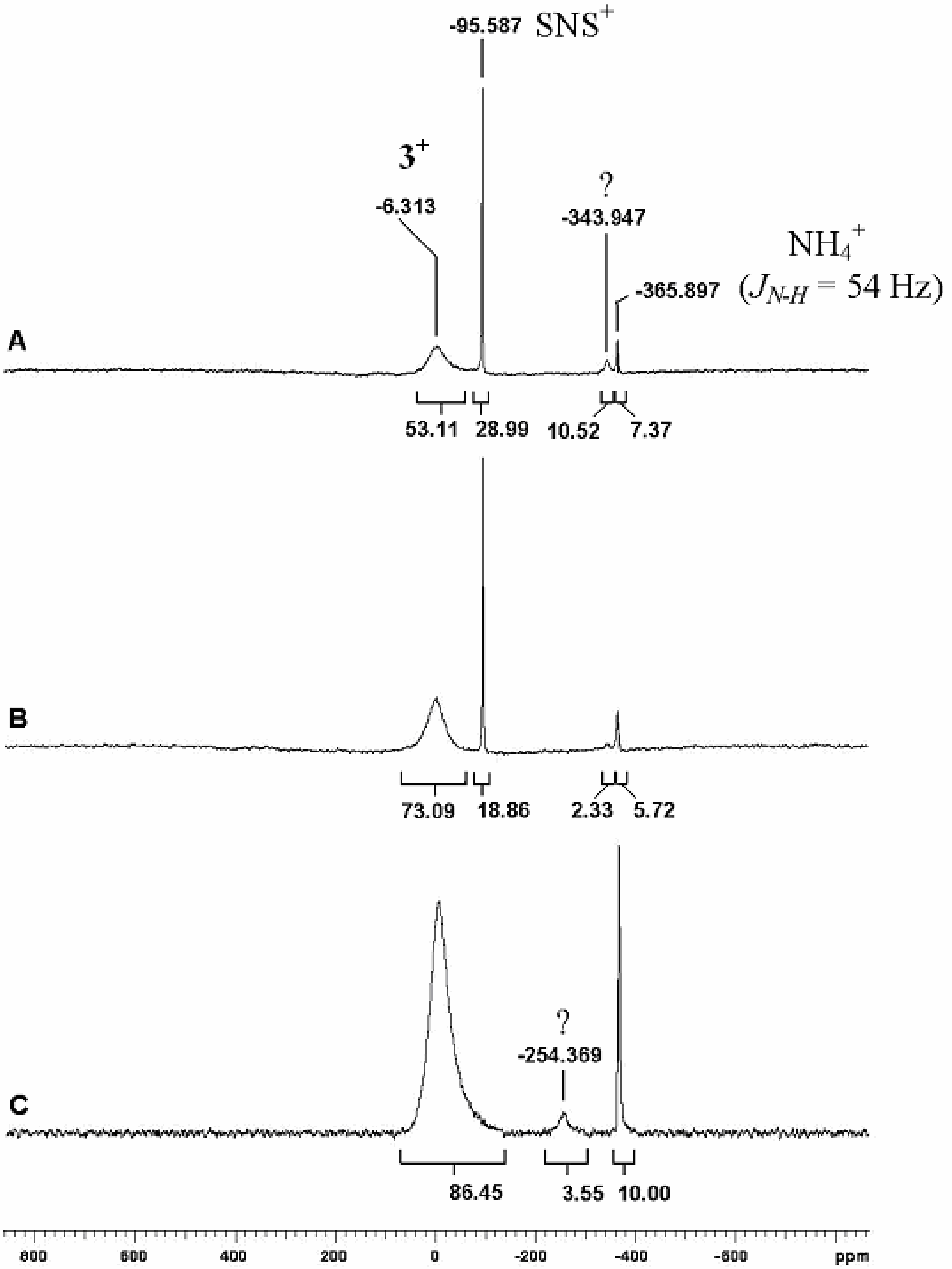

Figure S4: ^{14}N-NMR spectra of reaction of 1,4-naphthoquinone and $SNSSbF_6$ in 1:2 molar ratio in liquid SO_2 after a) ~ 15 min. (initial), b) after 24 hours and c) after 1 week at RT according to Equation 1-3 in Scheme S1 on pg. 11.

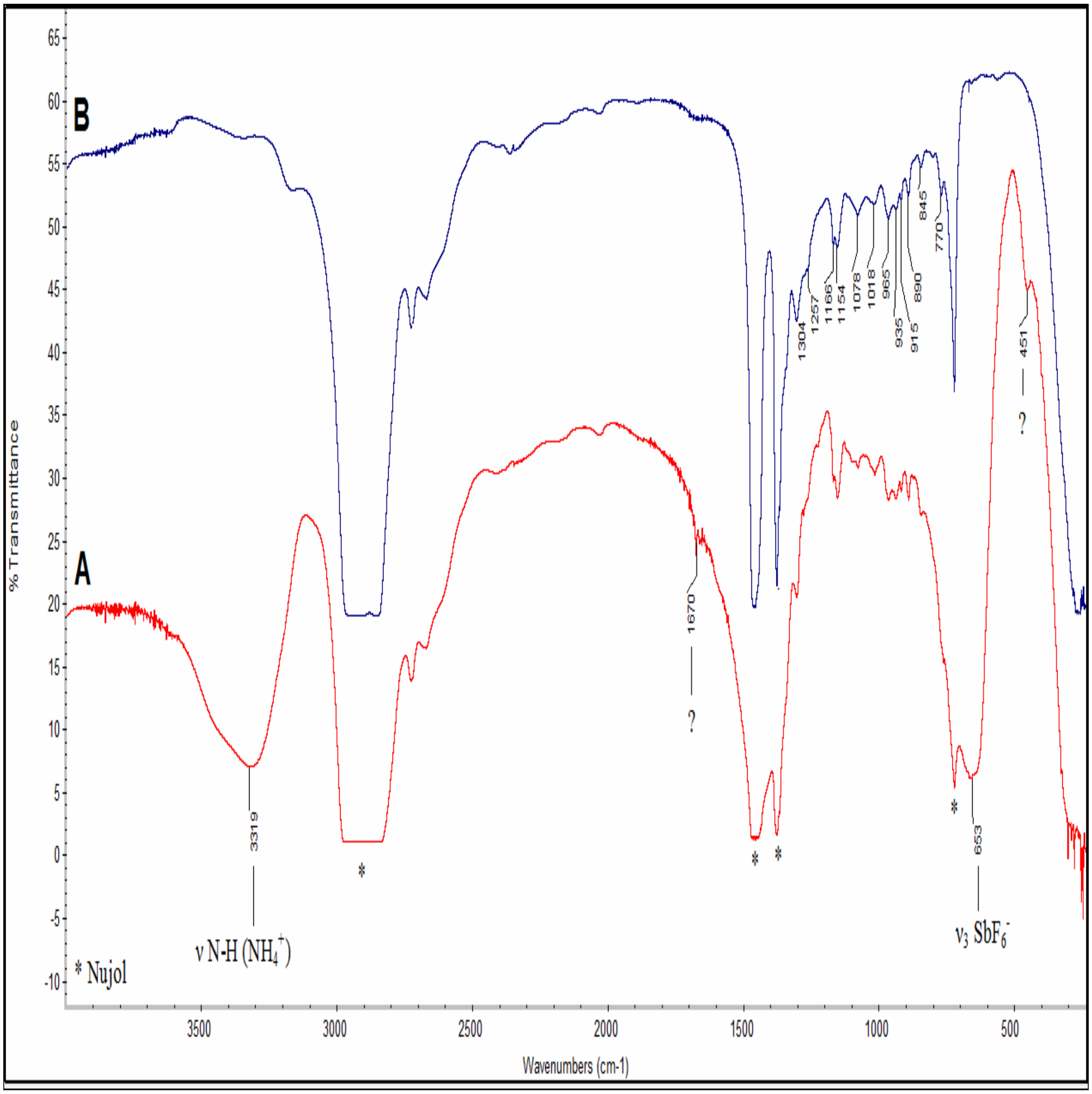

Figure S5: FT-IR spectra of a) white insoluble solid (c.f. NH_4SbF_6 and S_8) prepared according to Equation 1-3 in Scheme S1 on pg. 11 as a Nujol mull on KBr plates and b) Nujol on KBr plates. Note the assignments are tentative and based on visualization of the vibrational modes in *ChemCraft*[8]: ν = stretch, δ = bending, asym. = asymmetric and sym = symmetric, opp = out-of-plane, inp = in-plane.

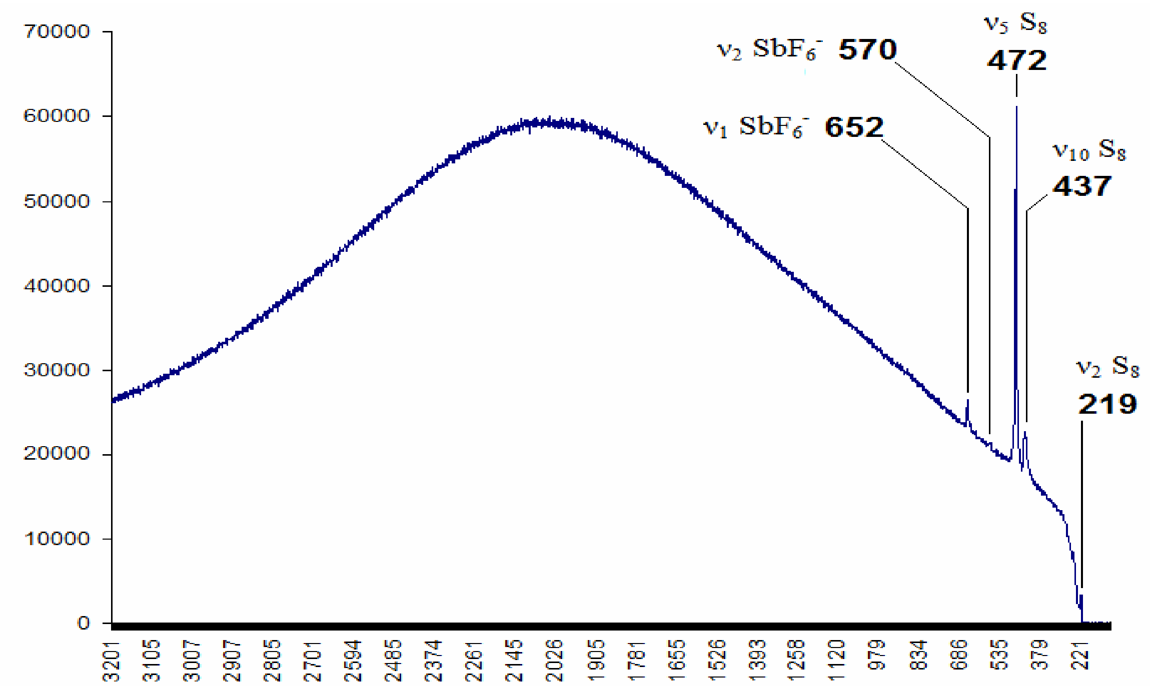

Figure S6: Raman microscopy spectrum of white insoluble solid (c.f. NH_4SbF_6 and S_8) obtained according Equation 1-3 in Scheme S1 on pg. 11 prepared as Nujol mull on KBr plates. Note the assignments are tentative and based on visualization of the vibrational modes in *ChemCraft*[8]: ν = stretch, δ = bending, asym. = asymmetric and sym = symmetric, opp = out-of-plane, inp = in-plane.

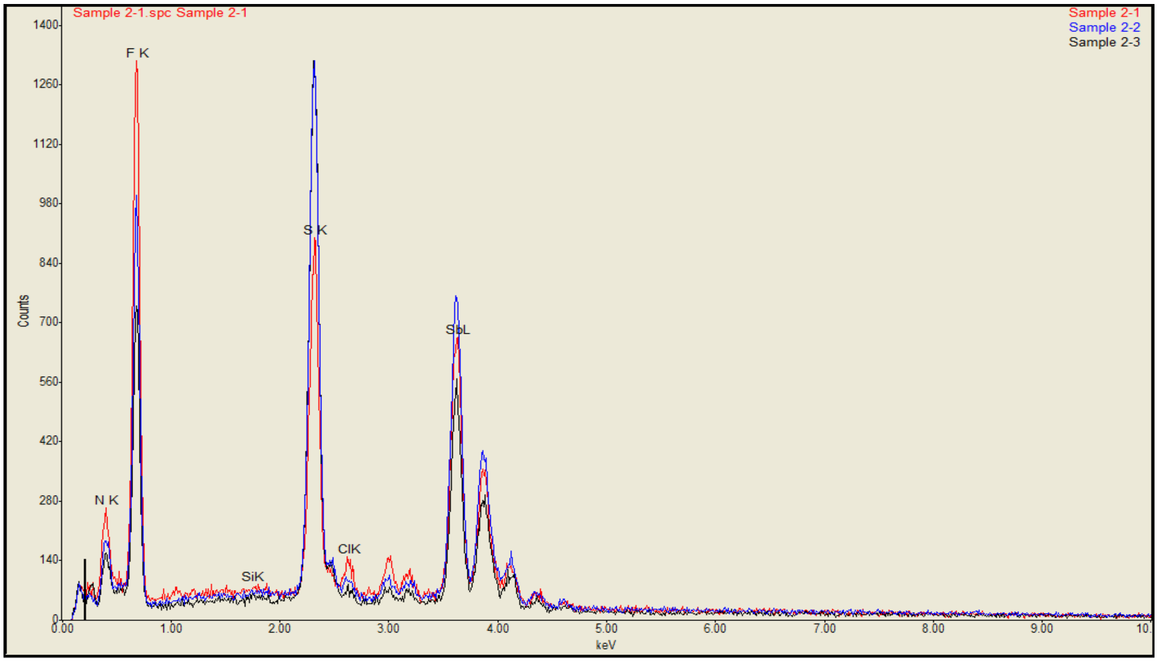

Figure S7: The stacked plot of three separate qualitative EDX microanalysis spectra of the insoluble solid (c.f. NH_4SbF_6 and S_8) prepared according to Equation 1-3 in Scheme S1 on pg. 11.

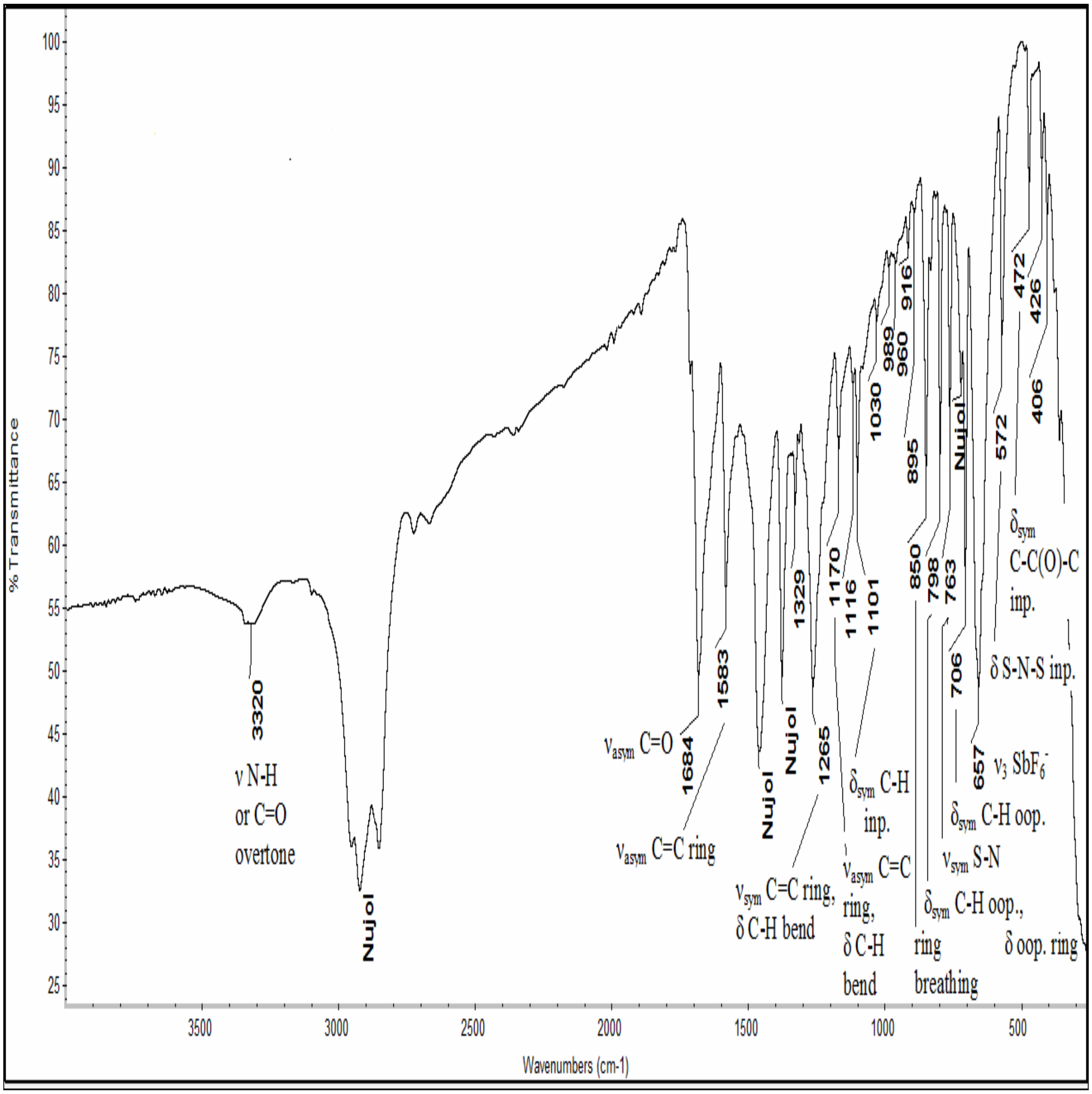

Figure S8: FT-IR spectrum of **3**SbF_6 prepared as Nujol mull on KBr plates prepared according to Equation 1-3 in Scheme S1 on pg. 11 (32 scans, 2 cm^{-1} resolution). See Table S2 on pg. 22 for comparison of experimental and calculated IR frequencies and tentative assignments. Note the assignments are tentative and based on visualization of the vibrational modes in *ChemCraft*[8]: ν = stretch, δ = bending, asym. = asymmetric and sym = symmetric, opp = out-of-plane, inp = in-plane.

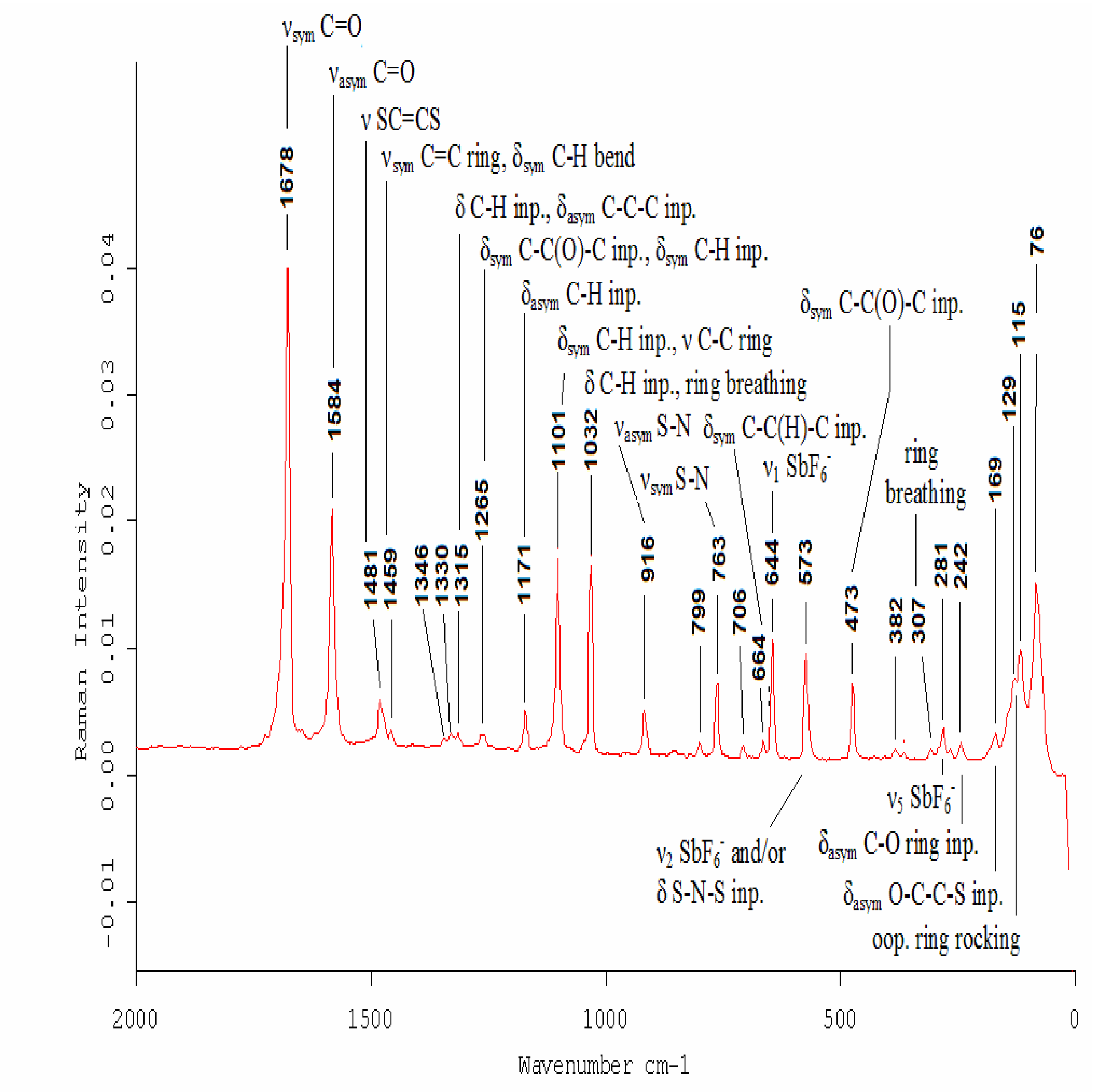

Figure S9: FT-Raman spectrum of **3**SbF_6 prepared according to Equation 1-3 in Scheme S1 on pg. 11. See Table S2 on pg. 22 for comparison of experimental and calculated Raman frequencies of **3**SbF_6 and tentative assignments. Note the assignments are tentative and based on visualization of the vibrational modes in *ChemCraft*[8]: ν = stretch, δ = bending, asym. = asymmetric and sym = symmetric, opp = out-of-plane, inp = in-plane.

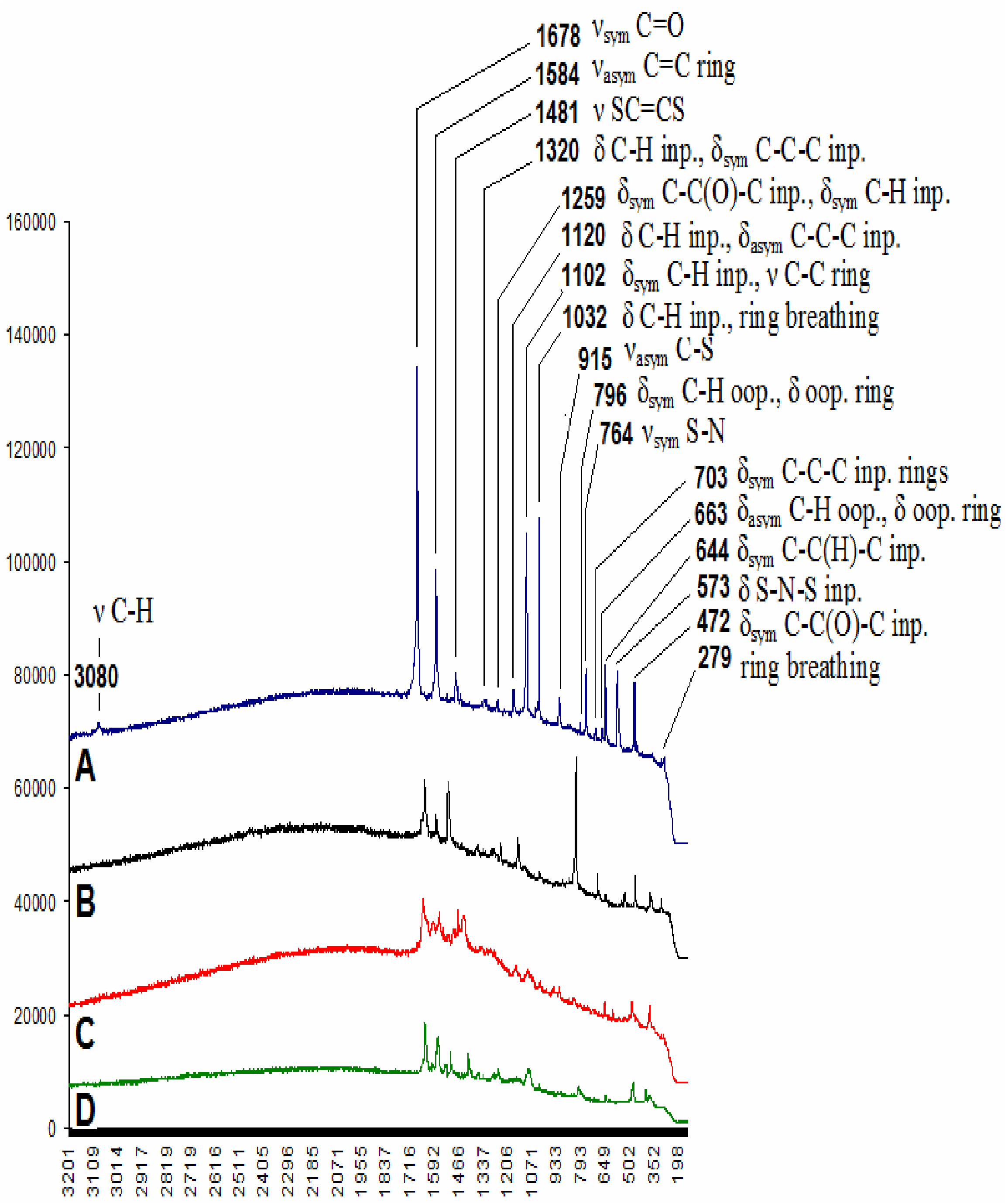

Figure S10: Raman microscopy spectra of a) **3**SbF$_6$ prepared according to Equation S1 on pg. 13 b) $\mathbf{3}^{\bullet}$ prepared according to Equation S2 on pg. 29 c) $\mathbf{3}^{\bullet}$ prepared according to Equation S6 on pg. 73 and d) $\mathbf{3}^{\bullet}$ prepared according to Equation S7 on pg. 75. See Table S2 on pg. 22 for comparison of experimental and calculated Raman frequencies of **3**SbF$_6$ and tentative assignments. Note the assignments are tentative and based on visualization of the vibrational modes in *ChemCraft*[8]: ν = stretch, δ = bending, asym. = asymmetric and sym = symmetric, opp = out-of-plane, inp = in-plane.

Table S2: Comparison of the experimental and calculated (PBE0/6-311G(d)) IR and Raman frequencies and intensities for **3**MF$_6$ (M = As, Sb) and **3**$^{\bullet}$ and tentative assignments. See pg. 19-21, 29, 30, 56, 64, 71, 74 and 76 for actual IR and Raman spectra.

3MF$_6$ (M = As, Sb)			Tentative Assignments^{a}	**3**$^{\bullet}$			Tentative Assignments^{a}
IR/Raman (Calc.)	IR (Obs.)	Raman (Obs.)		IR/Raman (Calc.)	IR (Obs.)	Raman (Obs.)	
	3320m, br		ν N-H (NH_4^+) or C=O overtone				
3081 (0/100)			ν C-H	3072 (2/23)			ν C-H
3076 (0/20)			ν C-H	3069 (0/3)			ν C-H
3069 (0/31)			ν C-H	3058 (2/16)			ν C-H
3061 (0/16)			ν C-H	3045 (1/10)			ν C-H
1706 (62/6)	1684s		ν_{asym} C=O	1682 (0/100)	1680w		
1697 (13/72)		1678s	ν_{sym} C=O	1679 (100/65)	1652s	1655w	ν_{asym} C=O
					1631s	1640m	ν_{sym} C=O
1562 (21/70)	1583m	1584m	ν_{asym} C=C ring	1581 (14/1)	1582s	1583w	ν_{asym} C=C ring
1554 (0/21)							
1460 (0/26)		1481w	ν SC=CS	1522 (31/65)	1519s	1521m	ν SC=CS
1446 (1/7)		1459vw	ν_{sym} C=C, δ_{sym}C-H	1449 (2/0)			
1422 (0/1)				1424 (1/0)			
						1366vw	ν_{sym} C=C, δ C-H
1339 (0/3)		1346vw			1340vw		
	1329w	1330vw		1328 (2/2)	1325w		ν_{sym} C=C
		1315vw	δ C-H $_{inp.}$, δ_{asym} C-C-C $_{inp.}$			1276vw	ν C-C ring, δ_{sym} C-H $_{inp.}$
1267 (0/1)				1252 (7/42)			
1234 (100/4)	1265s	1265vw	δ_{sym} C-C(O)-C$_{inp.}$, δ C-H$_{inp.}$	1250 (83/16)	1260s,br	1241w	ν C-C ring, δ_{asym} C-H $_{inp.}$
1221 (1/1)				1203 (13/68)	1149m	1147m	δ_{asym} C-H $_{inp.}$
1142 (0/3)	1170w	1171w	$\delta_{asym.}$ C-H $_{inp.}$	1131 (1/2)			
1140 (5/3)	1116vw			1105 (40/100)			
1068 (4/63)	1101w	1101m	$\delta_{sym.}$ C-H $_{inp.}$, ν C-C ring	1091 (0/1)	1098w	1113vw	$\delta_{asym.}$ C-H $_{inp.}$, $\delta_{asym.}$ C-C-C $_{inp.}$
1098 (0/3)				1057 (2/5)			
1044 (0/59)	1030vw	1032m	$\delta_{.}$ C-H, ring breathing	1013 (1/5)	1027vw	1032vw	$\delta_{asym.}$ C-H $_{inp.}$, $\delta_{sym.}$ C-C-C $_{inp.}$
1021 (0/1)				970 (0/1)	978w		$\delta_{asym.}$ C-H $_{oop.}$
995 (1/0)	989vw			949 (1/0)			
	960vw						
941 (0/1)	916vw	916w	ν_{asym} S-N	906 (0/1)			
912 (0/1)	895vw			885 (4/12)	895w		ν_{asym} C-S
881 (0/8)				856 (2/3)			
860 (1/0)				830 (16/3)	817m		ν_{asym} S-N
827 (12/0)	850m		ring breathing	812 (7/86)		822s	
801 (3/0)	798m	799vw	$\delta_{sym.}$ C-H $_{oop.}$	795 (3/0)	791w		ring breathing
745 (6/17)	763m	763w	ν_{sym} S-N	765 (0/1)			
734 (0/1)				715 (16/0)	703m		$\delta_{sym.}$ C-H $_{oop}$
718 (15/0)	706m	706vw	$\delta_{sym.}$ C-H $_{oop.}$	702 (0/2)		692m	δ_{asym} C-C-C $_{inp.}$
703 (1/1)				672 (0/1)			
670 (0/1)		664vw	$\delta_{sym..}$C-C(H)-C $_{inp.}$	668 (2/3)	684w		ν_{sym} S-N, δ S-N-S$_{inp.}$
	657vs		ν_3 SbF_6^-				
		644m	ν_1 SbF_6^-				
640 (1/5)				642 (2/0)	639w	639vw	$\delta_{sym..}$C-C(H)-C $_{inp.}$
582 (3/5)				545 (0/5)			
	572m	573m	ν_2 SbF_6^- and/or δ S-N-S $_{inp.}$				
553 (1/0)				524 (0/1)	530vw	529w	δ_{sym} C-S-N $_{inp}$

478 (0/1)				473 (0/1)			
468 (2/6)	472w	473m	δ_{sym} C-C(O)-C $_{inp.}$	466 (1/5)	468v	467m	δ_{sym} C-C(O)-C $_{inp}$
434 (1/0)	426w			421 (0/1)			
413 (2/0)				386 (0/1)		370m	δ_{sym} CSNSC $_{oop}$
407 (0/1)	406w			365 (3/0)	363w,sh		δ_{sym} C-O ring inp.
373 (1/2)		382vw		361 (1/14)			
359 (2/0)				302 (0/1)		304m	ring breathing
299 (3/1)		307vw	ring breathing	259 (0/2)		254w	δ_{asym} C-O ring inp.
		281w	ν_5 SbF_6^-				
255 (1/1)				238 (0/1)		202m	δ S-N-S oop.
231 (1/2)		242w	δ_{asym} C-O ring inp.	183 (2/0)			
170 (1/0)		169w		176 (0/1)		179w	δ O-C-C-S
149 (1/0)		129m	oop. ring rocking	146 (1/0)			
120 (0/1)		115m		122 (0/1)			
97 (0/1)		75m		93 (0/1)			
52 (1/0)				53 (1/0)			

[a] The vibrational modes are heavily mixed, therefore, only the major vibrational modes are assigned based on the scaled displacement vectors visualized using *ChemCraft*[8].

Table S3: Comparison of the experimental and calculated (PBE0/6-311G(d)) bond lengths (Å) and bond angles (°) of **3**MF$_6$ (M = As, Sb) and **3**$^{\bullet}$

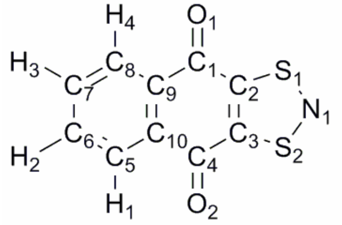

Bond	**3**SbF$_6$	**3**AsF$_6$•(SO$_2$)$_{0.5}$		**3**$^{\bullet}$		Calc. **3**$^+$ (C$_2$v)	Calc. **3**$^{\bullet}$ (C$_2$v)
	173(1)	198(1)		198(1)	296(1)		
Bond Length (Å)							
O1-C1	1.209(5)	1.213(3)	1.216(5)	1.220(3)	1.217(4)	1.206	1.213
O2-C4	1.211(6)	1.205(3)	1.215(5)	1.224(3)	1.221(4)	1.206	1.213
C1-C2	1.485(5)	1.489(4)	1.480(5)	1.478(3)	1.476(4)	1.500	1.474
C1-C9	1.465(6)	1.481(4)	1.472(6)	1.481(3)	1.483(5)	1.473	1.487
C2-C3	1.349(5)	1.361(4)	1.361(4)	1.354(3)	1.354(5)	1.366	1.354
C3-C4	1.502(6)	1.494(4)	1.490(5)	1.469(3)	1.462(5)	1.500	1.474
C4-C10	1.471(6)	1.477(4)	1.485(4)	1.483(3)	1.484(4)	1.473	1.487
C5-C6	1.387(7)	1.387(6)	1.373(6)	1.379(4)	1.373(5)	1.389	1.389
C5-C10	1.382(6)	1.394(6)	1.377(5)	1.387(3)	1.387(5)	1.392	1.391
C6-C7	1.380(7)	1.372(5)	1.387(6)	1.387(4)	1.379(6)	1.392	1.391
C7-C8	1.367(7)	1.387(6)	1.366(5)	1.386(4)	1.379(6)	1.389	1.389
C8-C9	1.387(7)	1.382(5)	1.389(5)	1.387(3)	1.391(4)	1.392	1.391
C9-C10	1.412(7)	1.412(4)	1.401(5)	1.410(3)	1.404(5)	1.414	1.403
C2-S1	1.692(4)	1.695(3)	1.692(3)	1.719(2)	1.716(3)	1.706	1.736
S1-N1	1.595(4)	1.597(3)	1.594(3)	1.645(2)	1.644(3)	1.606	1.672
S2-N1	1.597(4)	1.600(3)	1.598(3)	1.663(2)	1.654(4)	1.606	1.672
C3-S2	1.698(4)	1.695(3)	1.686(3)	1.729(2)	1.728(3)	1.706	1.736
C5-H1	0.950(5)	0.905(35)	0.828(45)	0.942(26)	0.943(33)	1.085	1.085
C6-H2	0.949(5)	0.928(45)	0.892(39)	0.947(26)	0.955(34)	1.085	1.085
C7-H3	0.951(5)	0.870(42)	1.012(41)	0.950(32)	0.956(34)	1.085	1.085
C8-H4	0.950(5)	0.908(36)	0.881(44)	0.935(27)	0.927(34)	1.085	1.085
Bond Angle (°)							
O1-C1-C2	119.48(37)	119.81(26)	118.82(35)	120.47(22)	120.62(27)	118.890	121.214
O1-C1-C9	125.42(41)	124.97(26)	124.54(39)	123.69(24)	123.67(34)	126.358	123.149
O2-C4-C3	120.23(38)	119.90(26)	119.72(35)	120.50(24)	120.70(33)	118.890	121.214
O2-C4-C10	125.20(31)	125.34(27)	124.96(28)	123.32(22)	123.13(27)	126.358	123.149
C1-C2-C3	124.22(35)	123.05(26)	122.33(28)	122.91(22)	122.67(27)	122.849	122.909
C1-C9-C10	121.16(40)	121.51(25)	120.86(35)	121.18(24)	121.36(32)	122.399	121.454
C1-C9-C8	118.50(37)	118.76(28)	119.34(31)	119.49(22)	119.40(28)	117.903	118.708
C2-C1-C9	115.09(33)	115.22(24)	116.60(32)	115.84(21)	115.71(26)	114.752	115.637
C3-C4-C10	114.57(32)	114.77(24)	115.33(25)	116.17(21)	116.16(26)	114.752	115.637
C4-C3-C2	121.62(35)	122.77(25)	122.32(28)	122.42(24)	122.74(33)	122.849	122.909
C4-C10-C9	123.07(38)	122.61(25)	122.23(26)	121.25(21)	121.15(25)	122.399	121.454
C4-C10-C5	117.66(35)	118.10(28)	118.86(29)	119.41(22)	119.52(27)	117.903	118.708
C5-C6-C7	121.01(48)	120.43(39)	120.15(39)	120.15(25)	119.77(31)	120.298	120.164
C5-C10-C9	119.25(41)	119.29(28)	118.91(31)	119.34(24)	119.33(33)	119.698	119.839
C6-C7-C8	120.45(47)	120.56(39)	119.78(39)	119.90(27)	120.54(41)	120.298	120.164
C6-C5-C10	119.34(39)	119.92(36)	120.92(37)	120.72(24)	120.91(31)	120.004	119.997
C7-C8-C9	119.61(46)	120.07(36)	120.49(37)	120.56(24)	120.21(31)	120.004	119.997
C8-C9-C10	120.34(40)	119.73(29)	119.73(30)	119.34(23)	119.24(26)	119.698	119.839
C1-C2-S1	121.79(28)	123.66(21)	123.96(24)	122.93(19)	122.85(23)	123.518	122.355
C2-S1-N1	98.06(19)	98.58(14)	98.61(15)	99.10(12)	98.81(16)	98.046	98.214
C2-C3-S2	113.99(29)	113.75(22)	113.03(21)	114.51(18)	114.06(21)	113.633	114.736

C3-S2-N1	98.05(20)	98.27(14)	99.01(15)	98.15(13)	98.37(17)	98.046	98.214
C3-C2-S1	113.45(29)	113.28(21)	113.70(22)	114.03(21)	114.36(28)	113.633	114.736
S1-N1-S2	116.45(24)	116.12(17)	115.55(18)	113.89(15)	114.11(20)	116.641	114.101
C4-C3-S2	124.92(28)	122.77(25)	124.64(21)	122.80(18)	122.96(23)	123.518	122.355
H1-C5-C6	120.32(44)	120.57(191)	118.32(292)	121.66(166)	121.04(187)	121.107	121.479
H1-C5-C10	120.34(44)	119.45(260)	120.75(296)	117.58(181)	118.03(219)	118.889	118.524
H2-C6-C5	119.40(50)	117.72(265)	121.05(269)	119.31(168)	118.95(190)	119.676	119.808
H2-C6-C7	119.58(51)	121.66(260)	118.59(272)	120.54(179)	121.27(213)	120.026	120.028
H3-C7-C6	119.76(52)	120.64(277)	117.05(235)	120.50(190)	121.52(209)	120.026	120.028
H3-C7-C8	119.80(52)	118.71(272)	123.16(240)	119.60(185)	117.77(215)	119.676	119.808
H4-C8-C7	120.16(46)	124.47(262)	118.57(276)	120.168(183)	122.33(232)	121.107	121.479
H4-C8-C9	120.23(49)	115.43(189)	120.54(266)	119.276(176)	117.40(210)	118.88	118.524

Table S4: Comparison of the experimental bond distances (Å) and bond angles (°) of **3**MF_6 (M = As, Sb), **3**$^{\bullet}$, 1,4-naphthoquinone ($C_{10}H_6O_2$) [9], 1,4-naphthalenediol [10] ($C_{10}H_8O_2$) and anthraquinone ($C_{14}H_8O_2$), **23** [11]

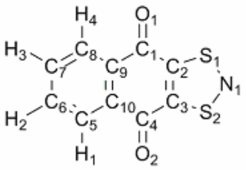

3$^{\bullet}$

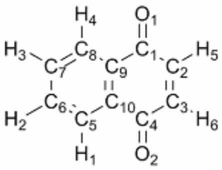

1,4-Np
($C_{10}H_6O_2$)

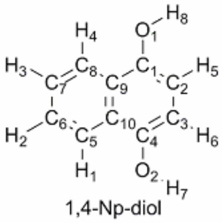

1,4-Np-diol
($C_{10}H_8O_2$)

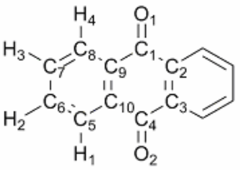

$C_{14}H_8O_2$
23

	3SbF_6	**3**AsF_6•$(SO_2)_{0.5}$		**3**$^{\bullet}$		$C_{10}H_6O_2$	$C_{10}H_8O_2$	**23**, $C_{14}H_8O_2$
	173 K	198 K		198 K	296 K	283-303 K	283-303 K	162 K
Bond Length (Å)								
O1-C1	1.209(5)	1.213(3)	1.216(5)	1.220(3)	1.217(4)	1.208[a]	1.377(6)	1.221(2)
O2-C4	1.211(6)	1.205(3)	1.215(5)	1.224(3)	1.221(4)	1.217[a]	1.377(6)	1.221(2)
C1-C2	1.485(5)	1.489(4)	1.480(5)	1.478(3)	1.476(4)	1.480[a]	1.353(7)	1.385(2)
C1-C9	1.465(6)	1.481(4)	1.472(6)	1.481(3)	1.483(5)	1.428[a]	1.428(10)	1.485(2)
C2-C3	1.349(5)	1.361(4)	1.361(4)	1.354(3)	1.354(5)	1.312[a]	1.419(10)	1.406(2)
C3-C4	1.502(6)	1.494(4)	1.490(5)	1.469(3)	1.462(5)	1.451[a]	1.353(7)	1.385(2)
C4-C10	1.471(6)	1.477(4)	1.485(4)	1.483(3)	1.484(4)	1.465[a]	1.428(10)	1.485(2)
C5-C6	1.387(7)	1.387(6)	1.373(6)	1.379(4)	1.373(5)	1.427[a]	1.360(9)	1.406(2)
C5-C10	1.382(6)	1.394(6)	1.377(5)	1.387(3)	1.387(5)	1.362[a]	1.399(8)	1.394(2)
C6-C7	1.380(7)	1.372(5)	1.387(6)	1.387(4)	1.379(6)	1.371[a]	1.385(13)	1.391(2)
C7-C8	1.367(7)	1.387(6)	1.366(5)	1.386(4)	1.379(6)	1.411[a]	1.360(9)	1.406(2)
C8-C9	1.387(7)	1.382(5)	1.389(5)	1.387(3)	1.391(4)	1.393[a]	1.399(8)	1.394(2)
C9-C10	1.412(7)	1.412(4)	1.401(5)	1.410(3)	1.404(5)	1.391[a]	1.403(10)	1.406(2)
C2-S1	1.692(4)	1.695(3)	1.692(3)	1.719(2)	1.716(3)	NA	NA	NA
S1-N1	1.595(4)	1.597(3)	1.594(3)	1.645(2)	1.644(3)	NA	NA	NA
S2-N1	1.597(4)	1.600(3)	1.598(3)	1.663(2)	1.654(4)	NA	NA	NA
C3-S2	1.698(4)	1.695(3)	1.686(3)	1.729(2)	1.728(3)	NA	NA	NA
C5-H1	0.950(5)	0.905(35)	0.828(45)	0.942(26)	0.943(33)	NA	0.968(57)	0.98(2)
C6-H2	0.949(5)	0.928(45)	0.892(39)	0.947(26)	0.955(34)	NA	0.964(52)	0.97(2)
C7-H3	0.951(5)	0.870(42)	1.012(41)	0.950(32)	0.956(34)	NA	0.964(52)	0.93(3)
C8-H4	0.950(5)	0.908(36)	0.881(44)	0.935(27)	0.927(34)	NA	0.968(57)	1.01(2)
C2-H5	NA	NA	NA	NA	NA	NA	0.969(43)	NA
C3-H6	NA	NA	NA	NA	NA	NA	0.969(43)	NA
O1-H8	NA	NA	NA	NA	NA	NA	0.950(41)	NA
O2-H7	NA	NA	NA	NA	NA	NA	0.950(41)	NA
S20-O21		1.402 (3)						
S20-O22		1.394 (3)						
Bond Angle (°)								
O1-C1-C2	119.48(37)	119.81(26)	118.82(35)	120.47(22)	120.62(27)	118.84[a]	121.28(29)	121.01(13)
O1-C1-C9	125.42(41)	124.97(26)	124.54(39)	123.69(24)	123.67(34)	119.35[a]	116.42(27)	121.00(14)
O2-C4-C3	120.23(38)	119.90(26)	119.72(35)	120.50(24)	120.70(33)	118.03[a]	121.28(29)	121.01(13)
O2-C4-C10	125.20(31)	125.34(27)	124.96(28)	123.32(22)	123.13(27)	118.84[a]	116.42(27)	121.00(14)
C1-C2-C3	124.22(35)	123.05(26)	122.33(28)	122.91(22)	122.67(27)	120.98[a]	119.46(28)	120.77(13)
C1-C9-C10	121.16(40)	121.51(25)	120.86(35)	121.18(24)	121.36(32)	118.25[a]	118.25(27)	119.90(13)
C1-C9-C8	118.50(37)	118.76(28)	119.34(31)	119.49(22)	119.40(28)	122.59[a]	122.64(28)	119.90(13)
C2-C1-C9	115.09(33)	115.22(24)	116.60(32)	115.84(21)	115.71(26)	121.75[a]	121.48(28)	118.00(12)
C3-C4-C10	114.57(32)	114.77(24)	115.33(25)	116.17(21)	116.16(26)	123.13[a]	121.48(28)	118.00(12)
C4-C3-C2	121.62(35)	122.77(25)	122.32(28)	122.42(24)	122.74(33)	117.90[a]	119.46(28)	120.77(13)
C4-C10-C9	123.07(38)	122.61(25)	122.23(26)	121.25(21)	121.15(25)	117.92[a]	118.25(27)	118.00(12)
C4-C10-C5	117.66(35)	118.10(28)	118.86(29)	119.41(22)	119.52(27)	122.41[a]	122.64(28)	119.90(13)

C5-C6-C7	121.01(48)	120.43(39)	120.15(39)	120.15(25)	119.77(31)	118.83[a]	120.33(37)	120.17(15)
C5-C10-C9	119.25(41)	119.29(28)	118.91(31)	119.34(24)	119.33(33)	119.64[a]	119.11(28)	119.32(14)
C6-C7-C8	120.45(47)	120.56(39)	119.78(39)	119.90(27)	120.54(41)	118.94[a]	120.33(37)	119.82(14)
C6-C5-C10	119.34(39)	119.92(36)	120.92(37)	120.72(24)	120.91(31)	121.66[a]	120.15(36)	120.47(15)
C7-C8-C9	119.61(46)	120.07(36)	120.49(37)	120.56(24)	120.21(31)	121.32[a]	120.15(36)	120.60(14)
C8-C9-C10	120.34(40)	119.73(29)	119.73(30)	119.34(23)	119.24(26)	119.31[a]	119.11(28)	119.61(14)
C1-C2-S1	121.79(28)	123.66(21)	123.96(24)	122.93(19)	122.85(23)	NA	NA	NA
C2-S1-N1	98.06(19)	98.58(14)	98.61(15)	99.10(12)	98.81(16)	NA	NA	NA
C2-C3-S2	113.99(29)	113.75(22)	113.03(21)	114.51(18)	114.06(21)	NA	NA	NA
C3-S2-N1	98.05(20)	98.27(14)	99.01(15)	98.15(13)	98.37(17)	NA	NA	NA
C3-C2-S1	113.45(29)	113.28(21)	113.70(22)	114.03(21)	114.36(28)	NA	NA	NA
S1-N1-S2	116.45(24)	116.12(17)	115.55(18)	113.89(15)	114.11(20)	NA	NA	NA
C4-C3-S2	124.92(28)	122.77(25)	124.64(21)	122.80(18)	122.96(23)	NA	NA	NA
H1-C5-C6	120.32(44)	120.57(191)	118.32(292)	121.66(166)	121.04(187)	NA	122.02(302)	119.9(12)
H1-C5-C10	120.34(44)	119.45(260)	120.75(296)	117.58(181)	118.03(219)	NA	116.40(305)	119.7(12)
H2-C6-C5	119.40(50)	117.72(265)	121.05(269)	119.31(168)	118.95(190)	NA	121.50(241)	118.2(14)
H2-C6-C7	119.58(51)	121.66(260)	118.59(272)	120.54(179)	121.27(213)	NA	117.20(241)	121.6(14)
H3-C7-C6	119.76(52)	120.64(277)	117.05(235)	120.50(190)	121.52(209)	NA	117.20(241)	119.8(13)
H3-C7-C8	119.80(52)	118.71(272)	123.16(240)	119.60(185)	117.77(215)	NA	121.50(241)	120.4(13)
H4-C8-C7	120.16(46)	124.47(262)	118.57(276)	120.168(183)	122.33(232)	NA	122.02(302)	120.2(12)
H4-C8-C9	120.23(49)	115.43(189)	120.54(266)	119.276(176)	117.40(210)	NA	116.40(305)	119.2(12)
H5-C2-C1	NA	NA	NA	NA	NA	NA	122.55(241)	NA
H5-C2-C3	NA	NA	NA	NA	NA	NA	117.15(241)	NA
H6-C3-C2	NA	NA	NA	NA	NA	NA	117.15(241)	NA
H6-C3-C4	NA	NA	NA	NA	NA	NA	122.45(241)	NA
H7-O2-C4	NA	NA	NA	NA	NA	NA	108.13(258)	NA
H8-O1-C1	NA	NA	NA	NA	NA	NA	108.13(258)	NA
O21-S20-O22		120.8 (3)						

[a] Standard deviations were not given in reference 6.

Discussion: Comparison of structural parameters in 3^+ to 23. Since **3^+** can be considered a thiazyl analog of 9,10-anthraquinone, **23** a comparison of the structural parameters indicates the affect on the quinone moiety by replacing a aromatic ring with a 6π 1,3,2-dithiazolylium ring. The most notable differences are the shortening of the C2-C3 bond (ca. 0.06 Å) and the lengthening of C1-C2 and C3-C4 (ca. ~ 0.10 Å) and C1-C9 and C4-C10 (ca. ~ 0.33 Å compared to the mean bond distance in 9,10-anthraquinone) bonds of the quinone moiety in **3^+** with respect to 9,10-anthraquinone[12] (See Table S4 on pg. 26). The structural parameters of C5-C10 of the aromatic rings are almost unaffected by the structural changes of the quinone moiety.

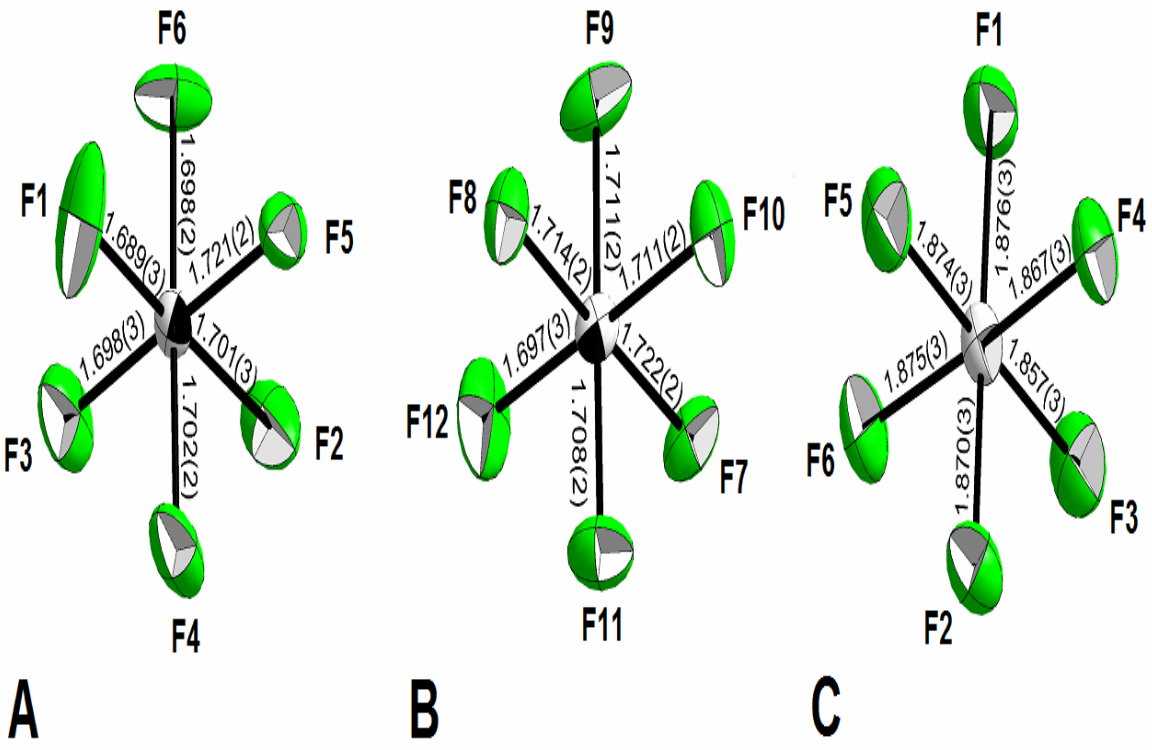

AsF_6^-: **A:** F1-As-F2 = 177.89(13), F1-As-F3 =91.63(13), F1-As-F4 = 91.49(13), F1-As-F5 = 88.64(12), F1-As-F6 = 89.68(13), F2-As-F3 = 90.48(13), F2-As-F4 = 88.52(12), F2-As-F5 = 89.25(12), F2-As-F6 = 90.29(12), F3-As-F4 = 89.44(13), F3-As-F5 = 179.24(12), F3-As-F6 = 91.15(12), F4-As-F5 = 89.84(11), F4-As-F6 = 178.67(11), F5-As-F6 = 89.57(11).

AsF_6^-: **B:** F7-As-F8 = 178.27(10), F7-As-F9 = 89.65(10), F7-As-F10 = 89.31(10), F7-As-F11 = 90.22(10), F7-As-F12 = 90.03(12), F8-As-F9 = 90.49(10), F8-As-F10 = 88.98(10), F8-As-F11 = 89.62(11), F8-As-F12 = 91.69(12), F9-As-F10 = 89.24(11), F9-As-F11 = 178.90(11), F9-As-F12 = 89.57(12), F10-As-F11 = 89.66(11), F10-As-F12 = 178.64(12), F11-As-F12 = 91.53(12).

SbF_6^-: **C:** F1-Sb-F2 = 177.40(14), F1-Sb-F3 =90.43(14), F1-Sb-F4 = 88.12(13), F1-Sb-F5 = 89.43(14), F1-Sb-F6 = 91.33(13), F2-Sb-F3 = 91.03(14), F2-Sb-F4 = 89.71(13), F2-Sb-F5 = 89.08(14), F2-Sb-F6 = 90.78(13), F3-Sb-F4 = 90.70(13), F3-Sb-F5 = 179.05(13), F3-Sb-F6 = 91.88(14), F4-Sb-F5 = 88.36(13), F4-Sb-F6 = 177.37(13), F5-Sb-F6 = 89.06(14).

Figure S11: The geometry of the AsF_6^- and SbF_6^- anions in the $\mathbf{3}^+$ salts. Thermal ellipsoids given at 50 % probability.

B. Reduction of $3SbF_6$ with ferrocene (Cp_2Fe) in refluxing acetonitrile (CH_3CN) according to Equation S2.

Procedure: CH_3CN (30 ml) was syringed onto **3**SbF_6 (1.170 g, 2.49 mmol) in bulb A through the pressure equilizing sidearm of a vessel of Type B (See Figure S1b). Ferrocene (Cp_2Fe; 0.521 g, 2.80 mmol) was placed onto the scintered glass frit of the reflux condenser. The yellow solution in bulb A was degassed by three freeze-pump-thaw cycles and then warmed to refluxed (*Note: The Teflon in glass valve to bulb B is closed only during reflux*, Figure S1b). The ferrocene (Cp_2Fe) on the scintered glass frit was slowly extracted into bulb A. After refluxing for 4 hours, a blue-green solution was obtained in bulb A which was allowed to slowly cool to ambient temperature. The more soluble blue-green fraction (*c.f.* Cp_2FeSbF_6) was filtered into bulb B leaving a green crystalline solid in bulb A. The volatiles (~ 15 ml) were condensed back to bulb A and the more soluble portion filtered to bulb B. The volatiles (~ 2-3 ml) were again condensed back to bulb A and the more soluble portion filtered to bulb B. This was repeated twice. The volatiles were removed under dynamic vacuum. The green crystalline solid in bulb A (0.423 g of **3**$^{\bullet}$, 73 % yield based on **3**SbF_6 and Equation 4) and blue solid (*c.f.* Cp_2FeSbF_6, 1.078 g) in bulb B were collected in the drybox. The FT-IR and Raman microscopy spectra of the green solid were consistent with **3**$^{\bullet}$. The actual spectra are given in Figure S12 and S13. Vibrational assignments for the experimental spectra are based on the calculated IR and Raman frequencies and intensities given in Table S2. The mass spectra, TGA and DSC are given in Figure S14-S16.

Equation S2 (Graphic depiction of Equation 4 in main text):

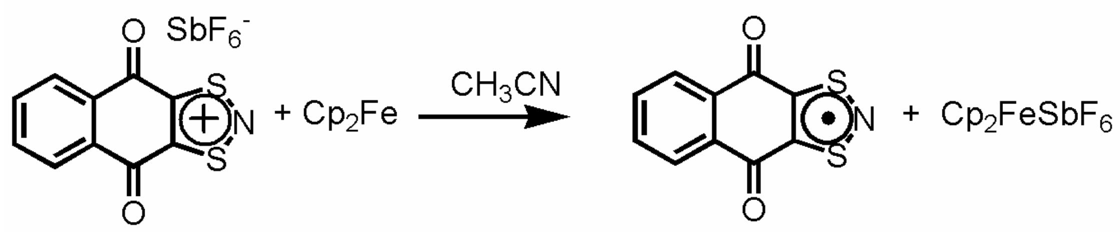

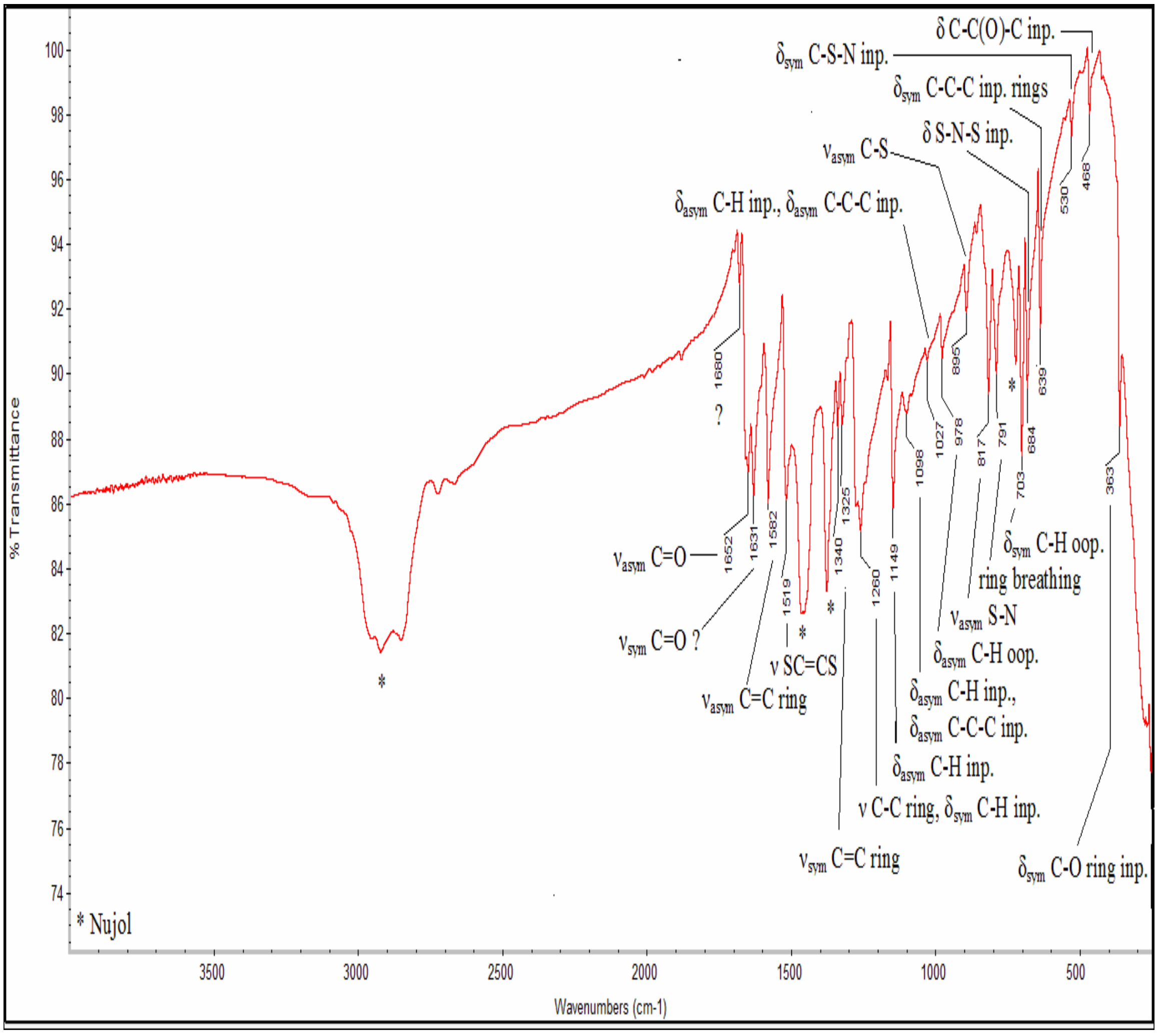

Figure S12: FT-IR spectrum of $\mathbf{3}^{\bullet}$ as a Nujol mull on KBr plates prepared according to Equation S2 on pg. 29 (32 scans, 2 cm^{-1} resolution). See Table S2 on pg. 22 for comparison of experimental and calculated IR frequencies and tentative assignments. Note the assignments are tentative and based on visualization of the vibrational modes in *ChemCraft*[8]: ν = stretch, δ = bending, asym. = asymmetric and sym = symmetric, opp = out-of-plane, inp = in-plane.

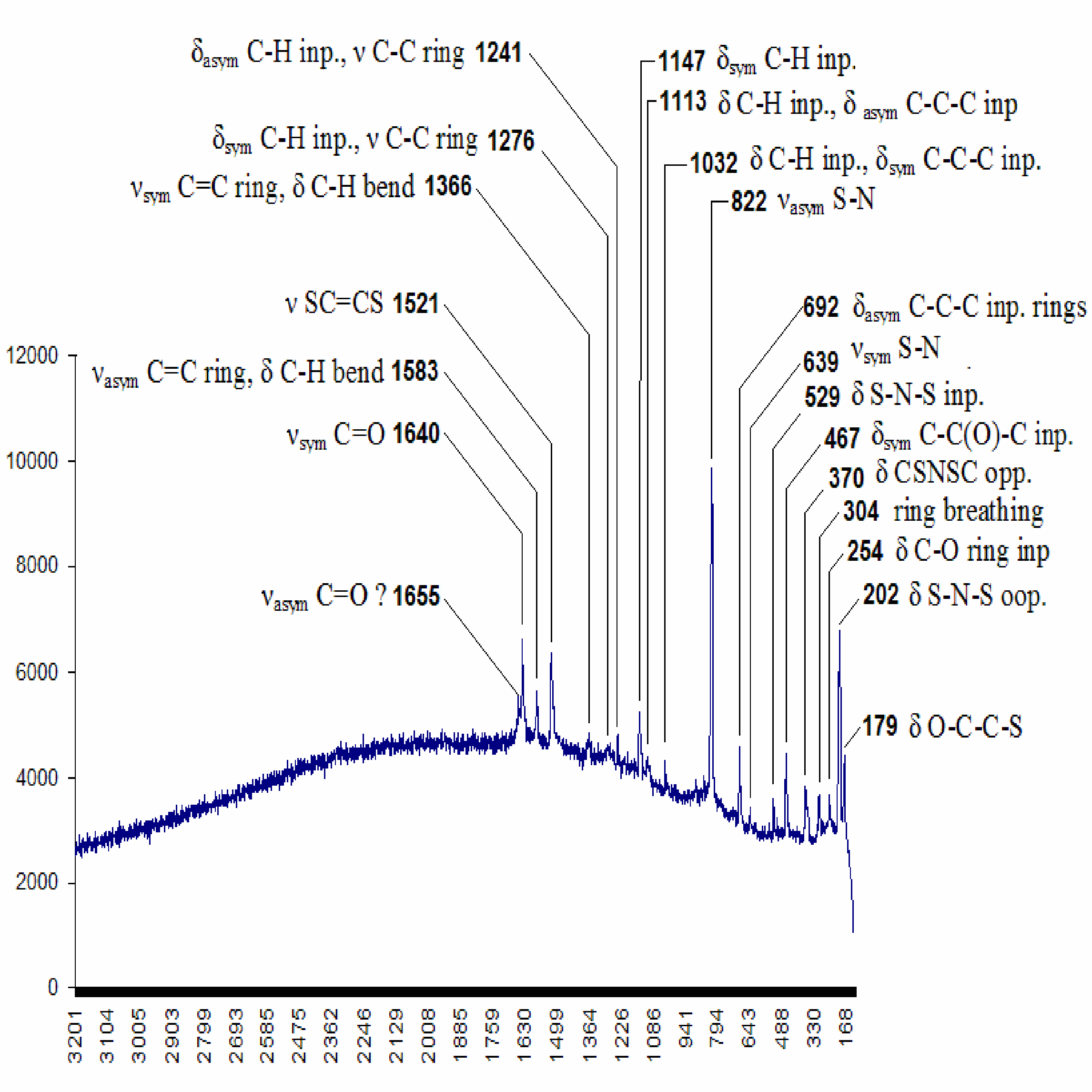

Figure S13: Raman microscopy spectrum of **3**$^{\bullet}$ prepared according to Equation S2 on pg. 29 (20 scans, 2 cm^{-1} resolution, 10 % laser power). See Table S2 on pg. 22 for comparison of experimental and calculated IR frequencies and tentative assignments. Note the assignments are tentative and based on visualization of the vibrational modes in *ChemCraft*[8]: ν = stretch, δ = bending, asym. = asymmetric and sym = symmetric, opp = out-of-plane, inp = in-plane.

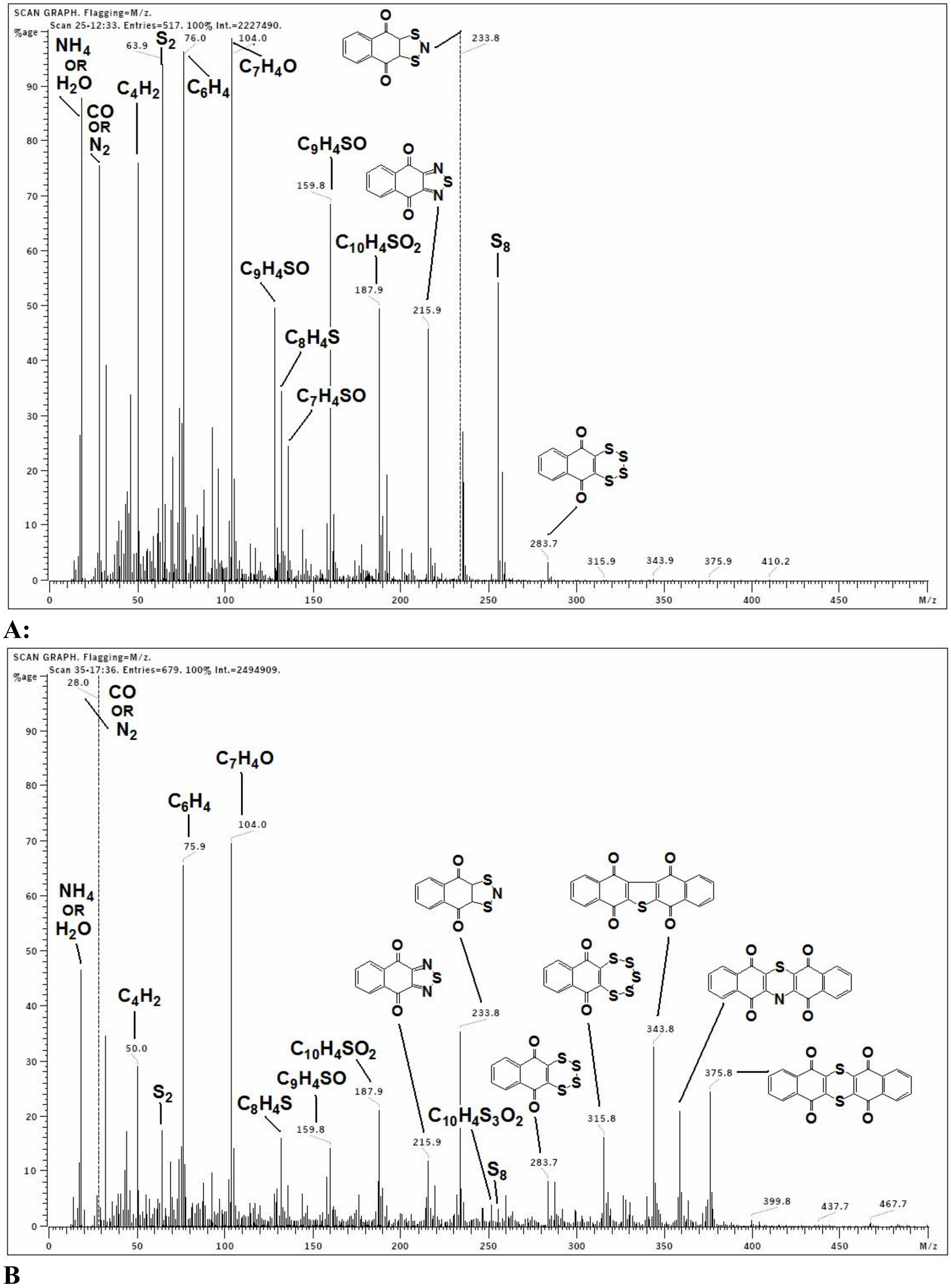

Figure S14: The mass spectra of $\mathbf{3}^{\bullet}$ prepared according to Equation S2 on pg. 29 a) scan 25, mz = 233.8, M^{+} = 100% and b) scan 35, mz = 233.8, M^{+} = 35% (See Table S5 on pg. 33 for details).

Table S5: Compilation of major fragmentation from mass spectra (EI, 70 eV, Scan 13) of **3**$^{\bullet}$ prepared according to Equation S2 (See Figure S14a and S14b on pg. 32) and **3**$^{\bullet}$ prepared according to Equation S5 (See Figure S40 on pg.72):

m/z	% scan 25 (See Figure S14a on pg. 32)	% scan 35 (See Figure S14b on pg. 32)	% scan 15 (See Figure S40 on pg. 72)	Fragmentation [a]	Proposed molecular formula of fragment
375.8	< 1	24	< 5	$M^+ + M^+ - S_2N$	$C_{20}H_8O_2S_2$
358.0	< 1	21	< 5	$M^+ + M^+ - S_3$	$C_{20}H_8O_2NS$
343.8	< 1	32	< 5	$M^+ + M^+ - S_3N$	$C_{20}H_4O_2S$
315.8	< 1	16	< 5	$M^+ + S_3 - N$	$C_{10}H_4O_2S_5$
283.8	3	8	66	$M^+ + S_2 - N$	$C_{10}H_4O_2S_4$
256.8	54	6	36		S_8
251.8	1	4	72	$M^+ + S - N$	$C_{10}H_4O_2S_3$
233.8	100	35	100	M^+	$C_{10}H_4O_2NS_2$
215.9	46	12	86	$M^+ - S + N$	$C_{10}H_4O_2N_2S$
187.9	50	21	74	$M^+ - SN$	$C_{10}H_4O_2S$
159.8	69	14	80	$M^+ - CO - SN$	C_9H_4OS
136.0	24	8	72	$M^+ - CO - C_2SN$	C_7H_4OS
132.0	34	16	71	$M^+ - 2\ CO - SN$	C_8H_4S
128.0	50	6	74	$M^+ - CO - S_2N$	C_9H_4O
104.0	99	70	76	$M^+ - C_2S_2N - CO$	C_7H_4O
76.0	96	66	78	$M^+ - C_2S_2N - 2\ CO$	C_6H_4
63.9	94	18	54		S_2
50.0	76	50	64		C_4H_2

[a] The inlet temperature (250 ^{o}C) leads to thermal decomposition of **3**$^{\bullet}$ leading to **10** (x = 1- 5) and **21** (and additional species from subsequent fragmentation) assuming decomposition occurs according to Scheme S3 (pg. 42) and Scheme S4 (pg. 52).

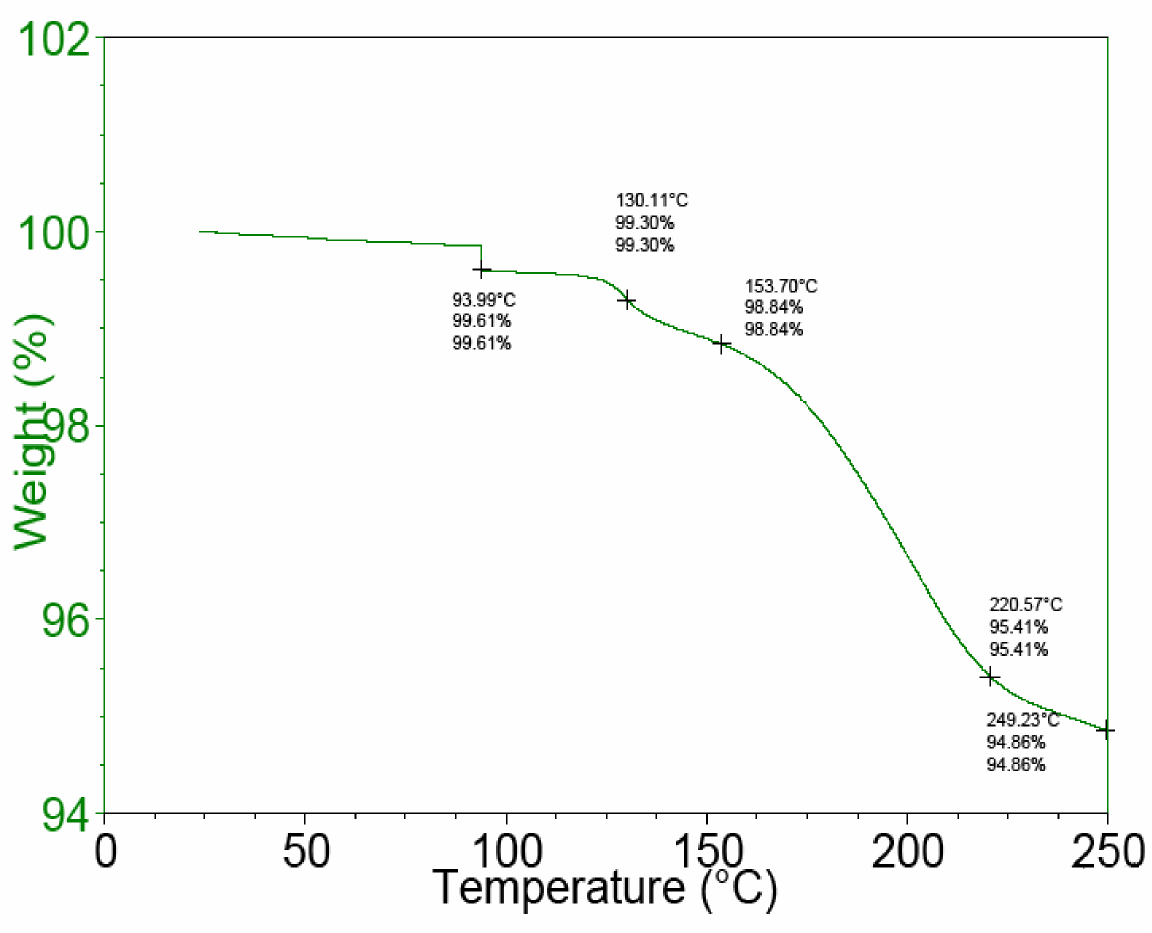

Figure S15: The Thermal Gravimetric Analysis (TGA) of **3**$^{\bullet}$ between 25-250 °C (65.286 mg) prepared according to Equation S2 on pg. 29.

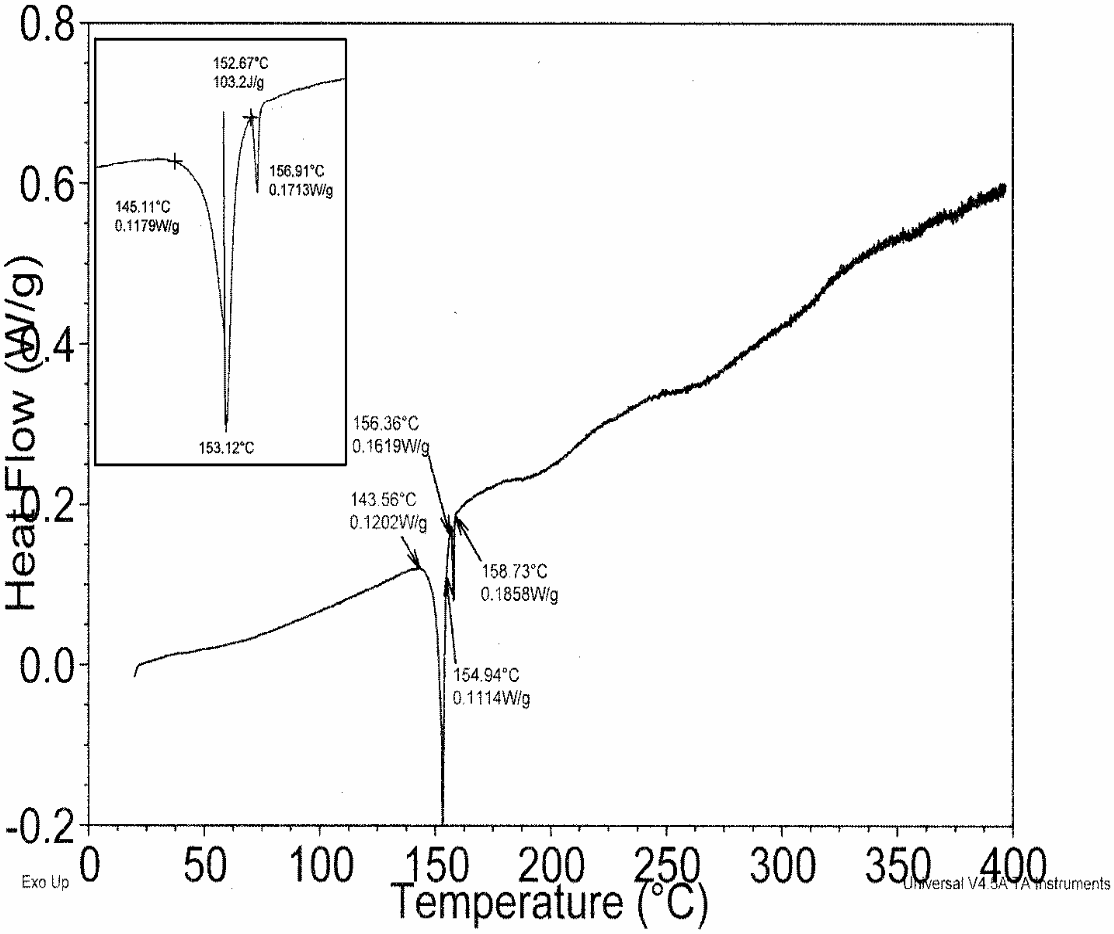

Figure S16: The Differential Scanning Calorimetry (DSC) of **3**$^{\bullet}$ between 25-250 °C (9.0 mg) prepared according to Equation S2 on pg. 29.

Table S6: Comparison of calculated (UB1LYP/EPR-III//6-31(3df))[13] and experimental[14] hyperfine coupling constants (G) for **3**$^\bullet$, **4**$^\bullet$, **8**$^\bullet$, **17**$^\bullet$, **18**$^\bullet$ and **19**$^\bullet$ (^{1}H, ^{13}C, ^{14}N and ^{33}S).

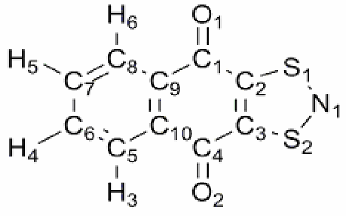

3$^\bullet$

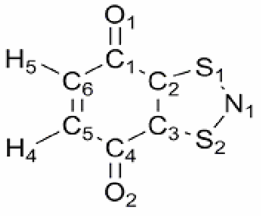

4$^\bullet$

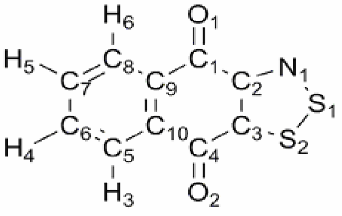

8$^\bullet$

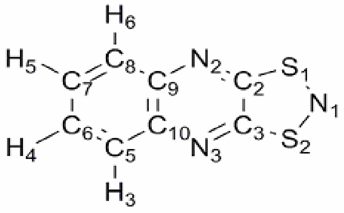

17$^\bullet$

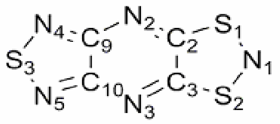

18$^\bullet$

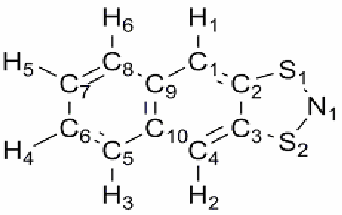

19$^\bullet$

	3$^\bullet$		**4**$^\bullet$		**8**$^\bullet$		**17**$^\bullet$		**18**$^\bullet$		**19**$^\bullet$	
g-value	2.0073		2.005		2.0095		2.0071		2.0072		2.0067	
	Calc.	Exp.	Calc.	Exp.	Calc.	Exp.	Calc.	Exp.	Calc.	Exp.	Calc.	Exp.
O1	0.09	[a]	-0.62	[a]	0.67	[a]	NA	[a]	NA	[a]	NA	NA
O2	0.09	[a]	-0.62	[a]	-3.48	[a]	NA	[a]	NA	[a]	NA	NA
C1	0.02	[a]	-0.65	[a]	1.55	[a]	NA	[a]	NA	[a]	0.12	[a]
C2	-2.00	[a]	-1.67	[a]	-9.57	[a]	-3.63	[a]	-3.63	[a]	-2.51	[a]
C3	-2.00	[a]	-1.67	[a]	11.31	[a]	-3.63	[a]	-3.63	[a]	-2.51	[a]
C4	0.02	[a]	-0.65	[a]	-5.03	[a]	NA	[a]	NA	[a]	0.12	[a]
C5	0.01	[a]	0.07	[a]	0.24	[a]	-0.33	[a]	-0.33	[a]	0.01	[a]
C6	0.01	[a]	0.07	[a]	-0.39	[a]	0.16	[a]	0.16	[a]	0.01	[a]
C7	0.03	[a]	NA	[a]	0.51	[a]	0.16	[a]	0.16	[a]	0.01	[a]
C8	0.03	[a]	NA	[a]	-0.47	[a]	-0.33	[a]	-0.33	[a]	0.01	[a]
C9	-0.20	[a]	NA	[a]	0.60	[a]	-0.78	[a]	-0.78	[a]	-0.55	[a]
C10	-0.20	[a]	NA	[a]	-1.06	[a]	-0.78	[a]	-0.78	[a]	-0.55	[a]
H1	NA	[a]	NA	[a]	NA	[a]	NA	[a]	NA	[a]	-0.12	[a]
H2	NA	[a]	NA	[a]	NA	[a]	NA	[a]	NA	[a]	-0.12	[a]
H3	-0.09	[a]	NA	[a]	-0.31	[a]	-0.54	0.65	-0.54	0.65	-0.24	[a]
H4	-0.11	[a]	NA	[a]	0.10	[a]	-0.26	0.23	-0.26	0.23	-0.24	[a]
H5	-0.11	[a]	-0.29	[a]	-0.39	[a]	-0.26	0.23	-0.26	0.23	-0.30	[a]
H6	-0.09	[a]	-0.29	[a]	0.18	[a]	-0.54	0.65	-0.54	0.65	-0.30	[a]
S1	4.040	[a]	2.26	[a]	5.08	[a]	2.47	[a]	2.47	[a]	3.55	[a]
S2	4.040	[a]	2.26	[a]	5.59	[a]	2.47	[a]	2.47	[a]	3.55	[a]
N1	10.86	10.89	10.63	10.13	4.60	4.90	10.81	10.89	10.81	10.89	11.04	11.26
N2	NA	NA	NA	NA	NA	NA	1.07	1.29	1.07	1.29	NA	NA
N3	NA	NA	NA	NA	NA	NA	1.07	1.29	1.07	1.29	NA	NA
N4	NA	NA	NA	NA	NA	NA	NA	NA	NA	NA	NA	NA
N5	NA	NA	NA	NA	NA	NA	NA	NA	NA	NA	NA	NA

[a] Not observed experimentally and/or not reported in the literature.

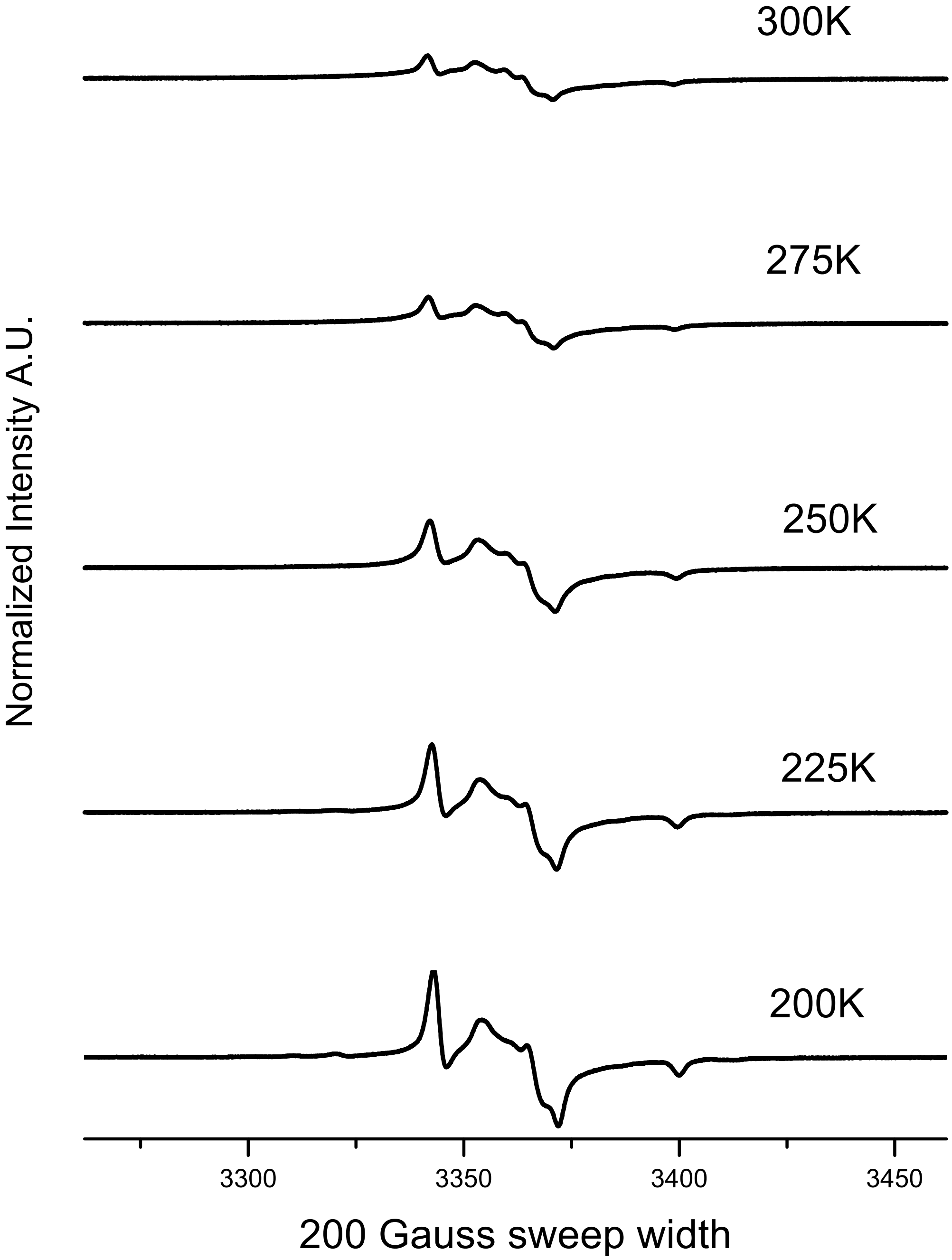

Figure S17: Variable temperature (300-200 K) powder X-band EPR spectra of **3**$^{\bullet}$

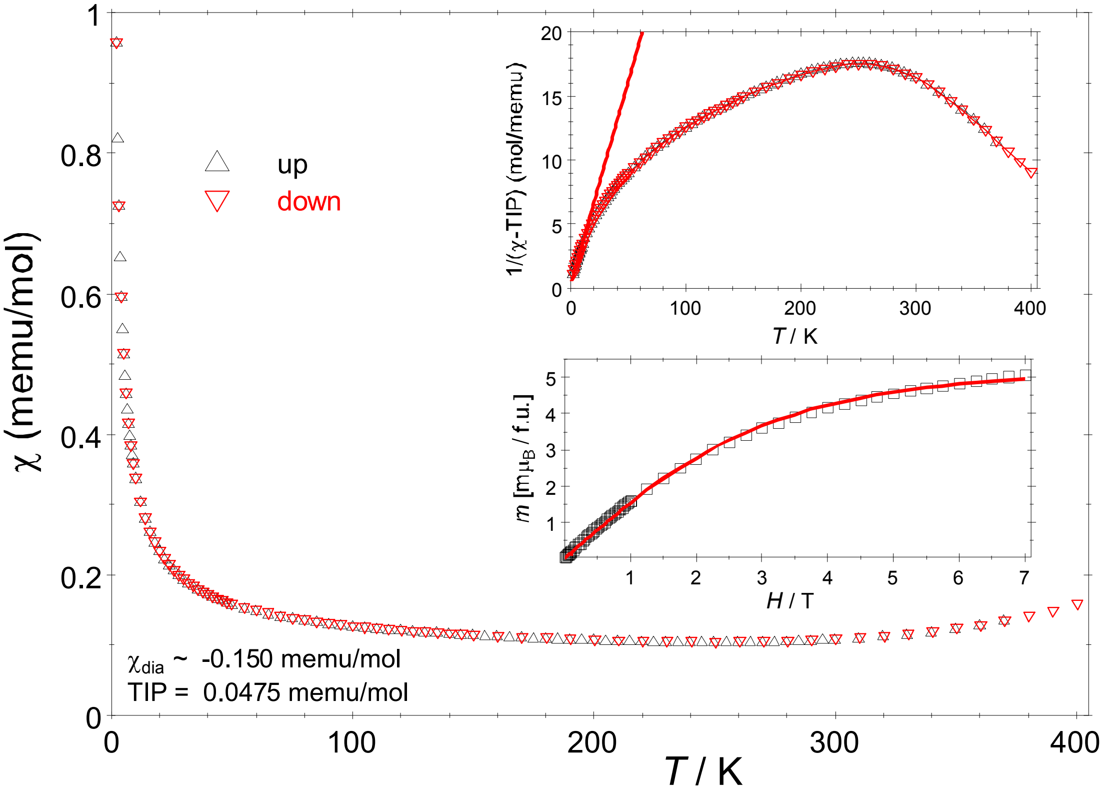

Figure S18: Temperature dependence of χ for **3**$^{\bullet}$. The sample cooling (▼) and sample heating (▲) of **3**$^{\bullet}$ over the temperature range 2 - 400 K.

Discussion: Magnetic susceptibility of 3$^{\bullet}$ and the small quantity of paramagnetic (S = ½) impurity.

Variable temperature magnetic susceptibility (χ) measurements have been performed on a crystalline sample of **3**$^{\bullet}$ for cooling-down and warming-up cycles (Figure S18). Data were corrected for both the sample holder and a molar core diamagnetism calculated from Pascal's constants of χ_{dia} = -150 memu mol^{-1} has been subtracted from the data. A linear temperature dependence of the inverse magnetic suceptibility (χ-TIP)$^{-1}$ (T) is observed below 8 K and a fit to a Curie-Weiss law yields an effective magnetic moment of 0.159 μ_B leading to a small paramagnetic impurity of around 0.8 % (Inset, top right of Figure S18). This is in line with the Brillouin fit of the magnetization curve at 2K for a S = ½ which includes a temperature independent paramagnetism (TIP) of 0.0475 memu mol^{-1} and yields a paramagnetic impurity of 0.45 % (Inset, bottom right of Figure S18). The presence of these small paramagnetic impurity was also inferred from the variable temperature (200-300 K) solid state EPR (See Figure S17 on pg. 37). Here the paramagnetic signal decreases with increasing temperature. The impurities likely arise from lattice defect sites in the crystalline sample of **3**$^{\bullet}$ which forms essentially centrosymmetric *trans* cofacial π^{*} - π^{*} dimers as described in Section 3.2.4 and shown in Figure 7 of the main text. However, the magnetic susceptibility of **3**$^{\bullet}$ increases slightly in the 300 – 400 K range, which may result from dissociation of a small portion of dimers [**3**$^{\bullet}$]$_2$ into monomers **3**$^{\bullet}$ producing paramagnetic S = ½ sites. The related **10**$^{\bullet}$ (R = H) is also dimerizes below 320 K, yet exhibits a high temperature (c.f. 324 K) phase transition from a dimeric to paramagetic state with a small hysteresis loop (ΔT = 26 K)[15]. While we postulated **3**$^{\bullet}$

may exhibit similar behaviour to $\mathbf{14}^{\bullet}$, the possibility of thermally accessible triplet states in the π^{*} - π^{*} dimers analogous to related thiazyl radicals[16] may be possible at elevated temperature based on the relatively long S---S separation (c.f. 3.276(2) Å) at 296 K (Figure 7, main text). Therefore, the thermal stability was first investigated by TGA and DSC measurements (See Figure S15 and S16 on pg. 34 and 35). The DSC indicated the onset ~ 417 K of an irreversible exothermic modification of $\mathbf{3}^{\bullet}$. However, the TGA indicates no substantial decrease in mass (≤ 5 %), corresponding to the temperature range 298-493 K. The moderate thermal stability of $\mathbf{3}^{\bullet}$ prohibited further investigation of the magnetic susceptibility above 400 K and broken symmetry calculations suggest a large S-T gap of 33 kJ mol^{-1} for $[\mathbf{3}^{\bullet}]_2$ at an intradimer S---S separation of 3.276(2) Å) corresponding to the HT single crystal X-ray structure.

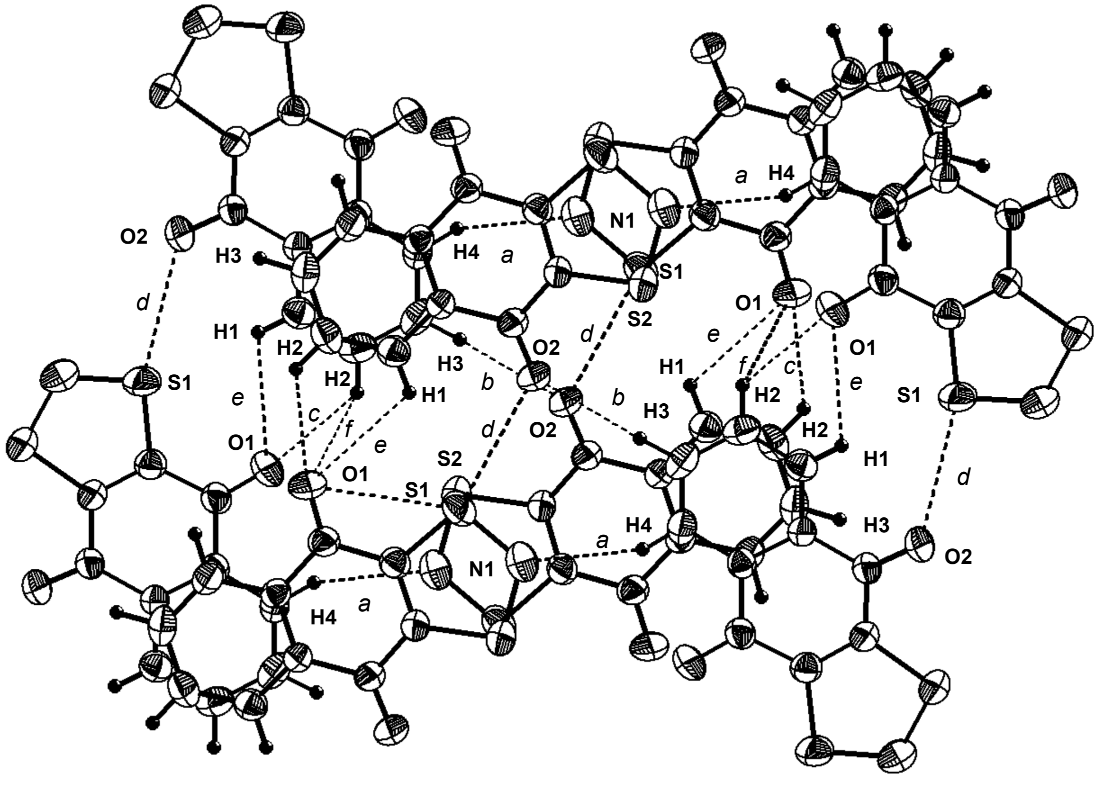

Figure S19: The principal intermolecular interactions between $\mathbf{3}^{\bullet}$ leading to zig-zag chains viewed in the *bc*-plane. Thermal ellipsoids are drawn at 35 % probability and hydrogen atoms are given as solid black spheres (0.135 Å) for clarity. The intermolecular contacts (Å) and Brown's bond valence units [vu] [40]: a = 2.512(35), [0.097]; b = 2.540(34), [0.095]; c = 2.840(24), [0.074]; d = 3.579(3), [0.005]; e = 3.214(36), [0.056] and f = 2.885(24), [0.072] are indicated above.

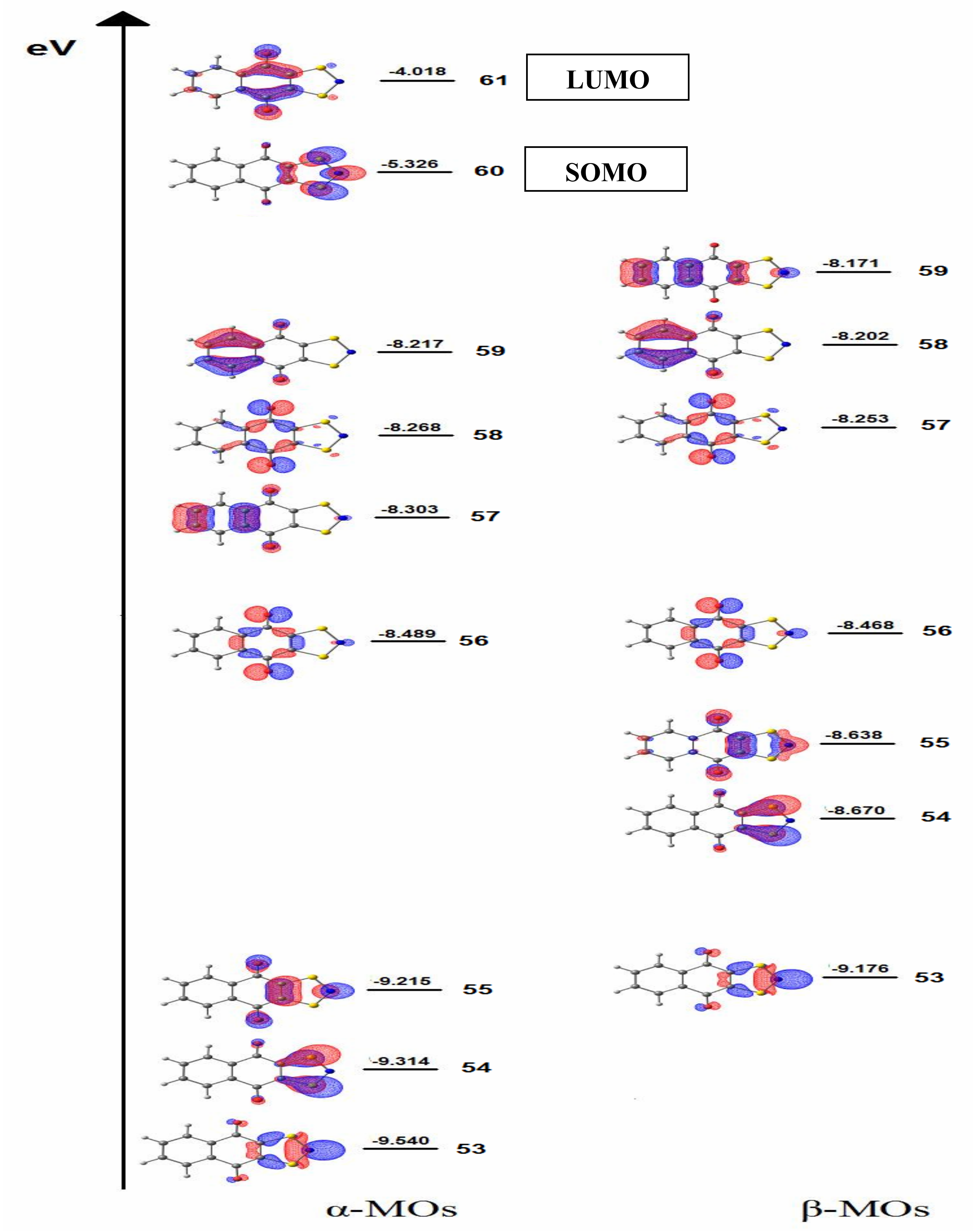

Figure S20: Frontier molecular orbitals (MOs 61-50) and energies of **3**$^{\bullet}$ (UPBE0/6-311G(d))

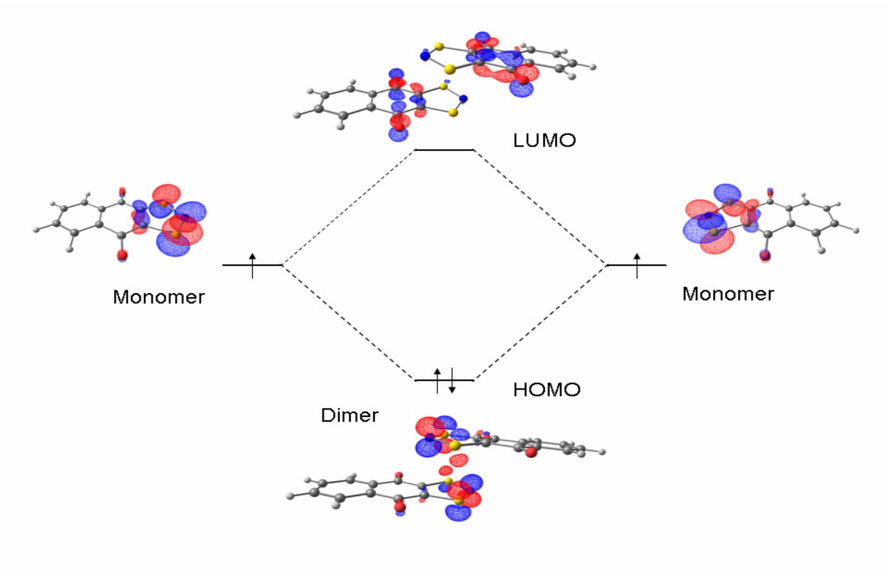

Figure S21: Schematic diagram illustrating formation of the $[\mathbf{3}^{\bullet}]_2$ dimer from two monomers. Orbitals are drawn at the isosurface of 0.05 au.

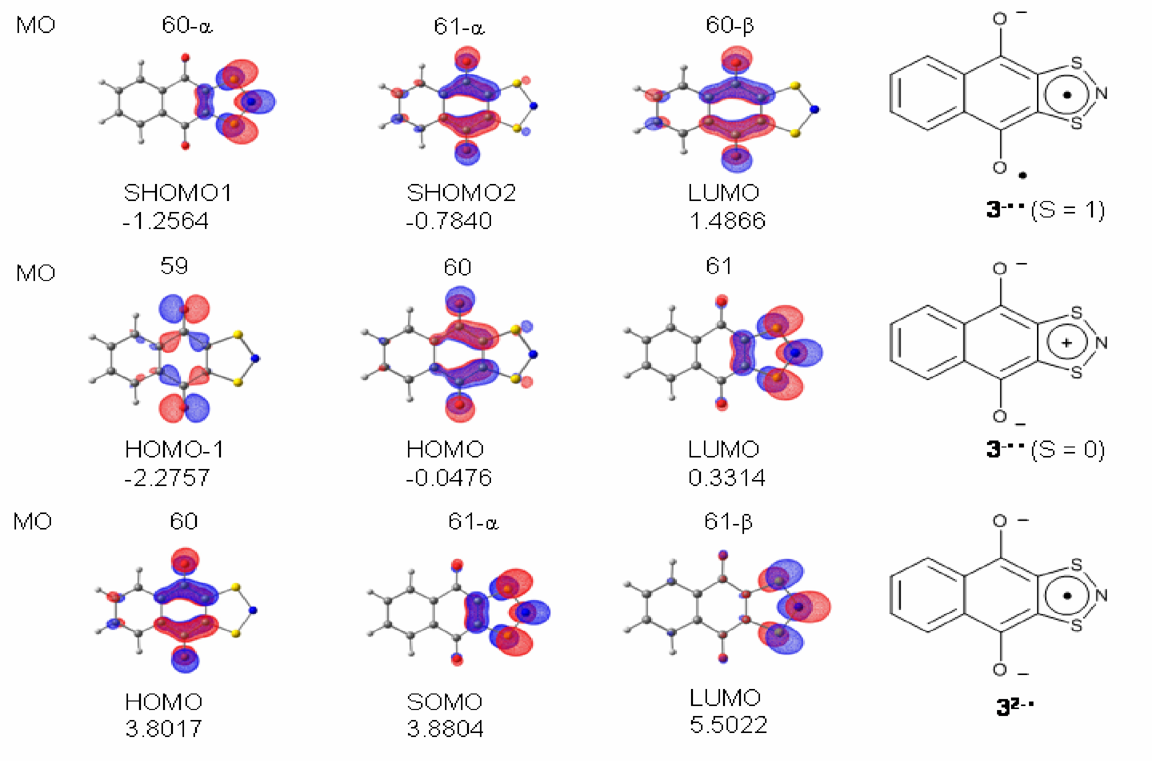

Figure S22: The π MOs 60 – 61 and PBE0/6-311G(d) orbital energies (eV) for the molecules $\mathbf{3}^{-\bullet\bullet}$ (S = 1 and S = 0) and $\mathbf{3}^{2-\bullet}$. Orbitals are drawn at the isosurface 0.05 au.

C. Thermal decomposition of $3^{\bullet}$ prepared according to Equation S2 (See pg. 29) by dynamic vacuum sublimation (10^{-2} Torr) in a three zone sublimation furnace.

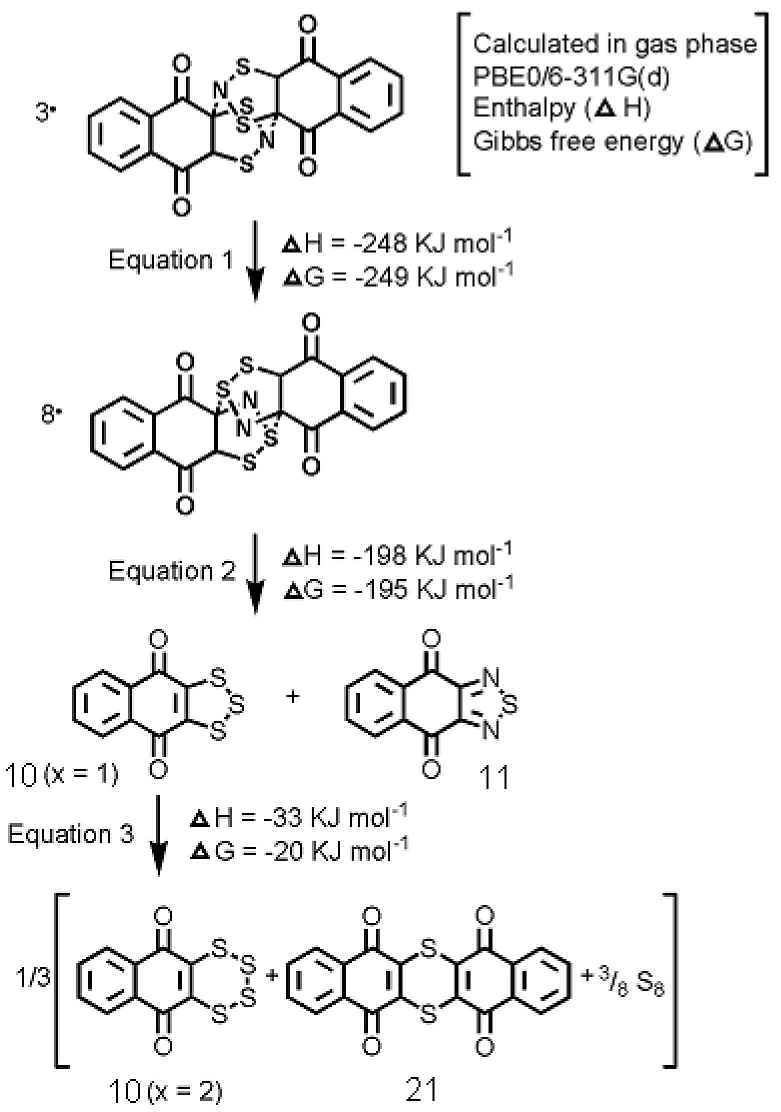

Scheme S3: Proposed route of thermal decomposition of $3^{\bullet}$ to 10 (x = 2) and 11

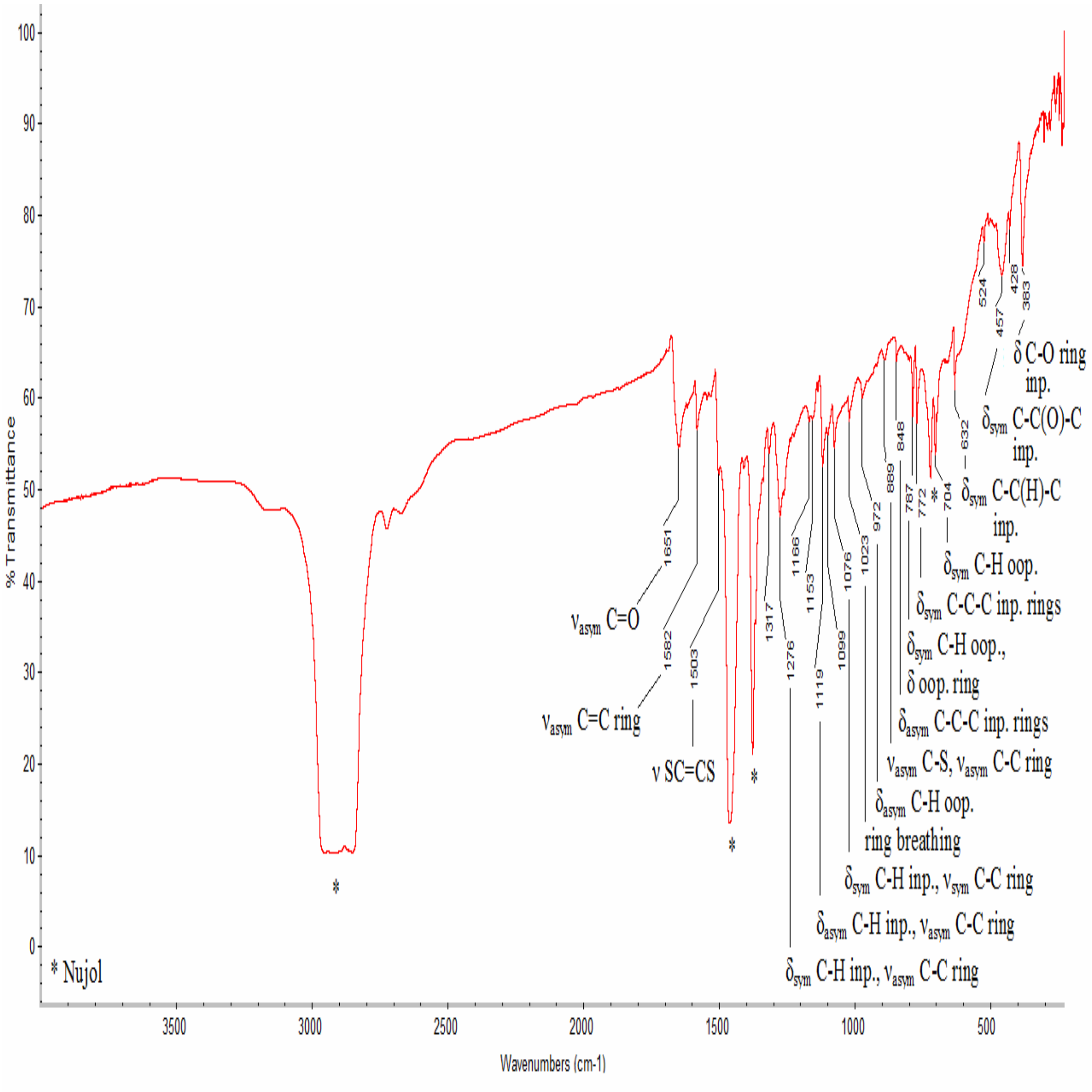

Figure S23: FT-IR spectrum of **10** (x = 2) prepared as Nujol mull on KBr plates prepared according to Equation 1-3 in Scheme S3 on pg. 42 (32 scans, 2 cm^{-1} resolution). See Table S7 on pg. 45 for comparison of experimental and calculated IR frequencies and tentative assignments. Note the assignments are tentative and based on visualization of the vibrational modes in *ChemCraft*[8]: ν = stretch, δ = bending, asym. = asymmetric and sym = symmetric, opp = out-of-plane, inp = in-plane.

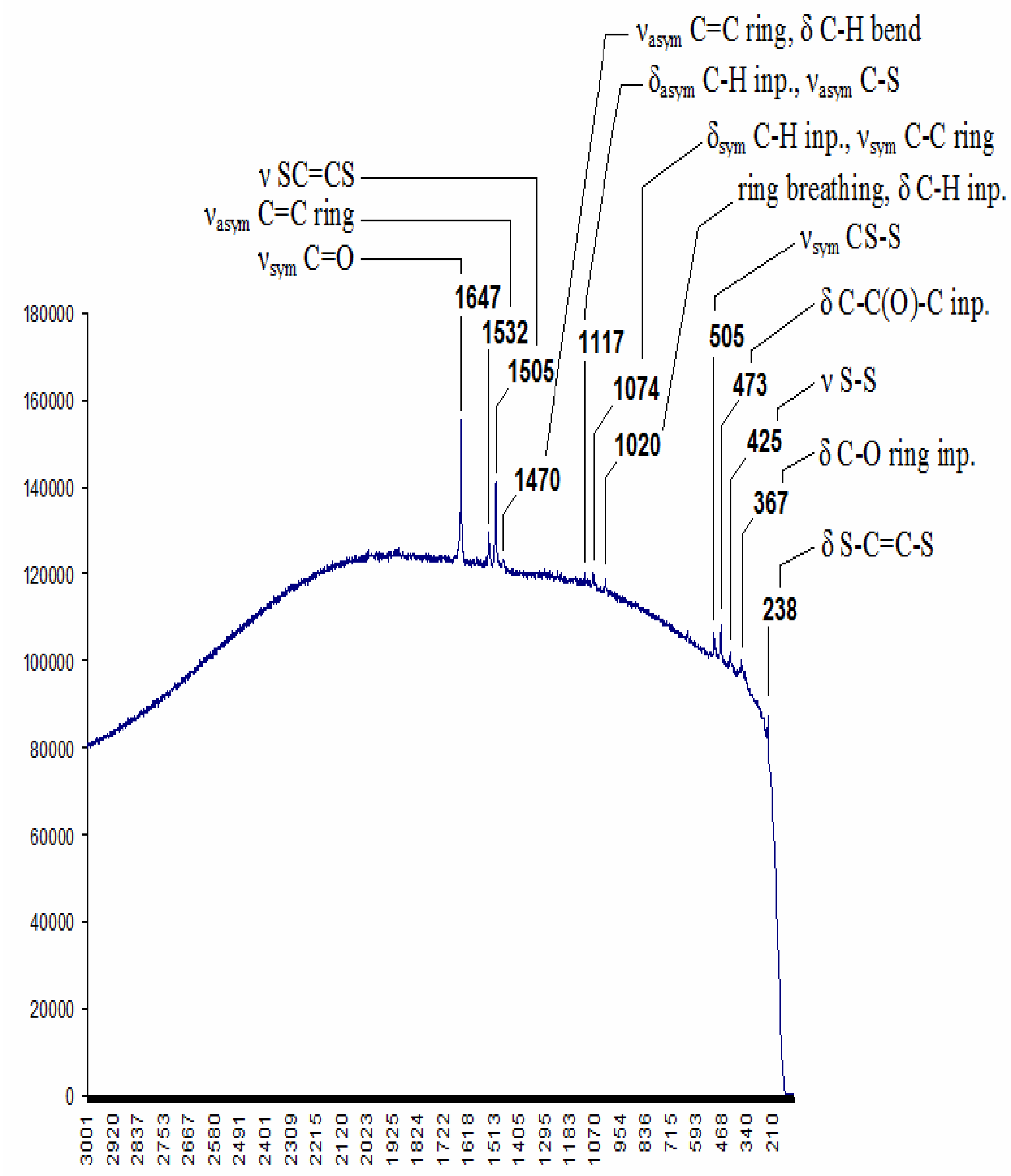

Figure S24: Raman microscopy spectrum of **10** (x = 2) prepared according to Equation 1-3 in Scheme S3 on pg. 42. See Table S7 on pg. 45 for comparison of experimental and calculated Raman frequencies and tentative assignments. Note the assignments are tentative and based on visualization of the vibrational modes in *ChemCraft*[8]: ν = stretch, δ = bending, asym. = asymmetric and sym = symmetric, opp = out-of-plane, inp = in-plane.

Table S7: Comparison of the experimental and calculated (PBE0/6-311G(d)) IR and Raman frequencies and intensities for **10** (x = 2) and the related trithiolane (**10**, x = 1) and pentathiine (**10**, x = 3) and tentative assignments. See pg. 43 and 44 for actual IR and Raman spectra.

10 (x = 2)			**10** (x = 1)	**10** (x = 3)	Tentative Assignments [a]
IR/Raman (Calc.)	IR (Obs.)	Raman (Obs.)	IR/Raman (Calc.)	IR/Raman (Calc.)	
3075 (2/57)			3073 (3/71)	3074 (2/65)	ν C-H
372 (0/9)			3069 (0/11)	3072 (0/10)	ν C-H
3058 (2/47)			3058 (2/50)	3059 (2/54)	ν C-H
3044 (1/19)			3045 (1/23)	3045 (1/22)	ν C-H
1675 (63/5)	1651s,br		1679 (93/13)	1679 (62/5)	ν_{asym} C=O
1674 (2/100)		1647s	1676 (0/100)	1677 (2/100)	ν_{sym} C=O
1583 (9/10)	1582m		1582 (13/8)	1582 (9/12)	ν_{asym} C=C ring
1579 (1/1)			1574 (6/1)	1579 (1/0)	
		1532w			ν_{asym} C=C ring
1494 (33/46)	1503m,sh	1505s	1534 (50/52)	1508 (34/45)	ν SC=CS
1455 (6/2)		1470vw	1452 (3/0)	1455 (4/1)	ν_{asym} C=C ring, δ C-H
1428 (1/0)			1473 (1/0)	1427 (1/0)	
1334 (2/2)			1330 (3/1)	1333 (2/2)	
	1317w				
1263 (3/10)			1261 (7/18)	1259 (3/11)	
1257 (100/12)	1276s,br		1256 (100/20)	1253 (100/16)	δ_{sym} C-H inp., ν_{asym} C-C ring
1203 (3/7)			1207 (7/15)	1201 (3/8)	
	1166w				
	1153w				
1131 (2/3)			1131 (1/4)	1131 (2/3)	
1095 (19/7)	1119m	1117w	1110 (27/13)	1092 (17/8)	δ_{asym} C-H inp., ν_{asym} C-C ring
	1099w				
1059 (6/8)	1076w	1074w	1086 (0/8)	1055 (6/7)	δ_{sym} C-H inp., ν_{sym} C-C ring
1054 (4/1)			1057 (2/0)	1051 (6/2)	
1007 (3/17)	1023w	1020w	1011 (1/16)	1007 (3/20)	ring breathing
970 (0/1)	972w		969 (0/1)	970 (0/1)	δ_{asym} C-H oop.
941 (1/0)			948 (1/0)	948 (1/0)	
907 (0/1)			906 (0/1)	907 (0/1)	
899 (2/0)	889w		879 (3/0)	876 (1/0)	ν_{asym} C-S
853 (1/0)	848w		854 (0/1)	847 (1/0)	δ_{asym} C-C-C inp. rings
811 (1/1)			817 (22/2)	819 (1/2)	
799 (2/0)	787w		796 (3/0)	798 (2/0)	δ_{sym} C-H oop., δ oop. ring
783 (9/1)	772w		786 (0/1)	780 (10/1)	δ_{sym} C-C-C inp. rings
723 (15/0)			719 (20/0)	720 (14/0)	
702 (1/0)	704w		702 (0/1)	699 (1/0)	δ_{sym} C-H oop.
693 (0/1)			678 (0/1)	694 (0/1)	
634 (5/1)	632w		640 (5/2)	631 (6/2)	δ_{sym} C-C(H)-C inp.
556 (0/1)			543 (0/1)	546 (0/1)	
526 (0/2)			500 (0/3)	524 (0/2)	
503 (1/6)		505m	498 (0/12)	493 (0/9)	ν_{sym} CS-S
489 (0/1)		473m	479 (1/2)	491 (0/1)	δ_{asym} C-C(O)-C inp., ν_{sym} S-S (x = 1)
473 (1/5)	457m,br		461 (0/1)	471 (1/2)	δ_{sym} C-C(O)-C inp., ν_{asym} S-S (x = 1)
430 (1/1)	428vw		425 (0/1)	446 (1/6)	ν_{sym} S-S (x = 3)
424 (0/1)		425m	385 (1/2)	426 (1/4)	ν_{asym} S-S (x = 2)
415 (1/2)			381 (2/1)	424 (1/1)	ν_{sym} S-S (x = 3)
382 (7/1)	383m		366 (3/0)	419 (0/2)	ν_{sym} S-S (x = 2,3), δ_{asym} C-C(O)-C

					inp. C=O wagging,
367 (0/1)		367m	352 (1/0)	372 (7/1)	δ_{sym} C-C(O)-C inp. C=O wagging
351 (0/1)			261 (1/1)	354 (1/1)	
285 (0/3)			260 (0/1)	302 (0/1)	
275 (0/1)			254 (1/2)	300 (0/3)	
255 (0/1)			170 (1/0)	289 (0/1)	
231 (1/1)		238w	169 (0/1)	270 (0/1)	δ S-C=C-S
206 (0/3)			124 (0/1)	227 (0/1)	
168 (0/1)			119 (0/1)	183 (0/2)	
166 (1/0)			83 (0/1)	173 (0/1)	
123 (0/1)			51 (1/0)	162 (0/1)	
89 (0/1)				150 (1/1)	
74 (0/1)				123 (0/1)	
37 (0/1)				106 (0/1)	
				67 (0/1)	
				58 (1/1)	
				29 (0/1)	

[a] The vibrational modes are heavily mixed, therefore, only the major vibrational modes are assigned based on the scaled displacement vectors visualized in *ChemCraft* [8].

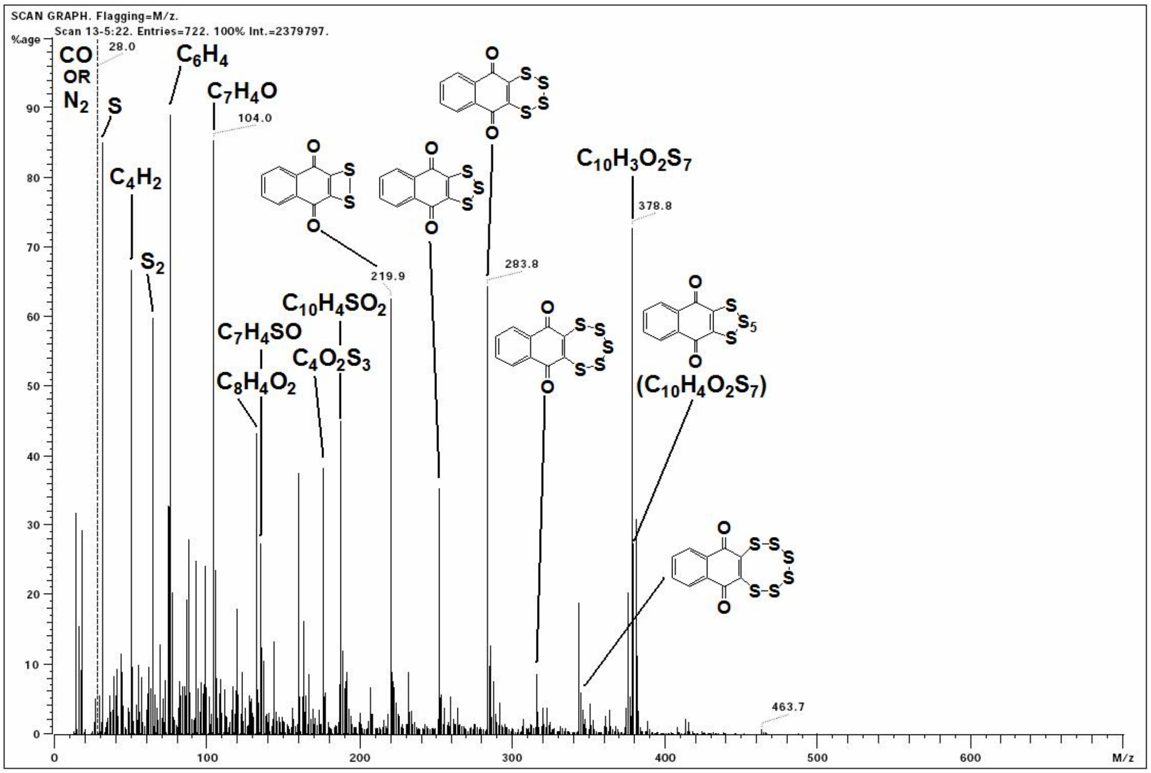

Figure S25: Mass spectra (EI, 70 eV) of **10** (x = 2; scan13, mz = 283.8 at 64 %, inlet temperature = 250 °C)

Table S8: Compilation of major fragmentation from mass spectra (EI, 70 eV, Scan 13) of **10** (x = 2) prepared according to Equation 1-3 in Scheme S3 on pg. 42 (See Figure S25 on pg. 46):

m/z	%	Fragmentation [a]	Proposed molecular formula of fragment
379.8	28	$M^+ + S_3$	$C_{10}H_4O_2S_7$
378.8	73	$M^+ + S_3 - H$	$C_{10}H_3O_2S_7$
376.0	20	$M^+ + M^+ - S_6$	$C_{20}H_8O_4S_2$
347.9	6	$M^+ + S_2$	$C_{10}H_4O_2S_6$
344.0	19	$M^+ + M^+ - S_7$	$C_{20}H_8O_4S$
315.9	8	$M^+ + S$	$C_{10}H_4O_2S_5$
283.8	64	M^+	$C_{10}H_4O_2S_4$
251.9	35	$M^+ - S$	$C_{10}H_4O_2S_3$
219.9	62	$M^+ - S_2$	$C_{10}H_4O_2S_2$
188.0	45	$M^+ - S_3$	$C_{10}H_4O_2S$
175.9	38	$M^+ - S - C_6H_4$	$C_4O_2S_3$
136.0	27	$M^+ - C_2S_3 - CO$	C_7H_4OS
132.0	43	$M^+ - C_2S_4$	$C_8H_4O_2$
104.0	85	$M^+ - C_2S_4 - CO$	C_7H_4O
76.0	89	$M^+ - C_2S_4 - 2\,CO$	C_6H_4
63.9	59		S_2
50.0	66		C_4H_2

[a] The inlet temperature (250 °C) leads to thermal decomposition of **10** (x = 2) leading to a **10** (x = 1-5) and **22** (and additional species from subsequent fragmentation) assuming decomposition occurs according to Scheme S3 (See pg. 42) and Scheme S4 (See pg. 52).

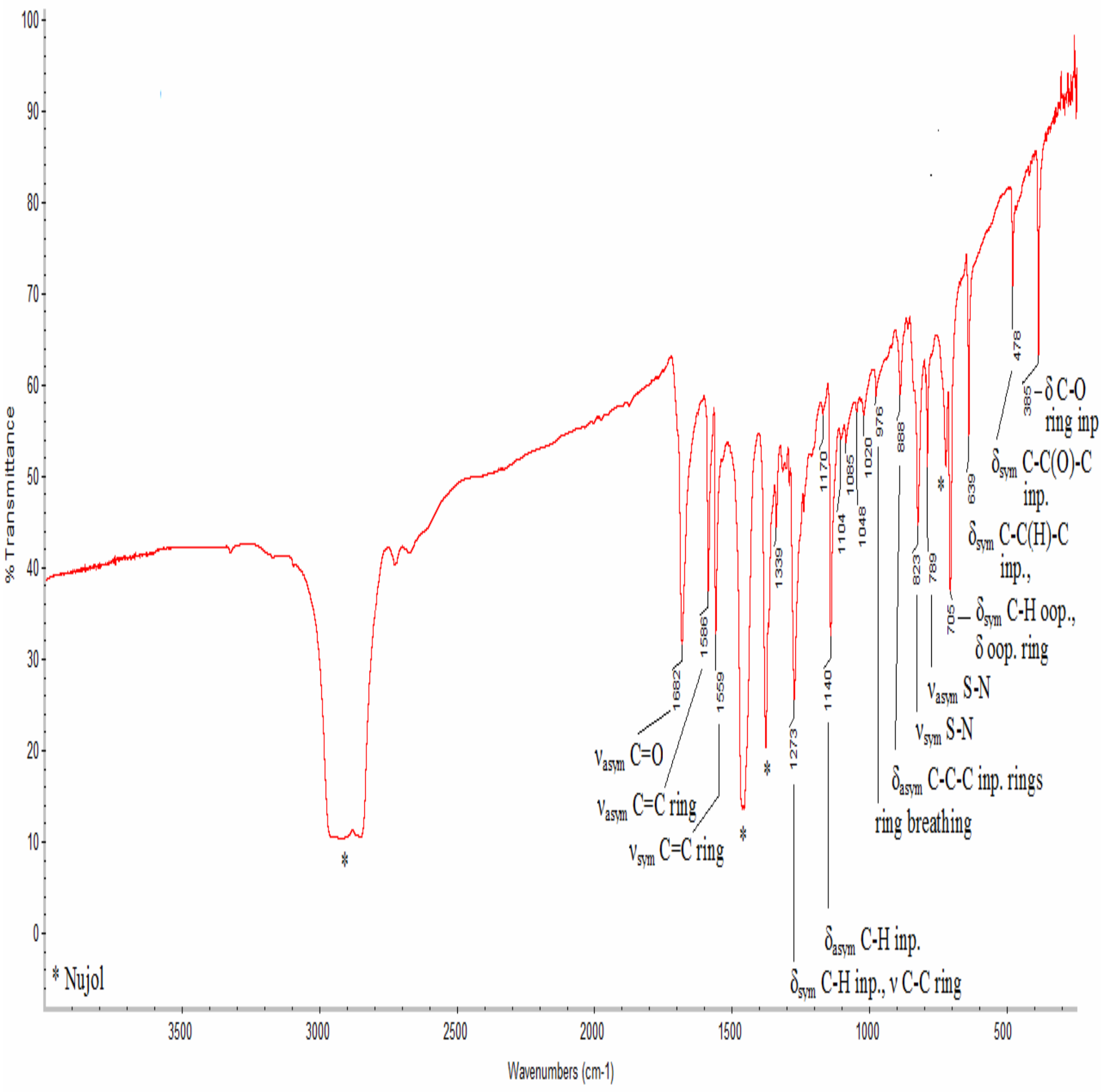

Figure S26: FT-IR spectrum of **11** prepared as Nujol mull on KBr plates prepared according to Equation 1-2 in Scheme S3 on pg. 42 (32 scans, 2 cm^{-1} resolution). See Table S7 on pg. 45 for comparison of experimental and calculated IR frequencies and tentative assignments. Note the assignments are tentative and based on visualization of the vibrational modes in *ChemCraft*[8]: ν = stretch, δ = bending, asym. = asymmetric and sym = symmetric, opp = out-of-plane, inp = in-plane.

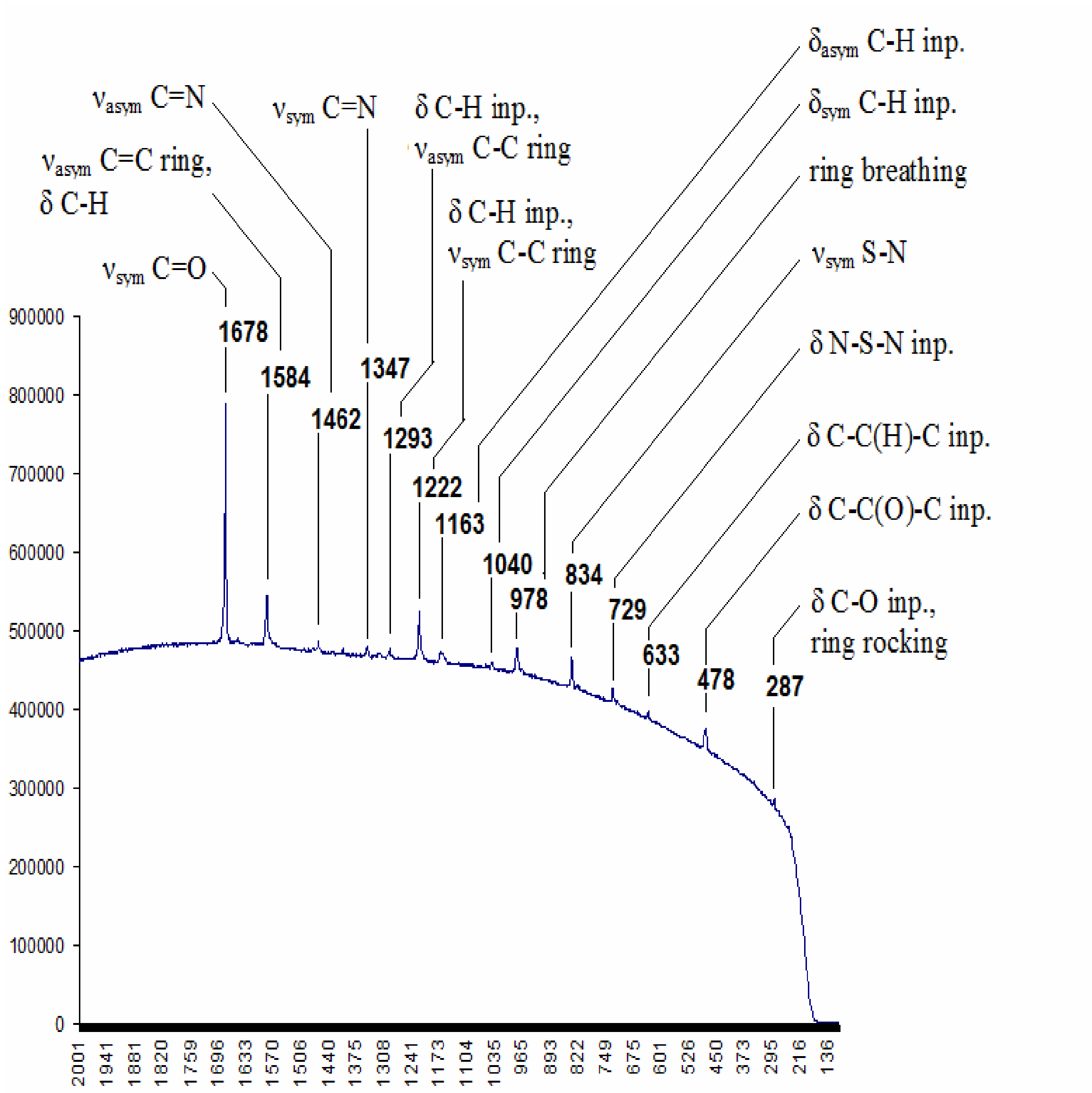

Figure S27: Raman microscopy spectrum of **11** prepared according to Equation1-2 in Scheme S3 on pg. 42. See Table S7 on pg. 45 for comparison of experimental and calculated Raman frequencies and tentative assignments. Note the assignments are tentative and based on visualization of the vibrational modes in *ChemCraft*[8]: ν = stretch, δ = bending, asym. = asymmetric and sym = symmetric, opp = out-of-plane, inp = in-plane.

Table S9: Comparison of the experimental and calculated (PBEO⁄6-311G(d)) bond distances (Å) and angles (^{o}) of **10** (x = 2) and the related trithiolane (**10**, x = 1) and pentathiine (**10**, x = 3).

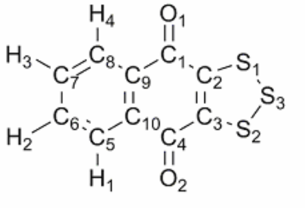

10 (x = 1)

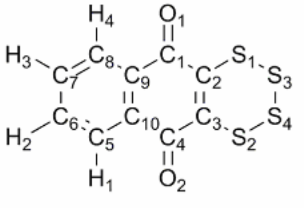

10 (x = 2)

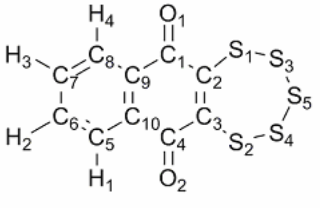

10 (x = 3)

Bond	**10** (x =2)	Calc. **10** (x =2) (C_2)	Calc. **10** (x =1) (C_2)	Calc. **10** (x =3) (~C_2)
Bond Length (Å)				
O1-C1	1.223(5)	1.215	1.214	1.214
O2-C4	1.225(4)	1.215	1.214	1.214
C1-C2	1.489(5)	1.493	1.477	1.496
C1-C9	1.482(4)	1.477	1.484	1.478
C2-C3	1.365(5)	1.363	1.351	1.357
C3-C4	1.499(4)	1.493	1.477	1.496
C4-C10	1.478(4)	1.477	1.484	1.214
C5-C6	1.387(5)	1.388	1.389	1.388
C5-C10	1.395(4)	1.391	1.390	1.391
C6-C7	1.387(5)	1.393	1.392	1.393
C7-C8	1.398(4)	1.388	1.389	1.388
C8-C9	1.395(5)	1.391	1.390	1.391
C9-C10	1.403(5)	1.395	1.400	1.395
C2-S1	1.752(3)	1.762	1.759	1.780
C3-S2	1.753(3)	1.762	1.759	1.780
S1-S3	2.035(1)	2.065	2.101	2.059
S2-S4	2.031(1)	2.065	NA	2.059
S3-S4	2.066(1)	2.086	NA	NA
S3-S5	NA	NA	NA	2.096
S4-S5	NA	NA	NA	2.096
C5-H1	0.950(4)	1.084	1.085	1.084
C6-H2	0.951(3)	1.085	1.085	1.085
C7-H3	0.950(3)	1.085	1.085	1.085
C8-H4	0.949(4)	1.084	1.085	1.084
Bond Angles (^{o})				
O1-C1-C2	118.87(29)	119.14	120.48	119.14
O1-C1-C9	122.15(27)	121.82	122.84	121.82
O2-C4-C3	118.98(25)	119.14	120.48	119.14
O2-C4-C10	122.31(29)	121.82	122.84	121.82
C1-C2-C3	121.11(28)	120.36	122.24	120.36
C1-C9-C10	119.96(25)	120.23	120.95	120.23
C1-C9-C8	119.76(26)	119.62	119.10	119.62
C2-C1-C9	118.97(25)	119.04	116.68	119.04
C3-C4-C10	118.71(25)	119.04	116.68	119.04
C4-C3-C2	120.38(26)	120.36	122.24	120.36
C4-C10-C9	120.58(28)	120.23	120.95	120.23
C4-C10-C5	119.68(26)	119.62	119.10	119.62
C5-C6-C7	120.85(29)	120.26	120.19	120.26
C5-C10-C9	119.74(26)	120.14	119.95	120.14
C6-C7-C8	120.00(26)	120.26	120.19	120.26

C6-C5-C10	119.68(26)	119.60	119.86	119.60
C7-C8-C9	119.41(26)	119.60	119.86	119.60
C8-C9-C10	120.29(29)	120.14	119.95	120.14
C1-C2-S1	107.52(20)	107.26	116.54	108.03
C2-S1-S3	105.00(11)	103.21	93.02	102.67
S1-S3-S4	98.99(5)	100.00	NA	NA
S1-S3-S5	NA	NA	NA	105.24
S1-S3-S2	NA	NA	96.93	NA
S2-S4-S5	NA	NA	NA	105.24
S2-S4-S3	99.18(5)	100.00	NA	NA
S3-S5-S4	NA	NA	NA	99.51
C3-S2-S4	103.34(10)	103.21	NA	102.67
C4-C3-S2	109.04(21)	107.26	116.54	108.03
H1-C5-C6	120.18(310)	121.64	121.53	121.64
H1-C5-C10	120.15(278)	118.77	118.61	118.77
H2-C6-C5	119.58(279)	119.80	119.80	119.80
H2-C6-C7	119.55(278)	119.94	120.00	119.64
H3-C7-C6	120.09(309)	119.64	120.00	119.64
H3-C7-C8	119.90(278)	119.80	119.80	119.80
H4-C8-C7	120.27(279)	121.64	121.53	121.64
H4-C8-C9	120.32(308)	118.77	118.61	118.77

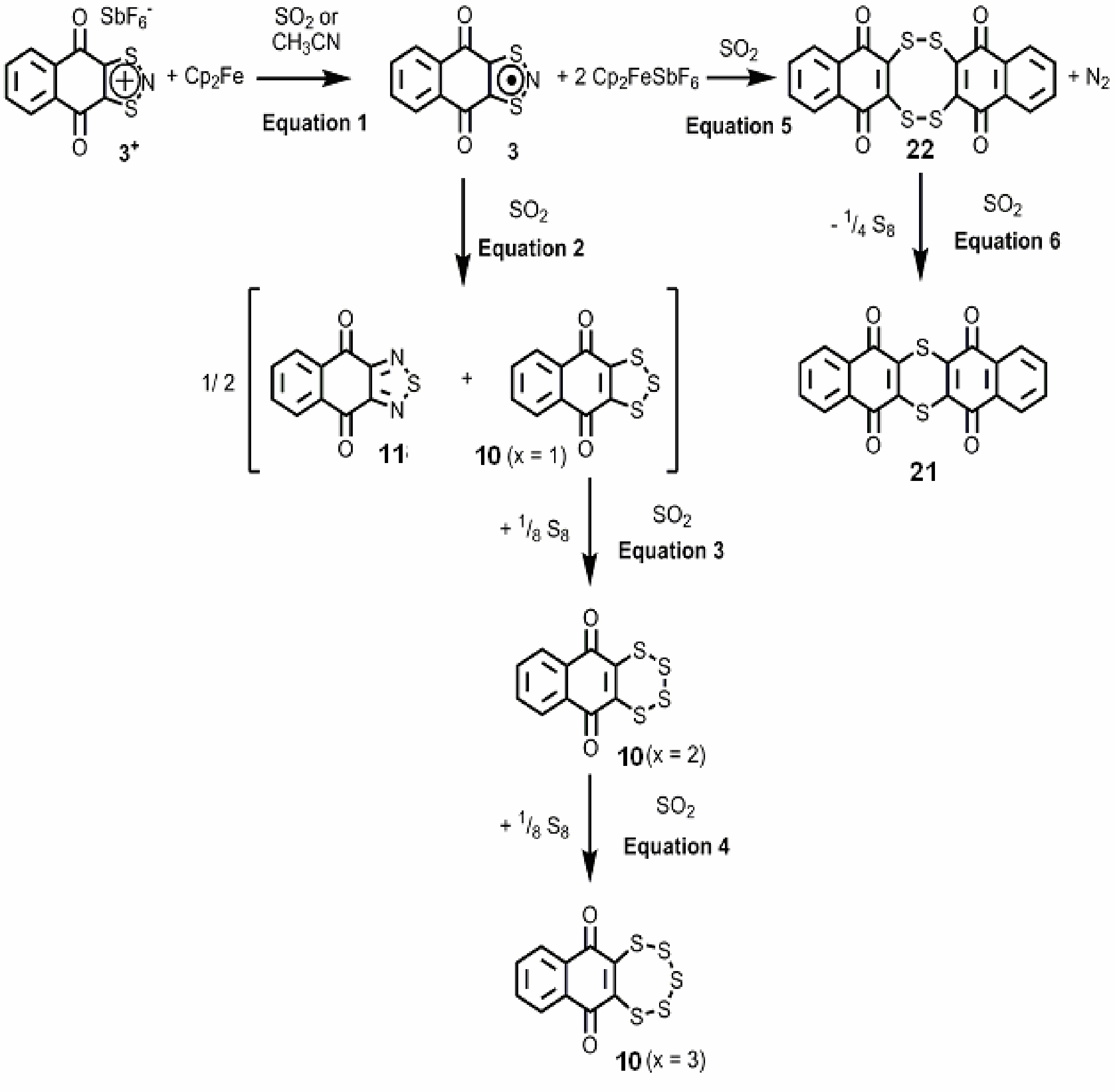

Scheme S4: Gas phase energetics of reduction of 3^+ and thermal decomposition of $3^\bullet$

Table S10: Calculated gas phase and SO_2 solution (PBE0/6-311G(d)) energetics

Compound [a]	Gas Phase (PBE0/6-311G(d))	Solution PBE0/6-311G(d)		Thermal Correction to Gibbs Free Energies [b]	Gas phase Enthalpy (ΔH) [c] kJ mol^{-1}	Solution Enthalpy (ΔH) kJ mol^{-1}	Solution Gibbs free energies (ΔG) kJ mol^{-1}
	Zero point energies (Hartrees)	Enthalpies (Hartrees)	Gibbs free energy (Hartrees)				
1,4-Np ($C_{10}H_6O_2$)	-534.485250	-534.633424	-534.624088	0.100335	NA	NA	NA
12^+	-1384.996612	-1385.226939	-1385.205183	0.103964	-141 Scheme S1, Eqn. 1	-80 Scheme S1, Eqn. 1 [c]	-119 Scheme S1, Eqn. 1 [c]
13^+	-1385.024445	-1385.250987	-1385.22936	0.103299	-73 Scheme S1, Eqn. 2	-63 Scheme S1, Eqn. 2 [c]	-62 Scheme S1, Eqn. 2 [c]
3^+	-1383.827929	-1384.032577	-1384.010829	0.082701	-84 Scheme S1, Eqn. 3	-108 Scheme S1, Eqn. 3 [c]	-105 Scheme S1, Eqn. 3 [c]
$3^•$	-1384.087505	-1384.218805	-1384.195219	0.079946	IP, 7.06 (eV) [e]		
$3^{-••}$ (S = 1 state) [d]	-1384.175138				IP, 2.38 (eV) [e]		
$3^{-••}$ (S = 0 state) [d]	-1384.126581				IP, 1.06 (eV) [e]		
$3^{2-•}$	-1384.084180 [f]				IP, -2.47 (eV) [f]		
11	-1040.76202	-1040.902802	-1040.881624	0.087666	-198 Scheme S3 and S4, Eqn. 2	-217 Scheme S4, Eqn. 2	-240 Scheme S4, Eqn. 2
$8^•$	-1384.112302				-248 Scheme S3, Eqn. 1		
10 (x = 1)	-1727.488347	-1727.617396	-1727.594979	0.077527	-198 Scheme S3 and S4, Eqn. 2	-217 Scheme S4, Eqn. 2	-240 Scheme S4, Eqn. 2
10 (x = 2)	-2125.556725	-2125.687502	-2125.664056	0.078423	- 33 Scheme S3, Eqn. 3		
					-15 Scheme S4, Eqn. 3	-15 Scheme S4, Eqn. 3	-28 Scheme S4, Eqn. 3
10 (x = 3)	-2523.608683	-2523.741717	-2523.716392	0.07648	28 Scheme S4, Eqn. 4	27 Scheme S4, Eqn. 4	23 Scheme S4, Eqn. 4
22	-1862.758552	-2659.11095	-2659.072032	0.178526	-276 Scheme S4, Eqn. 5	-271 Scheme S4, Eqn. 5	-291 Scheme S4, Eqn. 5
21	-2658.856685	-1863.007726	-1862.968614	0.179516	-71 Scheme S4, Eqn. 6	-68 Scheme S4, Eqn. 6	-41 Scheme S4, Eqn. 6
SNS^+	-850.457668	-850.562858	-850.53946	-0.01569			
NH_4^+	-56.789847	-56.953267	-56.97909	0.032369			

S_8	-3184.500057	-3184.51599	-3184.473046	-0.025148			
N_2	-109.423476	-109.429834	-109.423247	-0.012767			

[a] Based on Scheme S1 on pg. 11.

[b] Thermal correction from gas phase calculation applied to solution Gibbs free energies.

[c] Calculated enthalpies and Gibbs free energies are based on both Scheme S1 (See pg. 11) and the following proposed reaction: $SNS^+ + 4\ H^+ + 4\ e^- \rightarrow NH_4^+ + \frac{1}{4}\ S_8$ (c.f. Equation 3 in Scheme S1 on pg. 11).

[d] The singlet-triplet (S-T) gap is calculated as the difference in energy (Hartrees) between [**3**$^{-\bullet\bullet}$ (S=1) - **3**$^{-\bullet\bullet}$ (S=0)]*2625.5 kJ mol^{-1} Hartrees^{-1} = 127.3 kJ mol^{-1}.

[e] The adiabatic ionization potential (IP) in which case the ion has its lowest energy, optimized geometry.

[f] The gas phase (DFT) calculations do not favor the highly charged species (c.f. dianion) and as a result **3**$^{2-\bullet}$ is higher in energy than the related **3**$^{+}$, **3**$^{\bullet}$ and **3**$^{-\bullet\bullet}$ (S =1 and S = 0) and the adiabatic ionization potential with respect to **3**$^{-\bullet\bullet}$ (S = 1) is negative.[17]

Discussion of the thermal decomposition of 3$^{\bullet}$ and the theoretical calculations of 15 (x = 1-3). The proposed thermal decomposition route of **3**$^{\bullet}$ according to Scheme S3 on pg. 42 can be readily envisaged based on the established centrosymmetric dimer of **3**$^{\bullet}$ shown in Figure 7 of the main text. The HT dimer at 296 K shows a weak interaction between the N1-C3' (3.281(5) Å) which is outside the sum of the van der Waals radii (c.f. 2.99 Å), yet provides a mechanism for the formation of **8**$^{\bullet}$ by minimal atomic displacment according to Equation 1 in Scheme S3 on pg. 42. Similar switching of sulfur and nitrogen positions occurs in the photochemical rearrangment of 1,3,2,5-dithiadiazolyl ring to the thermodynamically more favorable 1,2,3,4-dithiadiazolyl isomer [18] which also can occur upon heating in the solid state[19]. The further rearrangment and disproportionation according to Equation 2 and 3 in Scheme S3 on pg. 42 leading to **10** (x = 2) and **11** appears reasonable based on the gas phase calculations (PBE0/6-311G(d)). The highly favorable calculated enthalpies (ΔH) for the decomposition of **3**$^{\bullet}$ according to Equation 1 and 2 in Scheme S3 (See pg. 42) is likely due to the greater bond strength of C-N (290-315 kJ mol^{-1}) and C=N (598 kJ mol^{-1}) versus the two C-S (143 kJ mol^{-1}) bonds and are non-isodesmic reactions.[20] In contrast, Equation 3 in Scheme S3 (See pg. 42) is isodesmic and leads only to a moderate exothermic reaction (c.f. -33 kJ mol^{-1}). The isolation of **10** (x = 2) may occur from the disporportionation of the trithiole, **10** (x = 1) to the ubiquitous **21**, **10** (x = 2) and S_8 according to Scheme S3 (pg. 42). While we recognize **10** (x = 1) and **21** were not directly isolated, the mass spectra of **3**$^{\bullet}$ provides indirect evidence for these and related species containing polysulfane rings (e.g. **10** (x = 0-5); See Figure S25 on pg. 46). The related **10** (x = 1) is only marginally more stable in the gas phase (~ 33 kJ mol^{-1}; PBE0/6-311G(d)) with respect to **10** (x = 2), the ubiquitous **21** and S_8 according to Equation 3 in Scheme S3 (See pg. 42). In the gas phase **10** (x = 3) is less favorable than **10** (x = 2) and 1/8 S_8 by 28 kJ mol^{-1} while **10** (x = 1) is marginally more stable (15 kJ mol^{-1}) than **10** (x = 2) and 1/8 S_8 (See Scheme S4 and Table S10 on pg. 52 and 53, respectively).

We note the DSC of **3**$^{\bullet}$ indicates two modest, irreversible exothermic transitions of 14 and 0.8 kJ mol^{-1} (See Figure S16 on pg. 35), while the TGA does not indicate any significant mass loss over the temperature range of 25-250 ^{o}C (See Figure S15 on pg. 34). Alternatively, the decomposition may occur via an excited state of **3**$^{\bullet}$ (i.e. thermally accessible triplet or semiquinone radical) and a variety of intermediate species.

D. Reaction of 1,4-naphthoquinone and $SNSSbF_6$ in a 1:1 molar ratio in liquid SO_2 expected to give 18^+ according to Equation S3a.

Equation S3a (A summary of Equation 1 and 2 in Scheme S1 on pg. 12):

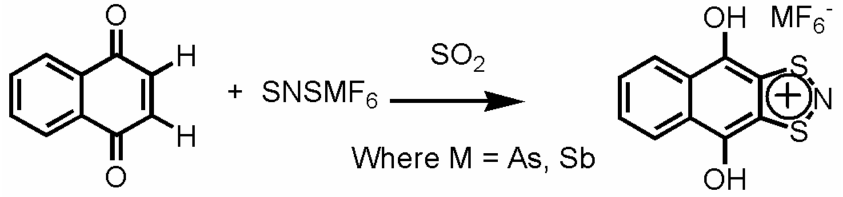

Equation S3b:

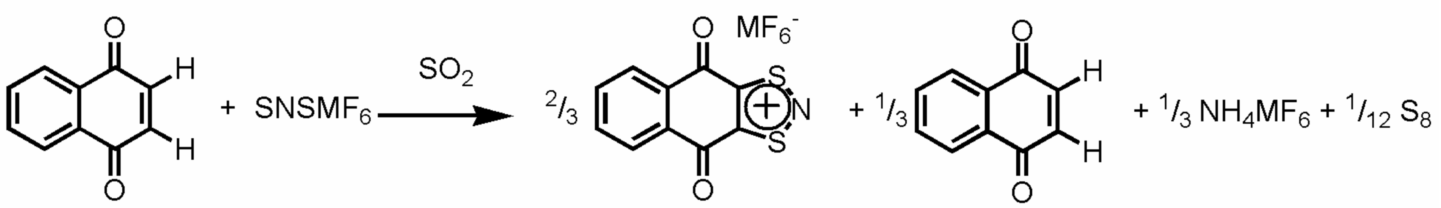

1,4-naphthoquinone (0.872 g, 5.51 mmol) and a stir bar were added to bulb B and $SNSSbF_6$ (1.741g, 5.55 mmol) was added to bulb C of a vessel of Type C (See Figure S1c on pg. 9). SO_2 (18.054 g, ~ 12 ml) was condensed into both bulb B and C and degassed. The two yellow solutions obtained in bulb B and C were mixed in bulb B. A brown solution over a yellow-orange insoluble was obtained after stirring for 1 hr. The more soluble fraction was filtered to bulb A. The volume of the volatiles in bulb A was reduced under dynamic vacuum to 8.934 g (~ 6 ml). Upon cooling to -78 °C a brown solution over a yellow-brown solid was obtained in bulb A. The more soluble fraction was filtered cold to bulb C. SO_2 (~ 3 ml) was condensed backed to bulb A. The yellow-brown solid was washed and the more soluble fraction filtered to bulb C. The washing was repeated (~ 4-6 times) until a bright yellow solid was obtained in bulb A. The volatiles were then condensed to bulb B. A pale yellow-brown solution over a yellow-orange solid was obtained in bulb B and the more soluble fraction decanted to bulb C. The volatiles were condensed back to bulb B and the yellow-orange solid washed and the more soluble fraction decanted to bulb C. The washing was repeated twice more to give a white solid in bulb B. The volatiles were removed and dark brown solid was obtained in bulb C. The bright yellow solid (0.989 g, 57% yield of **3**SbF_6 based on $SNSSbF_6$ and Equation S3b) in bulb A, white solid (0.042 g) in bulb B and brown solid (1.244 g) in bulb C was collected in the drybox. The IR (See Figure S28 on pg. 57) of the bright yellow solid (bulb A) was obtained as a Nujol mull on CsI plates and was consistent with **3**SbF_6. The calculated and experimental frequencies and intensities are compiled and compared in Table S2 on pg. 23.

The IR of the white solid (bulb B) was obtained as a Nujol mull on KBr and was consistent with NH_4SbF_6 (See Figure S29 on pg. 57). The EDX microanalysis (See Figure S30 on pg. 58) of the white solid (bulb B) was consistent with NH_4SbF_6 and S_8 assuming the reaction proceeded according to Equation S3b on pg. 55.

Multinuclear NMR: In a similar reaction, 1,4-naphthoquinone (0.369 g, 2.33 mmol) and $SNSSbF_6$ (0.964 g, 3.07 mmol) were added to bulb A of a vessel of Type A incorporating a 10 mm NMR tube directly attached via a ¼ inch Pyrex tube. SO_2 (8.547 g, ~ 6 ml) was condensed into bulb A. The reddish-brown solution obtained on warming was filtered into the attached 10 mm NMR and flame sealed at -196 °C. The NMR tube was warmed to ambient temperature and the multinuclear {^{1}H, ^{13}C, ^{14}N} NMR followed *in situ* over time (1 week). See Table S1 and S11 on pg. 13 and 63 for comparison of calculated and experimental ^{1}H, ^{13}C, ^{14}N-NMR chemical shifts and Figure S36-S38 on pg.6-69 for actual NMR spectra and tentative assignments.

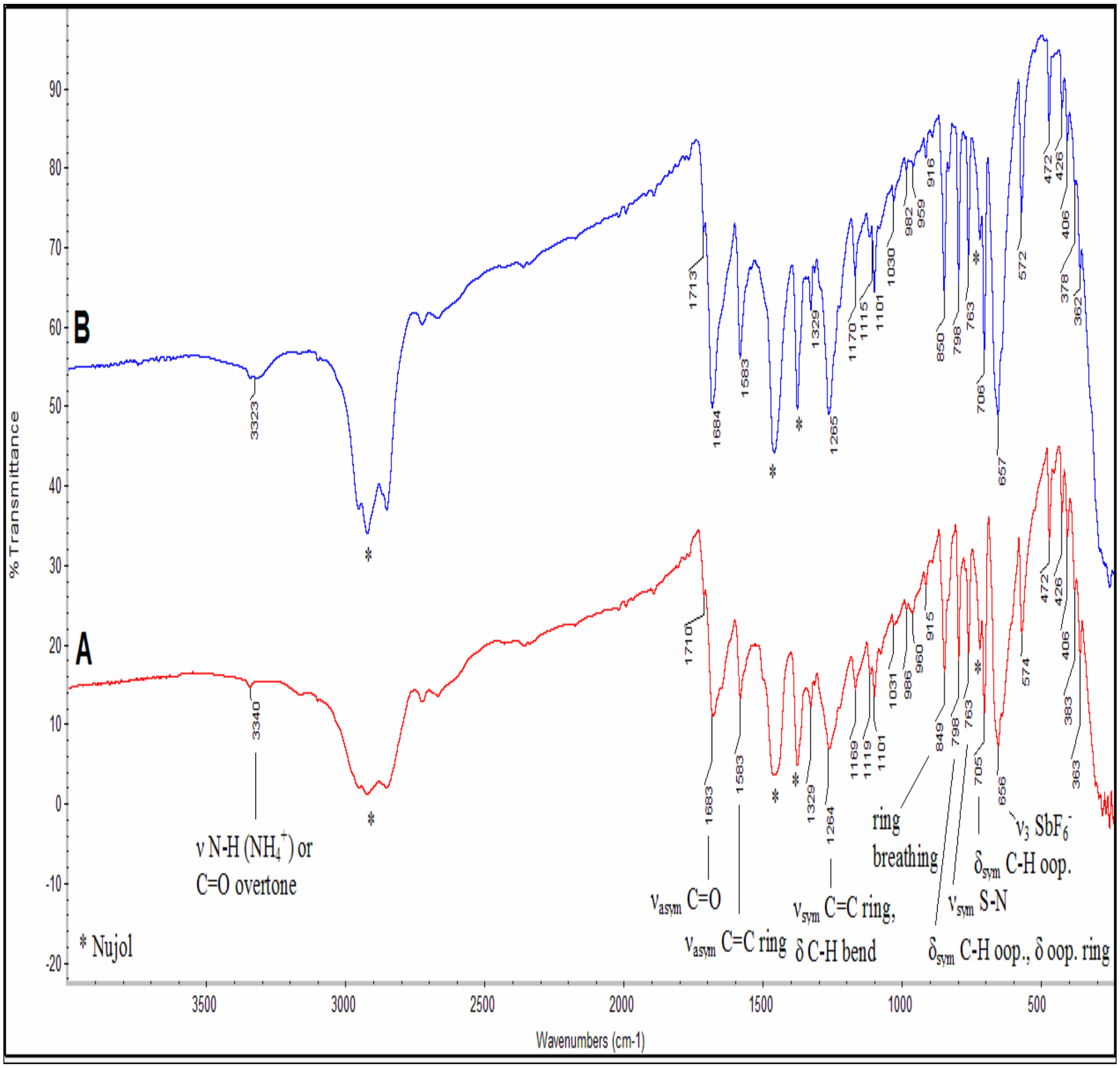

Figure S28: FT-IR spectra of a) **3**SbF_6 prepared from a 1:1 molar ratio of 1,4-naphthoquinone and $SNSSbF_6$ assuming reaction proceeded according to Equation S3b on pg. 55 and b) purified **3**SbF_6 prepared according to Equation 1-3 in Scheme S1 (See pg. 11) as Nujol mull on KBr plates (32 scans, 2 cm^{-1} resolution). See Table S2 on pg. 22 for comparison of experimental and calculated IR frequencies and tentative assignments. Note the assignments are tentative and based on visualization of the vibrational modes in *ChemCraft*[8]: ν = stretch, δ = bending, asym. = asymmetric and sym = symmetric, opp = out-of-plane, inp = in-plane.

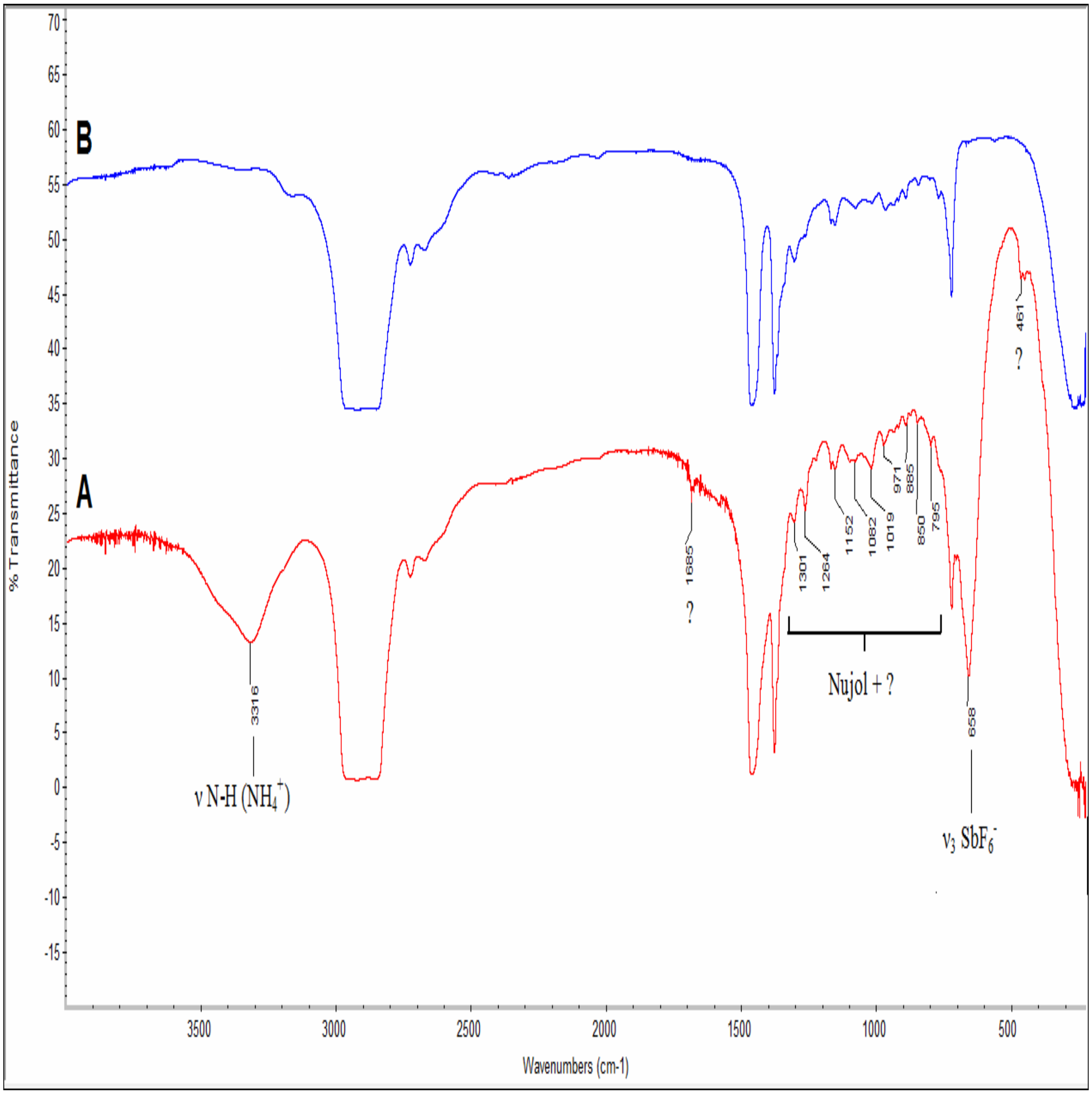

Figure S29: FT-IR spectra of a) white insoluble solid (c.f. NH_4SbF_6 and S_8) prepared from a 1:1 molar ratio of 1,4-naphthoquinone and $SNSSbF_6$ assuming reaction proceeded according to Equation S3b on pg. 55 as Nujol mull on KBr plates and b) Nujol on KBr plates (32 scans, 2 cm^{-1} resolution). Note the tentative assignments based on visualization of the vibrational modes in *ChemCraft*[8]: ν = stretch, δ = bending, asym. = asymmetric and sym = symmetric, opp = out-of-plane, inp = in-plane.

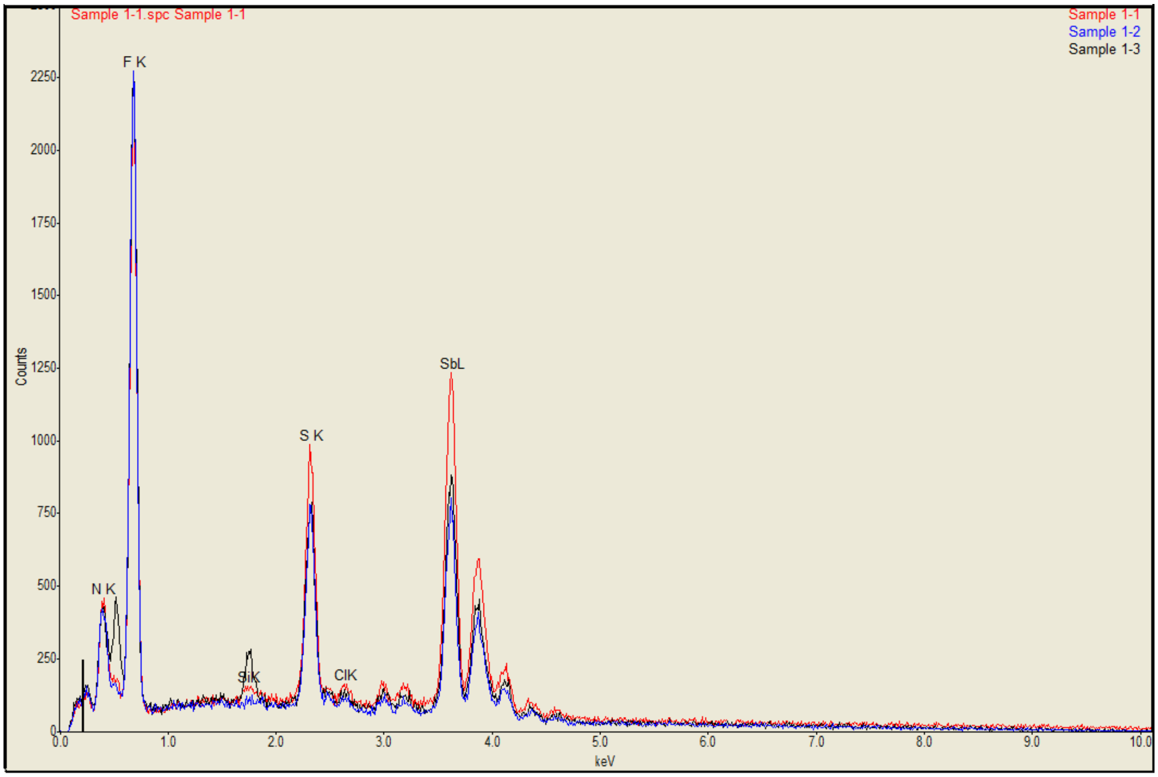

Figure S30: The stacked plot of three separate qualitative EDX microanalysis spectra of the insoluble white solid prepared from a 1:1 molar ratio of 1,4-naphthoquinone and $SNSSbF_6$ assuming reaction proceeded according to Equation S3b on pg. 55.

E. *In situ* multinuclear NMR of the reaction of 1,4-naphthoquinone and $SNSAsF_6$ in a 1:1 molar ratio in liquid SO_2 according to Equation S3a

*Synthesis.*1,4-naphthoquinone (0.161 g, 1.02 mmol), $SNSAsF_6$ (0.331 g, 1.24 mmol) and a stir bar were added to bulb A of a vessel of Type A (Figure S1a on pg. 9) incorporating a 10 mm NMR tube attached via a J.Young o-ringette valve and a Pyrex adaptor tube closed by a J. Young valve. SO_2 (6.577 g, ~ 5 ml) was condensed into bulb A producing a reddish-brown solution upon warming to ambient temperature. A small volume of the solution was poured into the attached NMR tube. The remaining solution was stirred at ambient temperature. A brown solution over a small amount of white insoluble was obtained after stirring for 8 hrs. The more soluble fraction was filtered to bulb B. A small volume of volatiles was condensed back to bulb A. The more soluble fraction was filtered to bulb B. The soluble fraction in bulb B was concentrated by slow evaporation of the volatiles to bulb A over a temperature gradient of 0-5 ^{o}C. The volatiles were removed in small aliquots under dynamic vacuum. The slow removal of the volatiles led to a mixture of beige-brown solid and bright red crystals in bulb B. The solid mixture (0.362 g, 74 % recovered based on $SNSAsF_6$ and Equation S3b on pg. 55) in bulb B and 10 mm NMR tube (See *Multinuclear NMR* below) and white insoluble (0.092 g; 48 % yield of NH_4SbF_6 and S_8 based on $SNSAsF_6$ and Equation S3b on pg. 55) in bulb A were recovered. Suitable crystals were mechanically separated from the solid and investigated

by X-ray crystallography and shown to be $(\mathbf{3}AsF_6)_2{\bullet}SO_2$ as given in Figure 3b of the main text. See also Table 1 in the main text for full crystallographic details.
The IR (See Figure S34 on pg. 64) of the solid mixture in bulb B was obtained as a Nujol mull on KBr plates and was consistent with $\mathbf{3}AsF_6$ based on comparison of the experimental and calculated IR frequencies and intensities given in Table S3 on pg. 24. See Figure S31-S33 on pg. 59-61 for actual NMR spectra.

Multinuclear NMR. The multinuclear $\{^1H, ^{13}C, ^{14}N\}$ NMR was followed *in situ* for 24 hours (See Figure S31-S33 on pg. 59-61). The initial solution was reddish-brown over a small quantity of white insoluble. After 24 hours a brown solution was obtained. The NMR tube was attached directly to the vacuum line via Swagelok compress fittings[21] and a Wilmad[22] Pyrex adaptor (6 mm O.D.) and a and the volatiles removed under dynamic vacuum. The solid was collected in the drybox and combined with the solid mixture from bulb B.

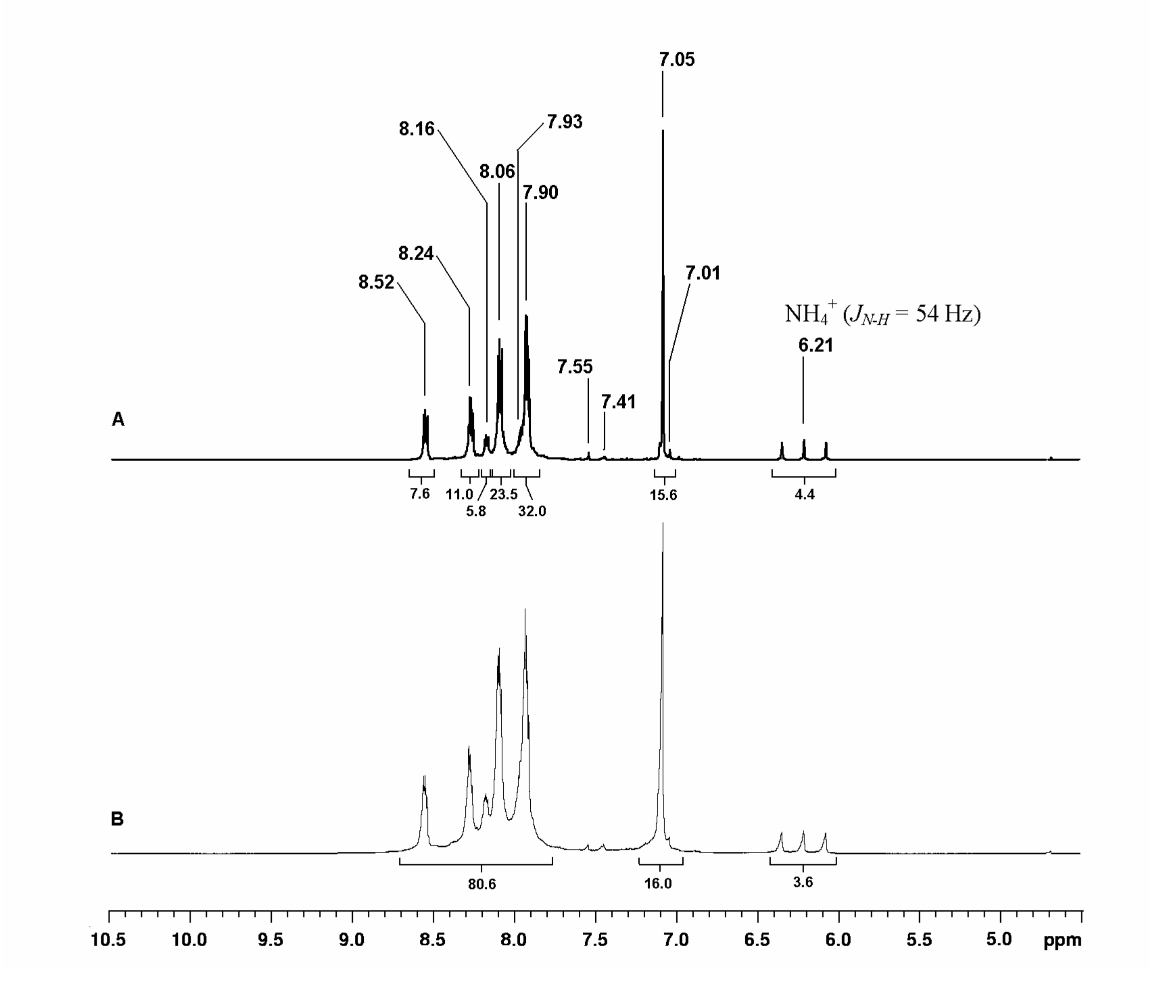

Figure S31: ^1H-NMR spectra of reaction of 1,4-naphthoquinone and $SNSAsF_6$ in 1:1 molar ratio after a) ~ 30 min. (initial) and b) after 24 hours at RT according to Equation S3a (See Table S1 and S11 on pg. 13 and 63 for comparison of experimental and calculated NMR tensors).

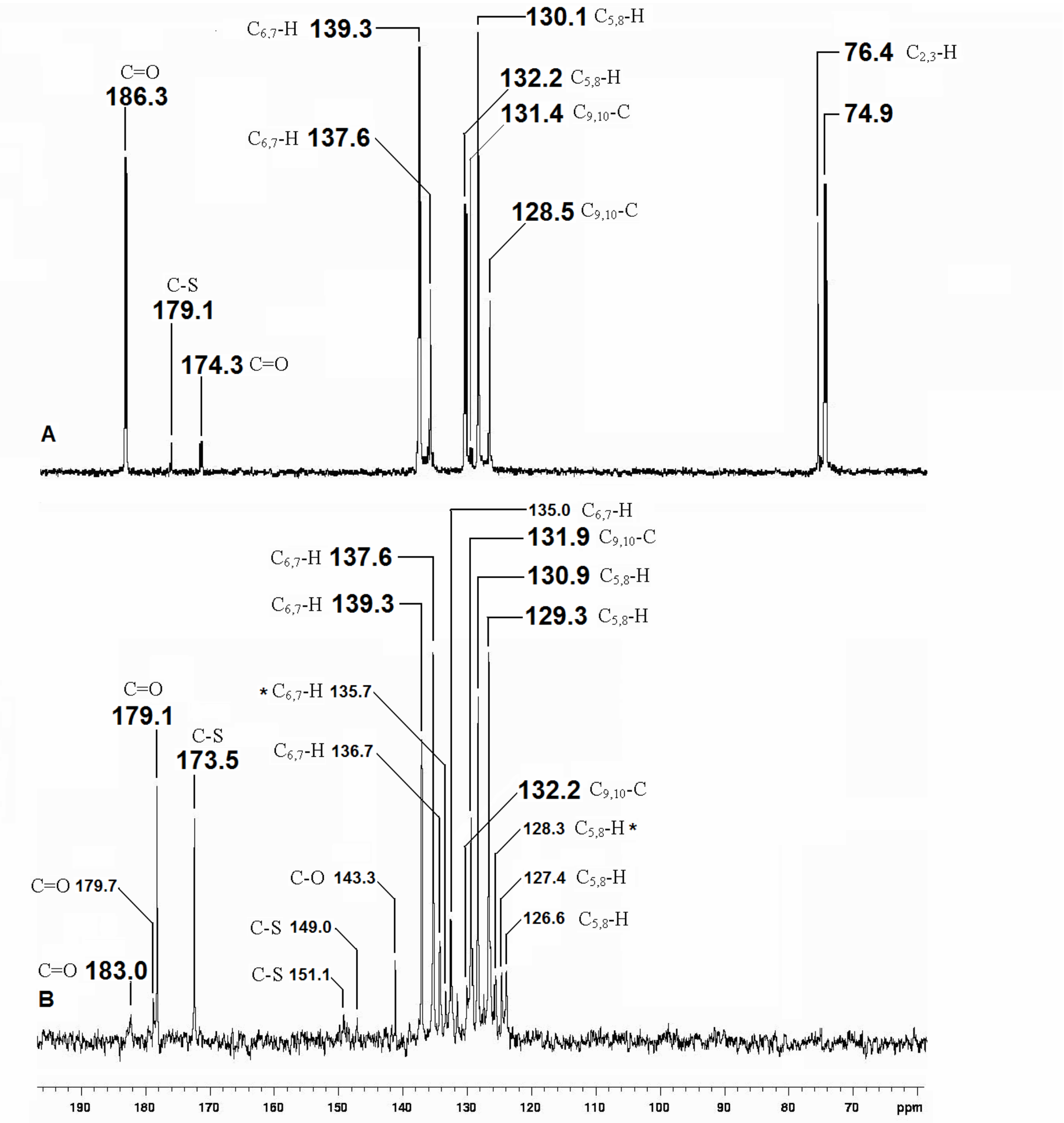

Figure S32: ^{13}C-NMR spectra of reaction of 1,4-naphthoquinone and $SNSAsF_6$ in 1:1 molar ratio after a) ~ 40 min. (initial) and b) after 24 hours at RT according to Equation S3a (See Table S1 and S11 on pg. 13 and 63 for comparison of experimental and calculated NMR tensors).

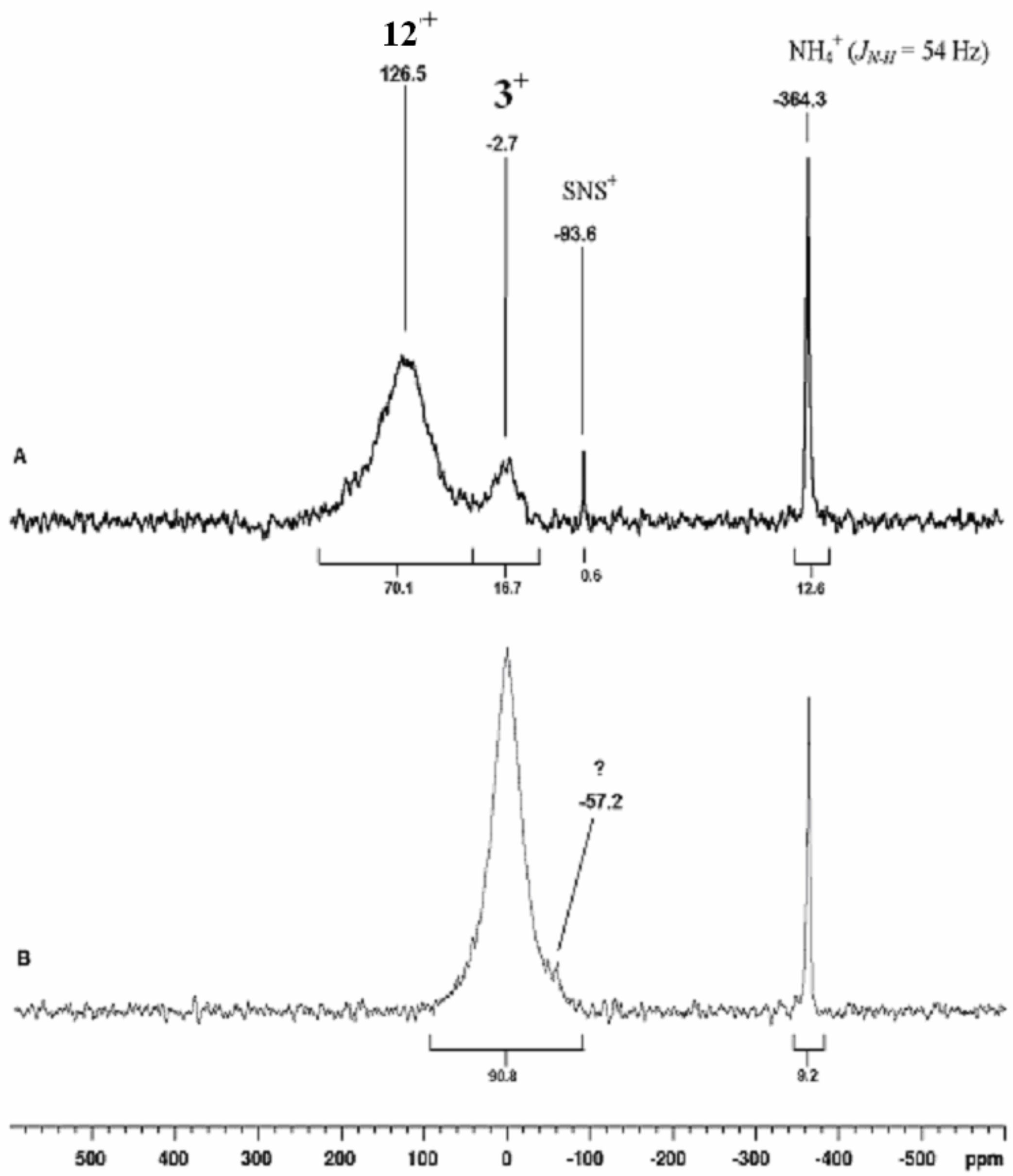

Figure S33: ^{14}N-NMR spectra of reaction of 1,4-naphthoquinone and $SNSAsF_6$ in 1:1 molar ratio after a) ~ 2 hours (initial) and b) after 24 hours at RT according to Equation S3a (See Table S1 and S11 on pg 13 and 63 for comparison of experimental and calculated NMR tensors).

Discussion: The reaction of $SNSAsF_6$ with 1,4-naphthoquinone in a 1:1 molar ratio in liquid SO_2 was followed by *in situ* multinuclear {^{1}H, ^{13}C, ^{14}N} NMR for 2 days (See Figure S31-S33 on pg. 59 - 61). Initially we believed the reaction would proceed according to Equation S3a (See also Equation 1 and 2 in Scheme S1 on pg. 11) leading to **18**AsF_6. The analogous reaction of $SNSAsF_6$ and 1,4-benzoquinone in a 1:1 molar ratio in liquid SO_2 leads to **2**AsF_6.[23] The initial ^{1}H, ^{13}C and ^{14}N-NMR were consistent with the formation of the intermediate $\mathbf{12}^+$ according to Equation 1 in Scheme S1 (See Table S1 on pg. 13). The ^{13}C-NMR spectrum at -70 °C displayed a singlet resonances at δ 186.3 and a doublet centered at δ 75.5 (J_{CH} 151 Hz) which are assigned to the carbonyl and bridge-head carbons of $\mathbf{12}^+$ (See Figure S32a on pg. 60).

This is consistent with the analogous dithiazolidine-like intermediate obtained from the cycloaddition of SNS^+ with olefins[1] and observed by ^{13}C-NMR resonances of δ 186 and 74.6 in the reaction of 1,4-benzoquinone with $SNSAsF_6$ in a 1:1 molar ratio.[23] Resonances attributable to **13**$^+$ were not observed. However, five resonances at δ 179.1, 174.3, 137.6, 132.2 and 131.4 were assigned to **3**$^+$. (See Figure S32b on pg. 60). The assignments were also consistent with the predicted ^{13}C-NMR (See Table S1 on pg 13 for tentative assignments). The initial ^{14}N-NMR at -70 °C (See Figure S33a on pg. 61) also supports the conclusions from the observed ^{13}C-NMR spectrum. The resonances in the initial ^{14}N-NMR at δ 126.5 ($\nu_{1/2}$ = 1246 Hz) and -2.7 ($\nu_{1/2}$ = 622 Hz) are consistent with the dithiazolidine-like intermediate **12**$^+$ and the 1,3,2-dithiazolylium **3**$^+$, respectively (See Figure S32a on pg. 60).[1] The two remaining resonances δ -93.6 ($\nu_{1/2}$ = 8 Hz) and -364.3 are assigned to SNS^+ and NH_4^+. After 1 day the ^{14}N-NMR spectrum (25 °C) only displays resonances at δ 3.1 ($\nu_{1/2}$ = 608 Hz) and δ 363.6 assigned to **3**$^+$ and NH_4^+ (See Figure S33b on pg. 61). However, the ^{13}C-NMR (25 °C) after 1 day is more complex, while the ^{1}H-NMR (25 °C) appears to contain at least three AA'BB' spin systems (See Figure S31 on pg. 59). We tentatively assign several resonances in the ^{13}C-NMR to **10** (x = 2) and **13**$^+$ based on the calculated NMR tensors (See Table S1 and S11 on pg. 13 and 63). The sensitivity of the ^{1}H-NMR chemical shift to the chemical environment (c.f. presence of labile species (e.g. H^+ in hydroquinones (c.f. **13**$^+$) and NH_4^+) and paramagnetic species from redox processes (e.g. oxidative dehydrogenation)) leads to complex ^{1}H-NMR spectra and shifts in peak positions (See Figure S36 on pg. 67) therefore ^{1}H-NMR assignments are tentatitive.

Table S11: Comparison of calculated (PBE0/6-311G(d)) and experimental ^{1}H, ^{13}C and ^{14}N-NMR tensors of proposed intermediates (Scheme S3 and S4 on pg. 42 and 52) **10**, **11**, **21** and **22**; For actual spectra see Figures S2-S4 on pg 14-16 and Figures S31-S33 on pg. 59-61.

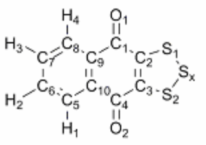

10

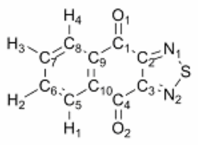

11

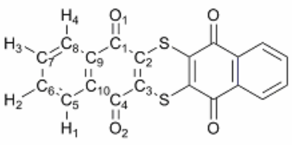

21

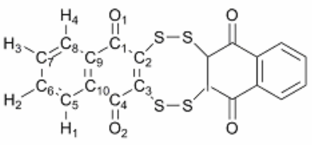

22

Molecule	**10 (x = 1)**		**10 (x = 2)**		**10 (x = 3)**		**11**		**21**		**22**	
Symmetry	$C_{2}v$		C_2		~C_2		$C_{2}v$		$D_{2}h$		C_2	
	Calc.	Exp.[a]	Calc.	Exp.[a]	Calc.	Exp.[a]	Calc.	Exp.[a]	Calc.	Exp.[a]	Calc.	Exp.[a]
^{13}C-NMR												
C1	176.9	179.2	178.1	183.0	181.1	183.5	175.4	-[b]	177.1	-[b]	183.0	-[b]
C2	154.2	151.2	148.7	149.1	147.0	-[b]	155.8	-[b]	143.0	-[b]	170.6	-[b]
C3	154.2	151.2	148.7	149.1	147.0	-[b]	155.8	-[b]	143.0	-[b]	141.1	-[b]
C4	176.9	179.2	178.1	183.0	181.2	183.5	175.4	-[b]	177.1	-[b]	176.0	-[b]
C5	128.6	127.4	129.3	131.0	128.6	-[b]	130.3	-[b]	128.5	-[b]	129.4	-[b]
C6	135.0	-[b]	135.4	-[b]	135.2	-[b]	135.7	-[b]	134.9	-[b]	135.9	-[b]
C7	135.0	-[b]	135.4	-[b]	135.2	-[b]	135.7	-[b]	134.9	-[b]	134.1	-[b]
C8	128.6	127.4	129.3	131.0	128.6	-[b]	130.3	-[b]	128.5	-[b]	128.5	-[b]
C9	131.7	-[b]	130.0	-[b]	130.9	-[b]	134.0	-[b]	130.0	-[b]	130.3	-[b]
C10	131.7	-[b]	130.0	-[b]	130.9	-[b]	134.0	-[b]	130.0	-[b]	131.9	-[b]
^{1}H-NMR												
H1	8.20	-[b]	8.36	-[b]	8.23	-[b]	8.63	-[b]	8.24	-[b]	8.29	-[b]
H2	7.81	-[b]	7.85	-[b]	7.80	-[b]	7.99	-[b]	7.80	-[b]	7.81	-[b]
H3	7.81	-[b]	7.85	-[b]	7.80	-[b]	7.99	-[b]	7.80	-[b]	7.74	-[b]
H4	8.20	-[b]	8.36	-[b]	8.23	-[b]	8.63	-[b]	8.24	-[b]	8.22	-[b]
^{14}N-NMR												
N1	NA	NA	NA	NA	NA	NA	-52.2	-57	NA	NA	NA	NA
N2	NA	NA	NA	NA	NA	NA	-52.2	-57	NA	NA	NA	NA

[a] The experimental assignments are based on the reaction of 1,4-naphthoquinone and $SNSSbF_6$ in 1:1, 2:1 and 1:2 molar ratios respectively and the comparison of the multinuclear NMR spectra given in Figures S34 - S36 on pg. 64-66. Assignments are tentative unless otherwise stated.

[b] Because of the low concentration of species or similarity in chemical shift in SO_2 solution the individual chemical shifts were not observed or resolved under these conditions and therefore not assigned.

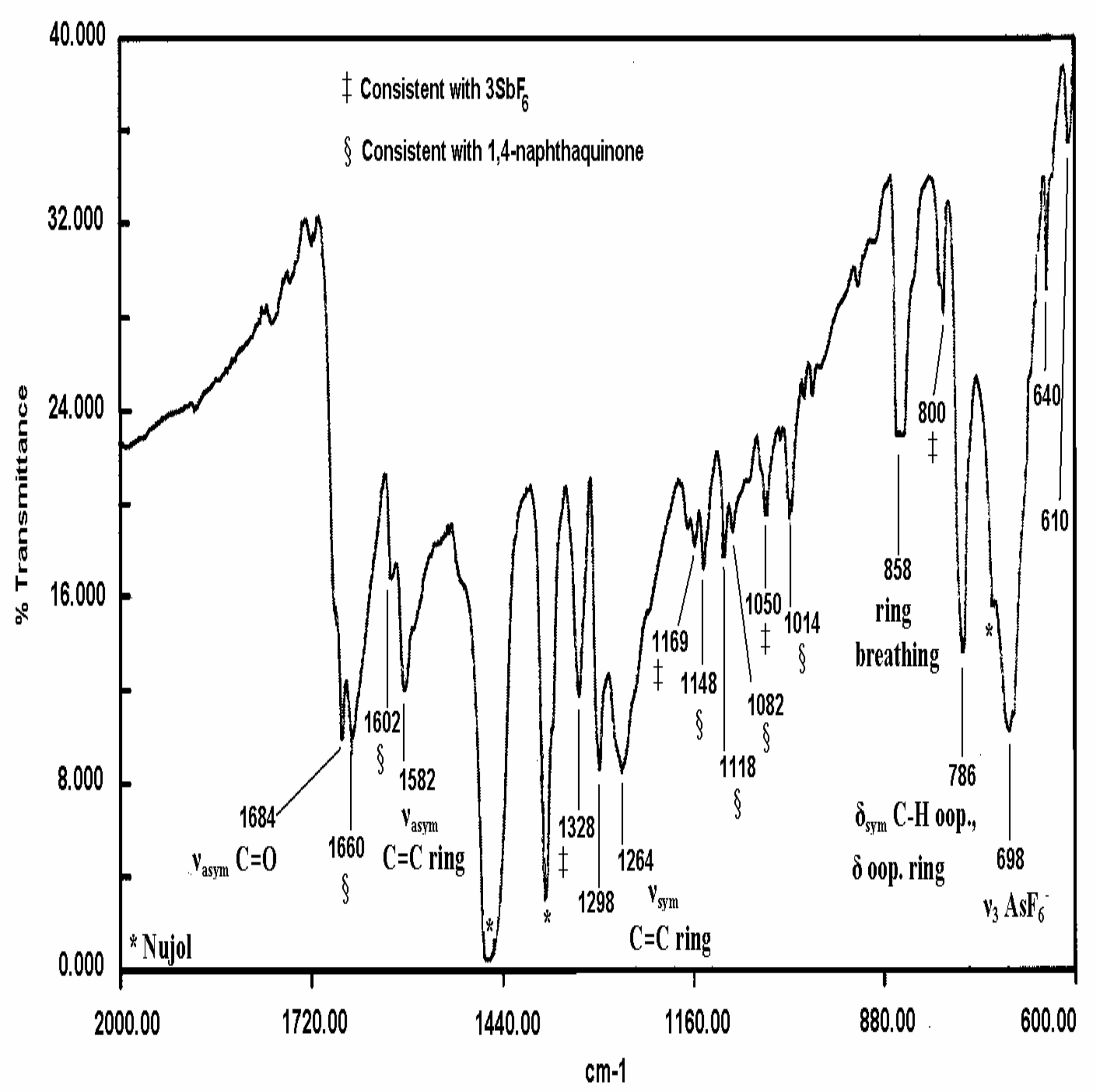

Figure S34: FT-IR spectrum of **3**AsF$_6$ prepared according to Equation S3b on pg. 55.[24]

F. Reaction of 1,4-naphthoquinone and $SNSSbF_6$ in a 2:1 molar ratio in liquid SO_2 assuming reaction proceeded according to Equation S4a.[25]

Equation S4a:

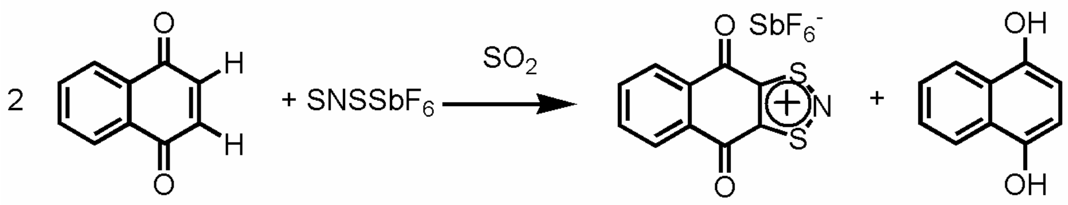

Equation S4b:

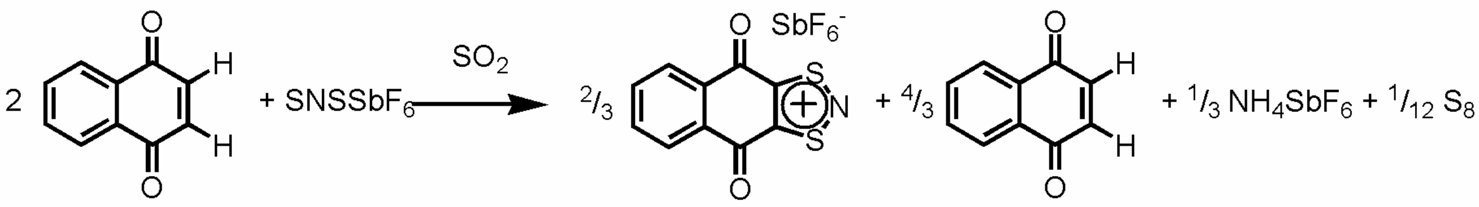

1,4-naphthoquinone (1.488 g, 9.41 mmol) and $SNSSbF_6$ (1.608 g, 5.12 mmol) were added to bulb B of a vessel of Type C. SO_2 (5.681 g, ~ 4 ml) was condensed into bulb B and degassed. A yellow-brown solution was obtained on warming to ambient temperature. After stirring for 4 days at ambient temperature a brown solution over a white insoluble solid was obtained. The more soluble fraction was filtered to bulb A. The volatiles were slowly condensed back to bulb B over a temperature gradient of 0-5 ^{o}C providing a solid mixture of brown solid and yellow crystals in bulb A. The volatiles were removed under dynamic vacuum. CH_2Cl_2 (2.687 g, ~ 2 ml) was condensed into bulb A. Upon warming to ambient temperature a yellow solution over a yellow-brown solid was obtained. The more soluble fraction was filtered to bulb C. The volatiles were condensed back to bulb A. The yellow-brown solid was washed and the more soluble yellow fraction filtered to bulb C. The washing of the yellow-brown solid in bulb A was repeated 6 more times and the more soluble yellow fractions collected in bulb C. The volatiles were condensed into bulb A. SO_2 (0.280 g, ~ 0.2 ml) was condensed into bulb A to give a 10:1 (v/v) mixture of CH_2Cl_2 and SO_2. Upon warming to ambient temperature a brown solution over a yellow-brown solid was obtained. The brown soluble fraction was filtered to bulb C. The volatiles were condensed back to bulb A and the washing of the yellow brown solid and filtration of the more soluble brown fraction to bulb C was repeated three times leading to a yellow solid in bulb A. The volatiles were removed under dynamic vacuum. The solids were collected in the drybox. The yellow solid was collected (0.385 g, 0.819 mmol of **3**SbF_6 in 24 % yield based on $SNSSbF_6$ according to Equation S4b on pg. 65) in bulb A. The IR as a Nujol mull on KBr plates was obtained and was consistent with **3**SbF_6 (See Figure S35 on pg. 66). A white insoluble solid (0.079 g; 15 % yield of NH_4SbF_6 and S_8 based on $SNSSbF_6$ and Equation S4b on pg. 65) was collected in bulb B and the brown solid (2.809 g) in bulb C.

Multinuclear NMR: In a similar reaction, 1,4-naphthoquinone (1.724 g, 10.90 mmol) and $SNSSbF_6$ (1.712 g, 5.45 mmol) were added to bulb A of a vessel of Type A incorporating a 10 mm NMR tube directly attached via a ¼ inch Pyrex tube. SO_2 (6.022 g, ~ 4 ml) was condensed into bulb A. The yellow-brown solution obtained on warming was filtered into the attached 10 mm NMR and flame sealed at -196 °C. The NMR tube was warmed to ambient temperature and the multinuclear {^{1}H, ^{13}C, ^{14}N} NMR followed *in situ* over time (1 week). See Table S1 and S11 for comparison of calculated and experimental ^{1}H, ^{13}C, ^{14}N-NMR chemical shifts and Figure S36-S38 on pg. 67-69 for actual NMR spectra and tentative assignments.

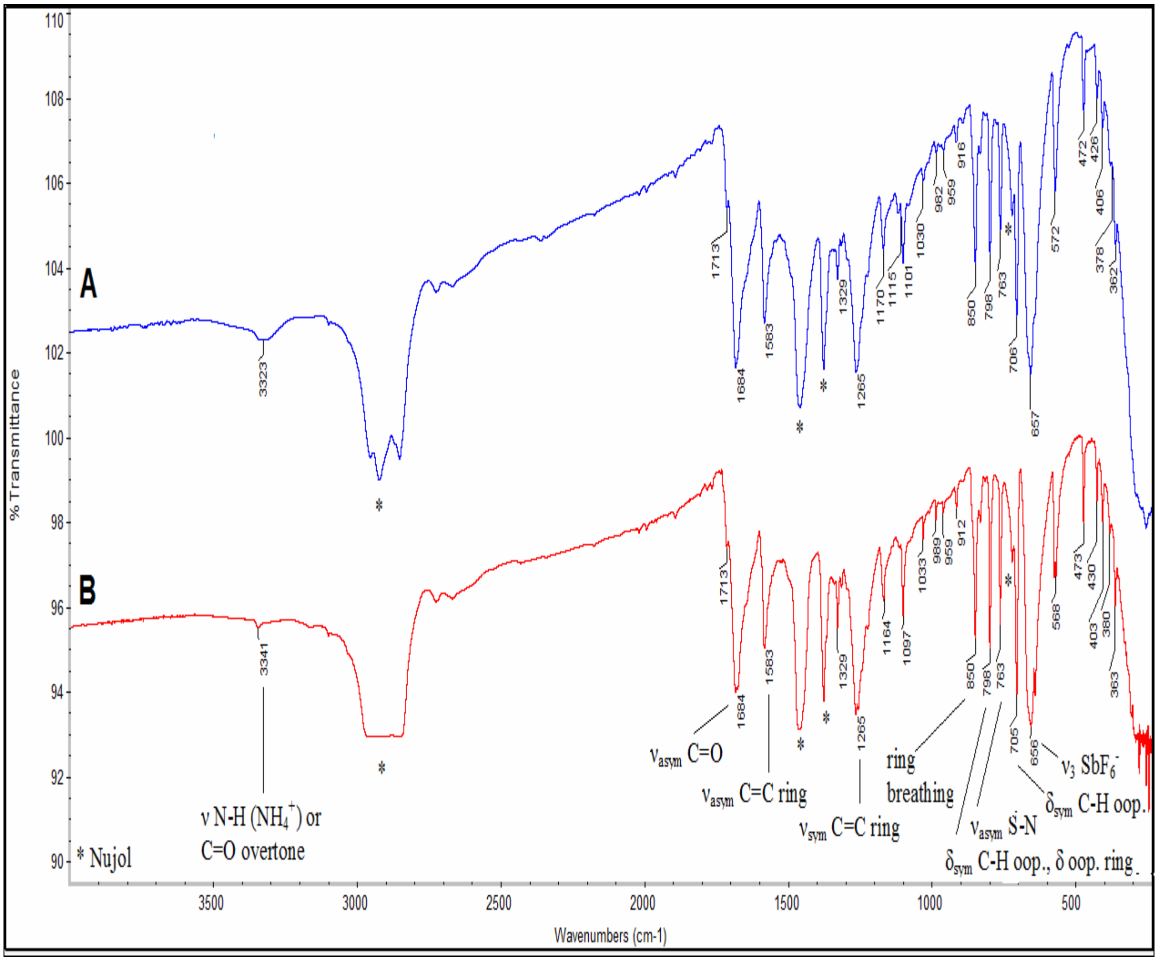

Figure S35: FT-IR spectra of a) **3**SbF_6 prepared from a 2:1 ratio of 1,4-naphthoquinone and $SNSSbF_6$ assuming reaction proceeded according to Equation S4b on pg. 65 as a Nujol mull on KBr plates and b) **3**SbF_6 prepared according to Equation 1-3 in Scheme S1 on pg. 11 as a Nujol mull on KBr plates. See Table S2 on pg 22 for comparison of experimental and calculated IR frequencies and tentative assignments. Note the assignments are tentative and based on visualization of the vibrational modes in *ChemCraft*[8]: ν = stretch, δ = bending, asym. = asymmetric and sym = symmetric, opp = out-of-plane, inp = in-plane.

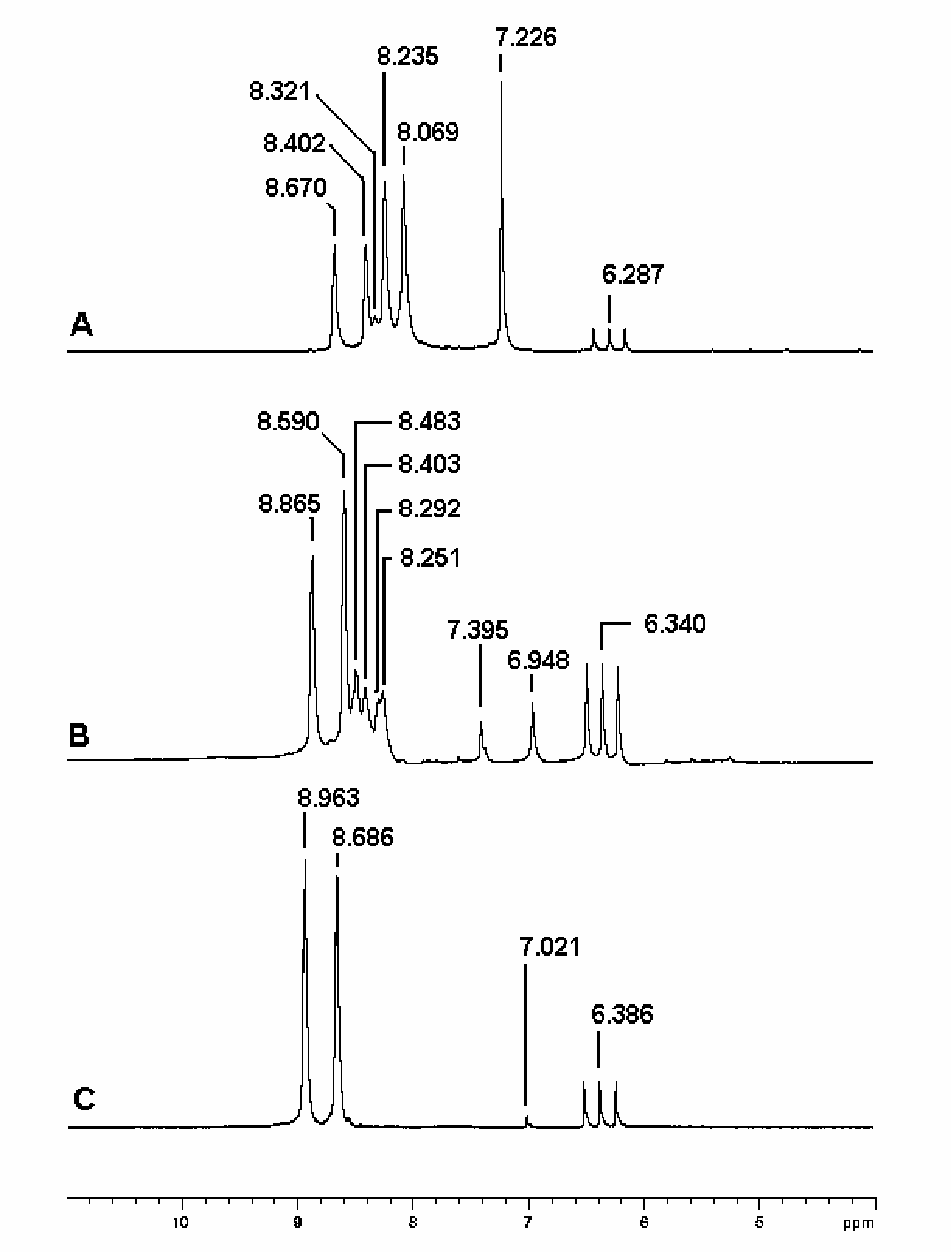

Figure S36: Comparison of the ^{1}H-NMR spectra of reaction of 1,4-naphthoquinone and $SNSSbF_6$ in liquid SO_2 of a) 1:1 molar ratio b) 2:1 molar ratio and c) 1:2 molar ratio after 1 week.

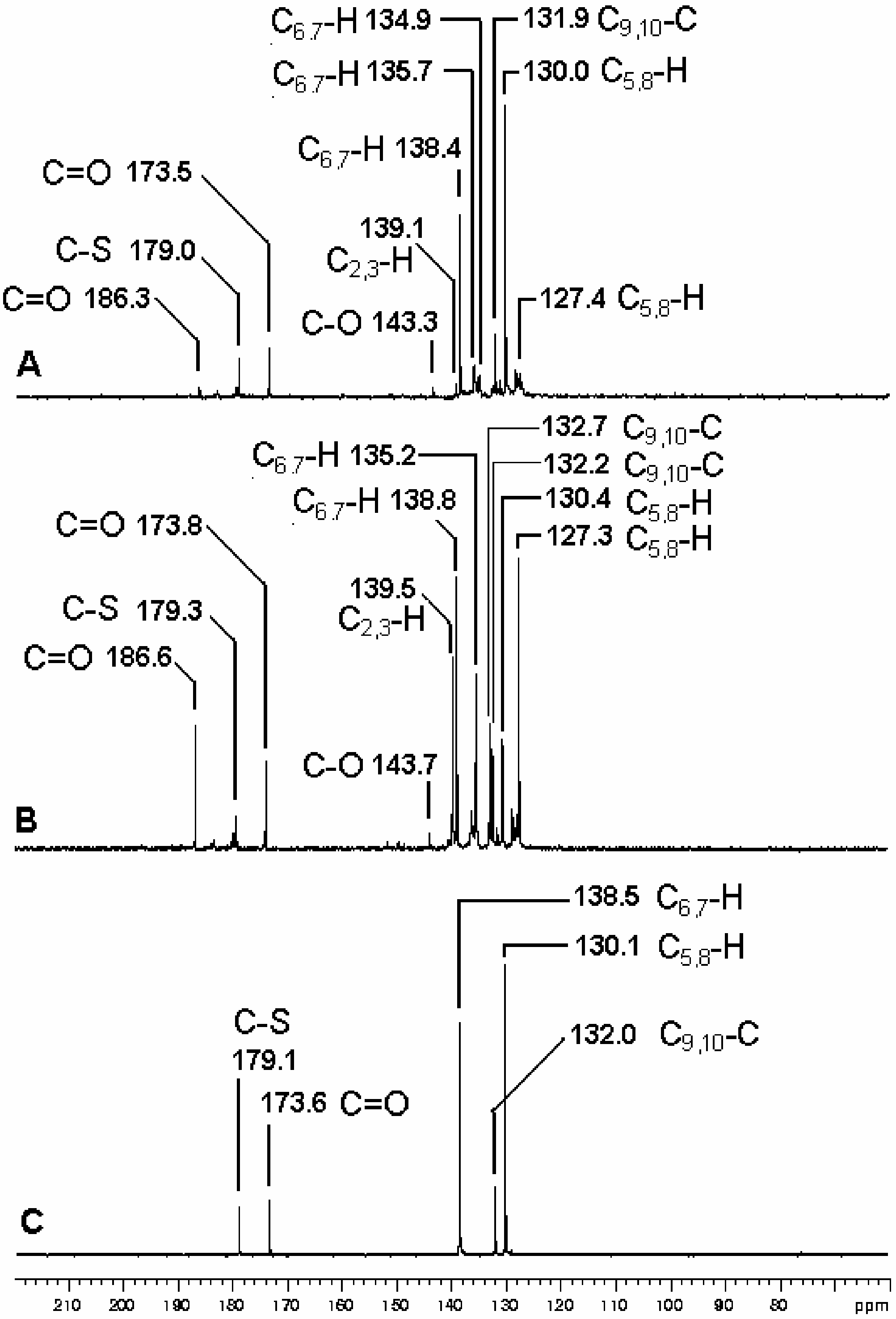

Figure S37: Comparison of the ^{13}C-NMR spectra of reaction of 1,4-naphthoquinone and $SNSSbF_6$ in liquid SO_2 of a) 1:1 molar ratio b) 2:1 molar ratio and c) 1:2 molar ratio after 1 week.

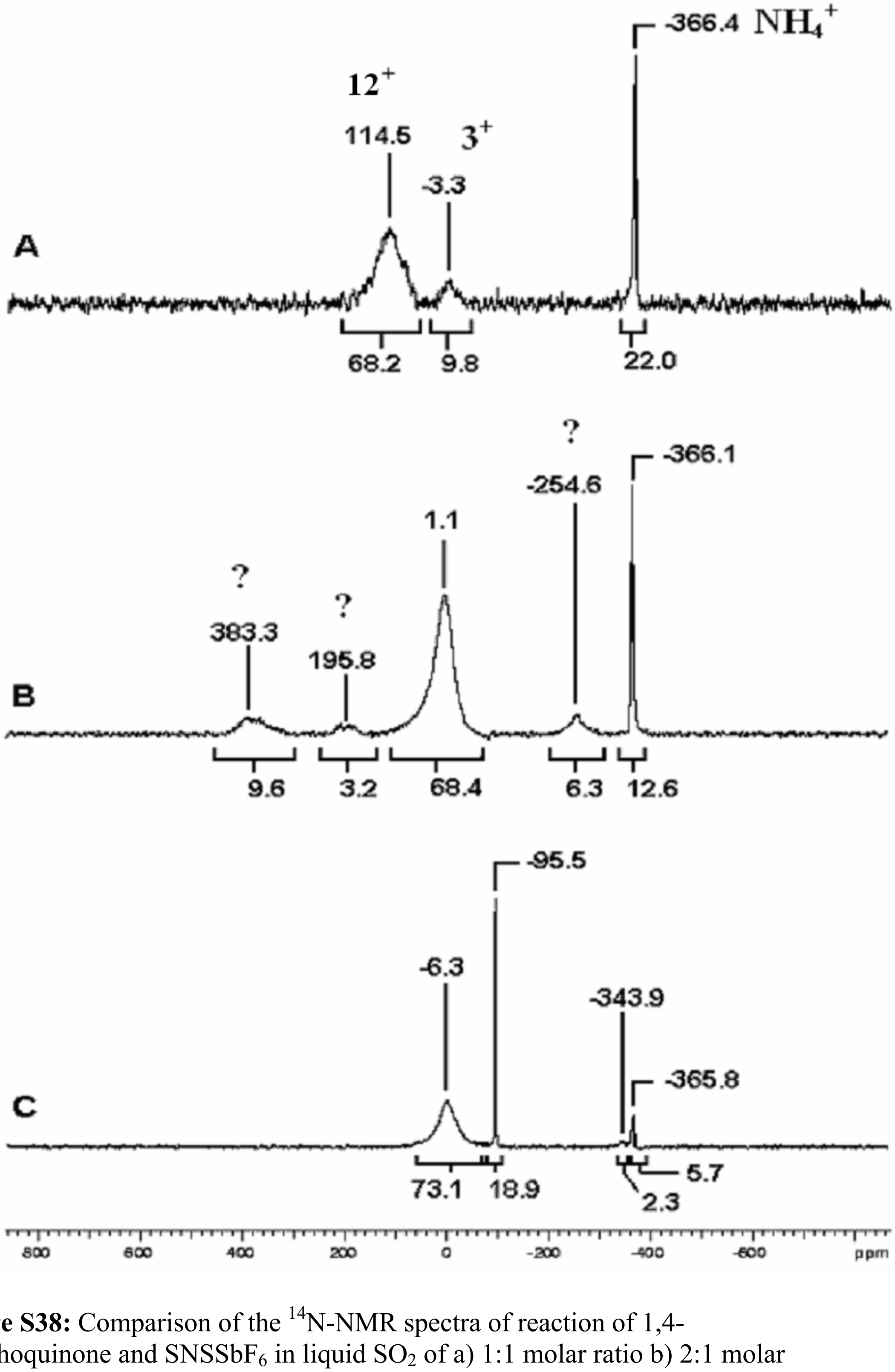

Figure S38: Comparison of the ^{14}N-NMR spectra of reaction of 1,4-naphthoquinone and $SNSSbF_6$ in liquid SO_2 of a) 1:1 molar ratio b) 2:1 molar ratio and c) 1:2 molar ratio after 1 week.

G. Reduction of 3SbF_6 with triphenylantimony ($SbPh_3$) and NBu_4Cl in liquid SO_2 according to Equation S5.

Equation S5 (Graphic depiction of Equation 5 in main text):

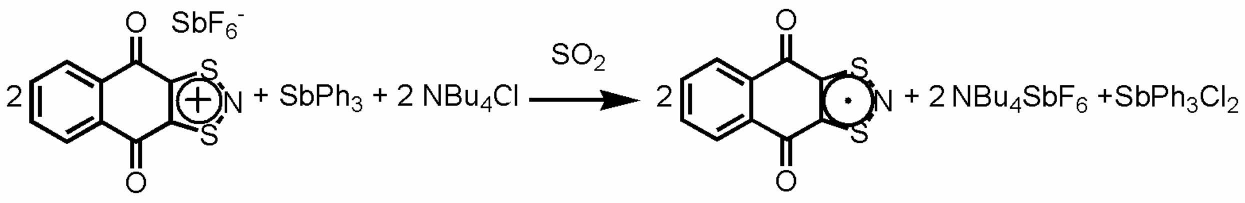

3SbF_6 (2.350 g, 5.00 mmol), triphenylantimony ($SbPh_3$; 0.883 g, 2.50 mmol), NBu_4Cl (1.390 g, 5.00 mmol) and a stir bar were added to bulb A of a vessel of Type B. SO_2 (7.688 g, ~ 5 ml) was condensed on to the solid mixture in bulb A. Upon warming to ambient temperature the yellow solution was obtained. After stirring for 1 hour a violet-brown solution was obtained. The SO_2 solution was concentrated (2.193 g, ~ 1.5 ml) under dynamic vacuum. CH_2Cl_2 (4.023 g, ~ 3 ml) was condensed into bulb A. Upon warming to ambient temperature a brown solution over a violet solid was obtained. The more soluble fraction was filtered to bulb B. The volatiles were condensed back to bulb A. The violet solid in bulb A was washed and the more soluble fraction filtered to bulb B. The washing was repeated five times until the washings were violet and the more soluble fractions collected in bulb B. The volatiles were removed under dynamic vacuum leaving a violet solid in bulb A and a brown solid in bulb B. The violet solid (0.240 g, 20 % yield based on **3**SbF_6 and Equation S5 on pg. 71) and the brown solid (4.317 g) were collected in the drybox. The IR (See Figure S39 on pg.72) of the violet solid (bulb A) was obtained as a Nujol mull on KBr and was consistent with **3**$^\bullet$ based on the calculated and experimental IR frequencies and intensities given in Table S2 on pg.23. Mass spectra (See Figure S40 on pg. 72) and SO_2 solution X-band EPR (See Figure S41 on pg. 73) of the violet solid (bulb A) prepared according to Equation S5 on pg. 70 were consistent with **3**$^\bullet$.

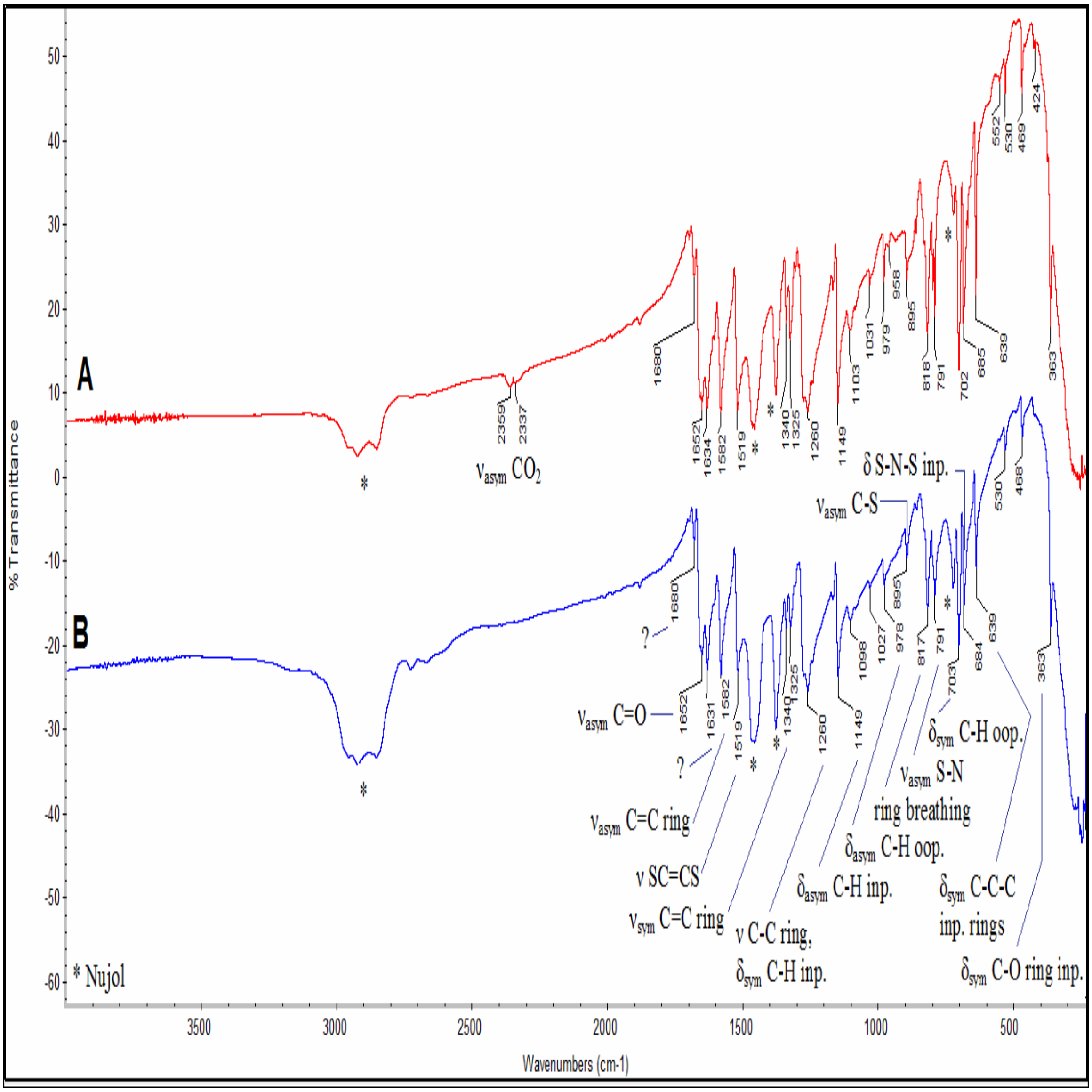

Figure S39: FT-IR spectra of a) **3**$^{\bullet}$ prepared according to Equation S5 on pg. 70 as Nujol mull on KBr plates and b) analytically pure **3**$^{\bullet}$ prepared according to Equation S2 on pg. 29 (32 scans, 2 cm^{-1} resolution). See Table S2 on pg. 22 for comparison of experimental and calculated IR frequencies and tentative assignments. Note the assignments are tentative and based on visualization of the vibrational modes in *ChemCraft*[8]: ν = stretch, δ = bending, asym. = asymmetric and sym = symmetric, opp = out-of-plane, inp = in-plane.

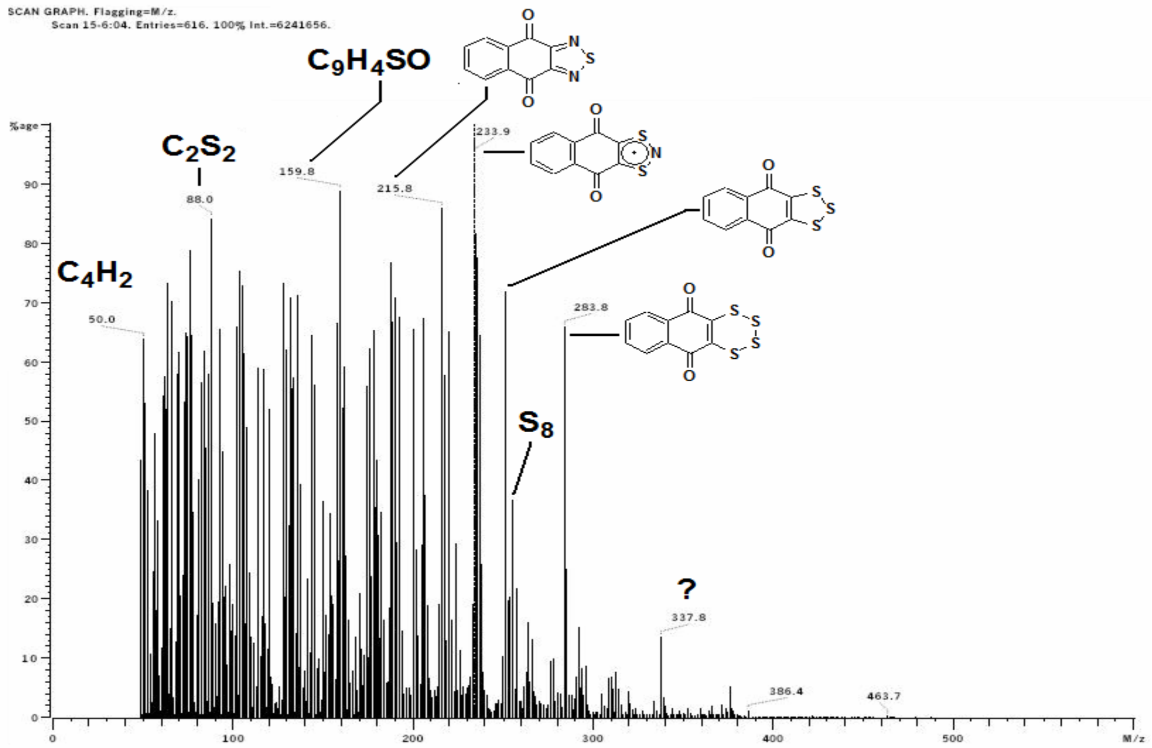

Figure S40: Mass spectra (EI, 30 eV) of **3$^\bullet$** (scan 15, mz = 233.9, 100%) prepared according to Equation S5 on pg. 70.

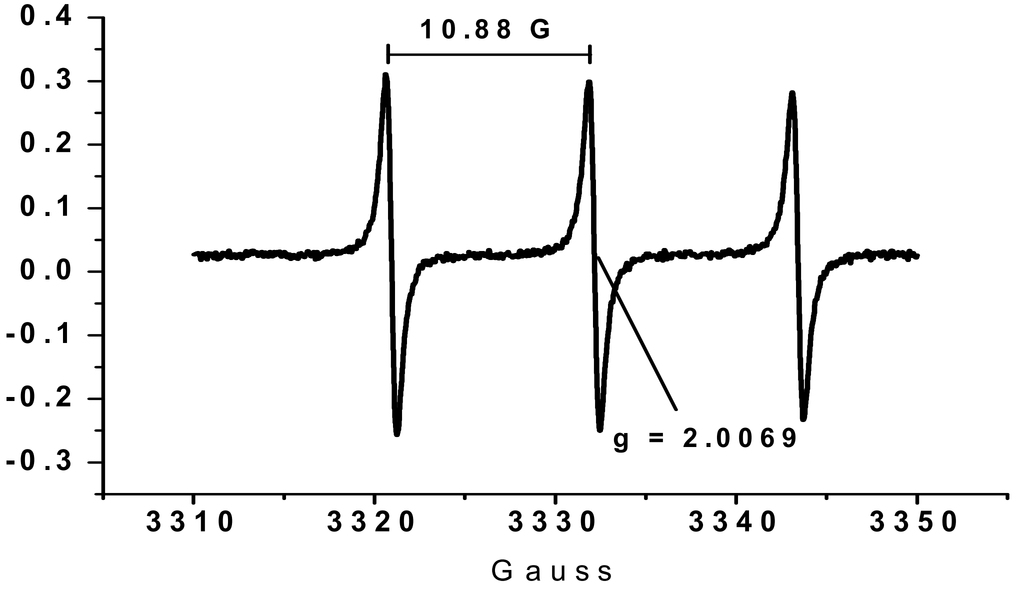

Figure S41: X-band EPR spectrum of **3$^\bullet$** in SO$_2$ solution prepared according to Equation S5 on pg. 70.

H. Reduction of $3SbF_6$ with one equivalent of NBu_4Cl and excess $Na_2S_2O_4$ in liquid SO_2 according to Equation S6.

Equation S6:

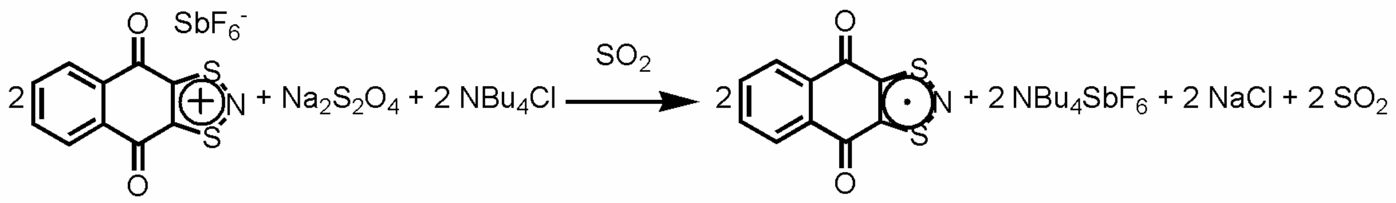

3SbF_6 (0.986 g, 2.10 mmol), NBu_4Cl (0.241 g, 2.20 mmol) and $Na_2S_2O_4$ (0.638 g, 3.67 mmol) were added to bulb A of a vessel of type A. SO_2 (5.414 g, ~ 4 ml) was condensed on to the solid mixture in bulb A. Upon warming to ambient temperature a yellow-brown solution over a white solid was obtained. After stirring for 12 hours the more soluble brown solution over a white solid was filtered to bulb B. The volatiles were condensed back to bulb A. The clear, colorless solution in bulb A was filtered to bulb B. A brown solution over a violet solid was obtained in bulb B. The more soluble fraction was filtered to bulb A. A small portion of the volatiles (~ 1 ml) was condensed to bulb B and the more soluble brown fraction over a violet solid was filtered to bulb A. This washing was repeated twice more and the volatiles removed under dynamic vacuum. The violet solid (0.243 g, 49 % yield based on **3**SbF_6 and Equation S6 on pg. 73) in bulb B and the brown-white solid (1.309 g) were collected in the drybox. The IR (See Figure S42a on pg. 74) of the violet solid (bulb B) obtained as a Nujol mull on KBr is compared to $\mathbf{3}^{\bullet}$ (See Figure S42b on pg. 74) prepared according to Equation S2 on pg. 29. See also the Raman microscopy spectra (See Figure S10d on pg. 21) compared to $\mathbf{3}^{\bullet}$ prepared according to Equation S2 on pg. 29 (See Figure S10b on pg. 21).

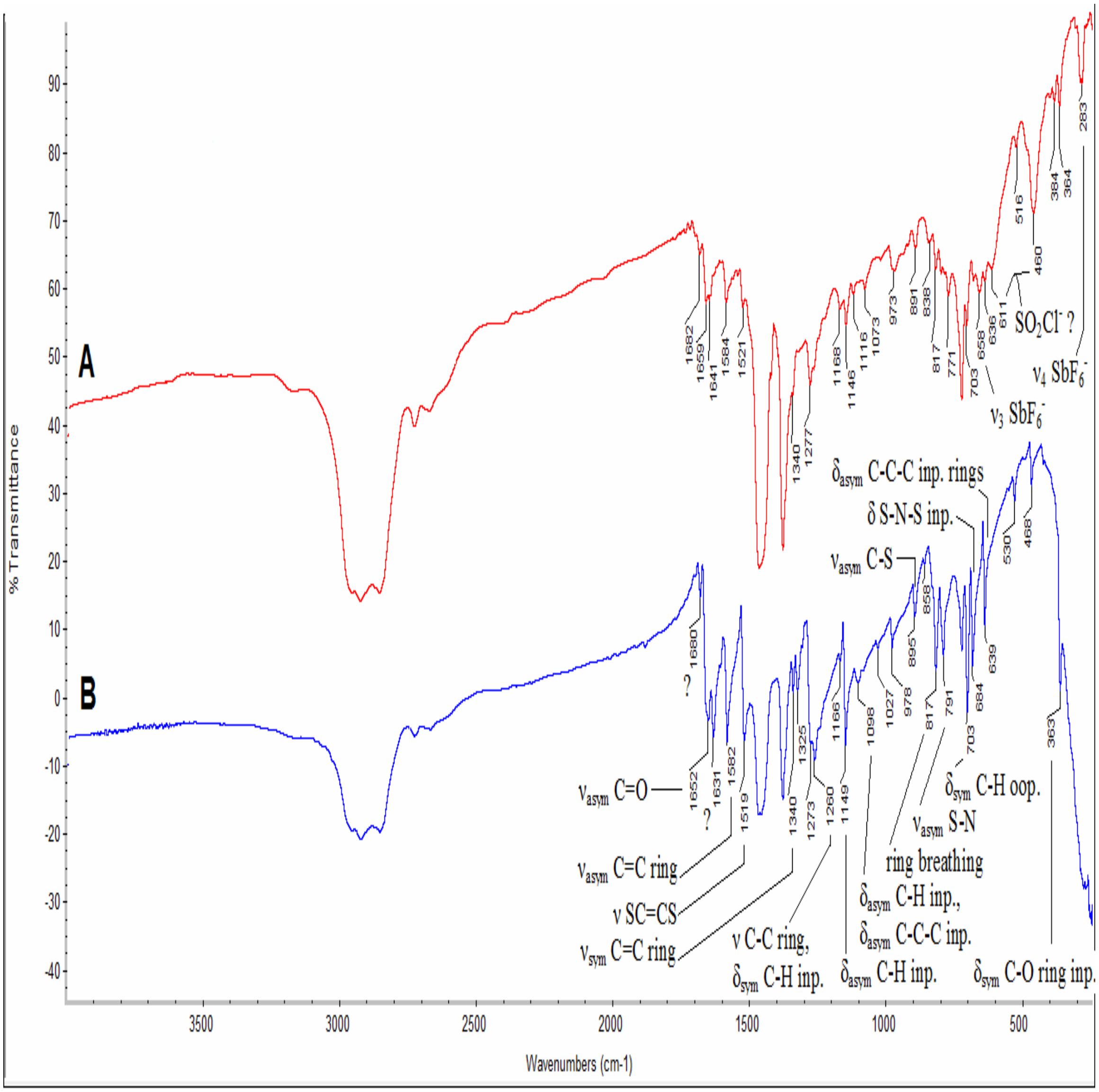

Figure S42: FT-IR spectra of a) **3**$^•$ prepared according to Equation S6 on pg. 75 as Nujol mull on KBr plates and b) analytically pure **3**$^•$ prepared according to Equation S2 on pg. 29 (32 scans, 2 cm^{-1} resolution). See Table S2 on pg. 22 for comparison of experimental and calculated IR frequencies and tentative assignments for **3**$^•$. Note the assignments are tentative and based on visualization of the vibrational modes in *ChemCraft*[8]: ν = stretch, δ = bending, asym. = asymmetric and sym = symmetric, opp = out-of-plane, inp = in-plane.

I. Reduction of 3SbF$_6$ with one equivalent of 18-benzocrown-6 and excess Na$_2$S$_2$O$_4$ in liquid SO$_2$ according to Equation S7

Equation S7:

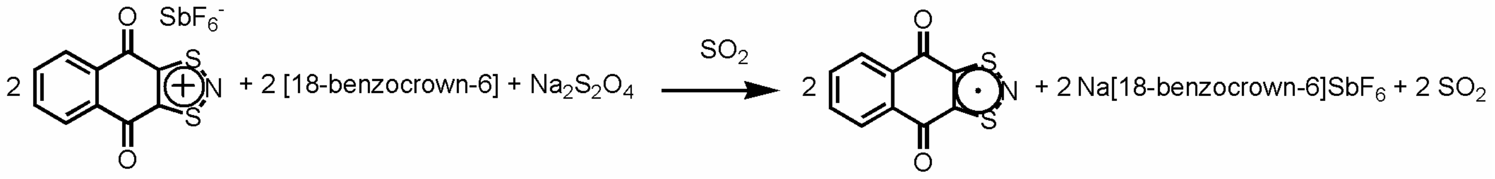

3SbF$_6$ (0.941 g, 2.00 mmol) was added to bulb A and 18-benzocrown-6 ($C_{20}H_{24}O_6$; 0.728 g, 2.02 mmol), Na$_2$S$_2$O$_4$ (0.218 g, 1.25 mmol) and a stir bar were added to bulb B of a vessel of Type A. SO$_2$ (11.982 g, ~ 8 ml) was condensed into bulb B. Upon warming to ambient temperature a pale yellow solution over a white solid was obtained in bulb B. The mixture in bulb B was stirred for 1 hour. Small quantities of SO$_2$ were condensed into to bulb A until the solid was dissolved and a yellow solution obtained. The two yellow solutions were mixed in bulb B. After stirring for 1 hour a violet solution was obtained over a white solid. The more soluble fraction was filtered to bulb A and the volatiles condensed back to bulb B. The volume of the volatiles was reduced (5.647 g, ~ 4 ml) under dynamic vacuum, than condensed back to bulb A. A yellow-brown solution over a dark violet solid was obtained in bulb A. The more soluble fraction was filtered to bulb B. The volatiles were removed under dynamic vacuum. CH$_2$Cl$_2$ (5.162 g, ~ 4 ml) was condensed into bulb A. A yellow-brown solution over a violet solid was obtained on warming to ambient temperature. The more soluble fraction was filtered to bulb B. The volatiles were back condensed onto the violet solid in bulb A and the more soluble fraction again filtered to bulb B. The volatiles were removed under dynamic vacuum. The violet solid (bulb A; 0.368 g, 78 % yield of **3**$^\bullet$ based on **3**SbF$_6$ and Equation S7 on pg. 75) and the white solid (bulb B; 1.347 g) were collected in the drybox. The IR (See Figure S43a on pg. 76) of the violet solid (bulb B) obtained as a Nujol mull on KBr is compared to **3**$^\bullet$ (See Figure S43b on pg. 76) prepared according to Equation S2 on pg. 29. See also the Raman microscopy spectra (See Figure S10c on pg. 21) compared to **3**$^\bullet$ prepared according to Equation S2 on pg. 29 (See Figure S10b on pg. 21).

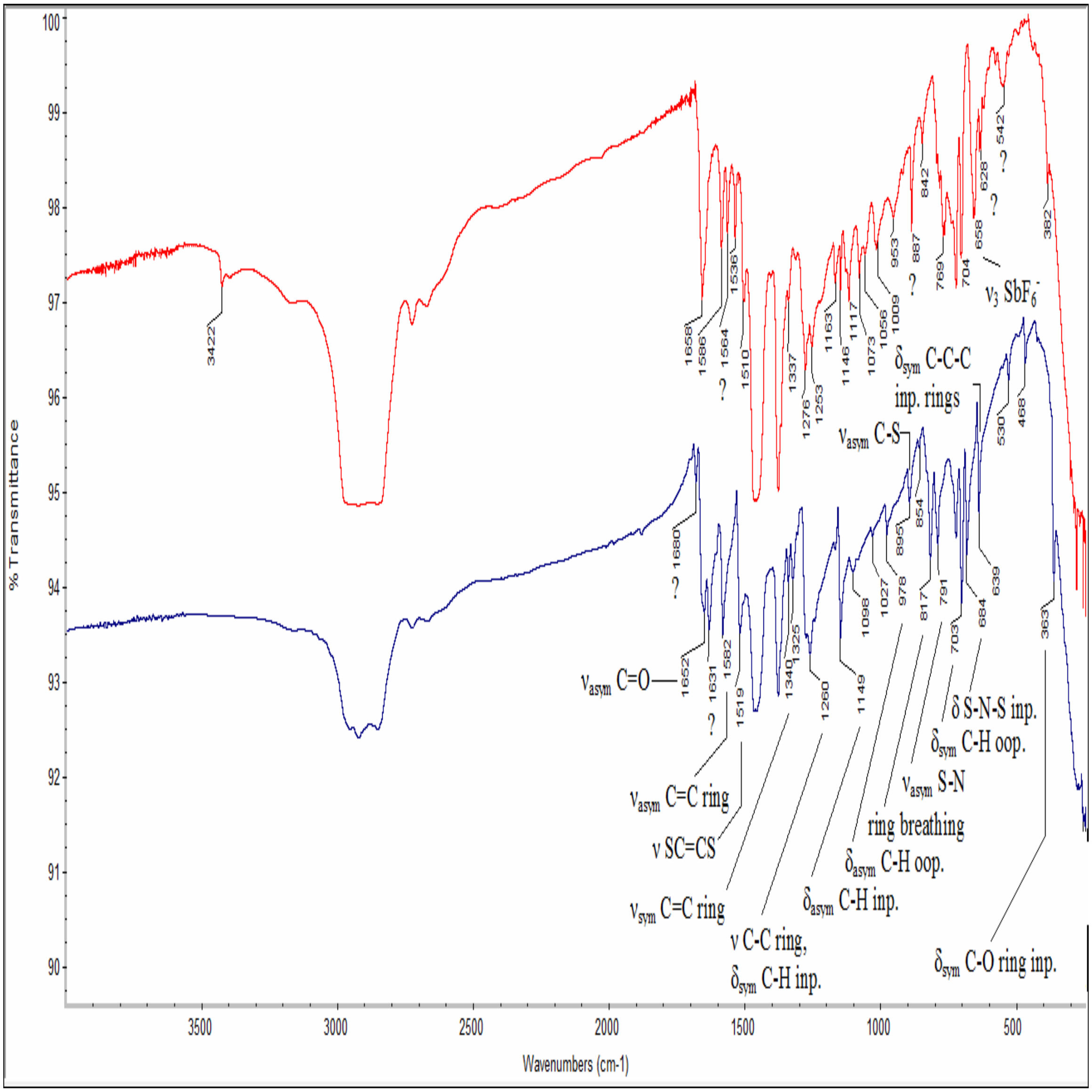

Figure S43: FT-IR spectra of a) **3**$^{\bullet}$ prepared as Nujol mull on KBr plates prepared according to Equation S7 on pg. 75 and b) analytically pure **3**$^{\bullet}$ prepared according to Equation S2 on pg. 29 (32 scans, 2 cm^{-1} resolution). See Table S2 on pg 22 for comparison of experimental and calculated IR frequencies and tentative assignments of **3**$^{\bullet}$. Note the assignments are tentative and based on visualization of the vibrational modes in *ChemCraft*[8]: ν = stretch, δ = bending, asym. = asymmetric and sym = symmetric, opp = out-of-plane, inp = in-plane.

9) **References**

---

[1] a) T.S. Cameron, A. Mailman, J. Passmore and K.V. Shuvaev, *Inorg. Chem.,* 2005, **44**, 6524; b) G. Antorena, S. Brownridge, T.S. Cameron, F. Palacio, S. Parsons, J. Passmore, L.K. Thompson and F. Zarlaida, *Can. J. Chem.,* 2002, **80**, 1568; c) E. Awere and J. Passmore, *Dalton Trans.,* 1992, 1343.

[2] Gaussian 03, Revision C. 02, M.J. Frisch, G.W. Trucks, H.B. Schlegel,G.E. Scuseria, M.A. Robb, J.R. Cheeseman, J.A. Montgomery, Jr., T. Vreven, K.N. Kudin, J.C. Burant, J.M. Millam, S.S. Iyengar, J. Tomasi, V. Barone, B. Mennucci, M. Cossi, G. Scalmani, N. Rega, G.A. Petersson, H. Nakatsuji, M. Hada, M. Ehara, K. Toyota, R. Fukuda, J. Hasegawa, M. Ishida, T. Nakajima, Y. Honda, O. Kitao, H. Nakai, M. Klene, X. Li, J.E. Knox, H.P. Hratchian, J.B. Cross, V. Bakken, C. Adamo, J. Jaramillo, R. Gomperts, R.E. Stratmann, O. Yazyev, A.J. Austin, R. Cammi, C. Pomelli, J.W. Ochterski, P.Y. Ayala, K. Morokuma, G.A. Voth, P. Salvador, J.J. Dannenberg, V.G. Zakrzewski, S. Dapprich, A.D. Daniels, M.C. Strain, O. Farkas, D.K. Malick, A.D. Rabuck, K. Raghavachari, J.B. Foresman, J.V. Ortiz, Q. Cui, A.G. Baboul, S. Clifford, J. Cioslowski, B.B. Stefanov, G. Liu, A. Liashenko, P. Piskorz, I. Komaromi, R.L. Martin, D.J. Fox, T. Keith, M.A. Al-Laham, C.Y. Peng, A. Nanayakkara, M. Challacombe, P.M.W. Gill, B. Johnson, W. Chen, M.W. Wong, C.Gonzalez, J.A. Pople, Gaussian, Inc., Wallingford CT, 2004.

[3] a) H.D.B. Jenkins, H.K. Roobottom, J. Passmore and L. Glasser, *Inorg. Chem.*, 1999, **38**, 3609; b) H.D.B. Jenkins, *J. Chem. Ed.*, 2005, **82**, 950; c) H.D.B. Jenkins and D. Tudela, *J. Chem. Ed.*, 2003, **80**, 1482.

[4] a) H.D.B. Jenkins, H.K. Roobottom, J. Passmore and L. Glasser, *Inorg. Chem.*, 1999, **38**, 3609; b) H.D.B. Jenkins, *J. Chem. Ed.*, 2005, **82**, 950; c) H.D.B. Jenkins and D. Tudela, *J. Chem. Ed.*, 2003, **80**, 1482.

[5] D.W.M. Hofmann, *Acta Cryst.,* **2002**, B57, 489-493.

[6] M.A.V. Ribeiro DaSilva, M.D.M.C. Ribeiro DaSilva, J.A.S. Teixeira, J.M. Bruce, P.M. Guyan, G. Pilcher, *J. Chem. Thermodyn.,* **1989**, 21, 265-274.

[7] C. Briske, N.H. Hartshorne and D.R. Stranks, *J. Chem. Soc.,* **1960**, 1200-1209.

[8] G.A. Zhurko, D.A. Zhurko, ChemCraft Version 1.5 (Build 275) , Tool for Treatment of the Chemical Data (http://www.chemcraftprog.com).

[9] J. Gaultier and C. Hauw, *Acta Cryst.,* 1965, **18**, 179.

[10] J. Gaultier and C. Hauw, *Acta Cryst.,* 1967, **23**, 1016.

[11] Y. Fu and C.P. Brock, *Acta Cryst.,* 1998, B**54**, 308.

[12] Y. Fu and C.P. Brock, *Acta Cryst.,* 1998, B**54**, 308.

[13] a) C. Adamo, V. Barone, *J. Chem. Phys.* 1998, **108**, 664; b) E. Cancès, B. Mennucci, J. Tomasi, *J. Chem. Phys.* 1997, **107**, 3032; c) M. Cossi, V. Barone, B. Mennucci and J. Tomasi, *Chem. Phys. Lett.* 1998, **286**, 253; d) V. Barone in : D.P. Chong (Ed.), Advances in Density Functional Methods, World Scientific, Singapore, 1995.

[14] See Table 1 in: J.L. Brusso, O.P. Clements, R.C. Haddon, M. E. Itkis, A.A. Leitch, R.T. Oakley, R.W. Reed, J.F. Richardson, *J. Am. Chem. Soc.,* 2004, **126**, 8256.

[15] W. Fujita, K. Awaga, Y. Nakazawa, K. Saito and M. Sorai, *Chem. Phys. Lett.*, 2002, **352**, 348.

[16] a) K.V. Shauvaev, A. Decken, F. Grein, T.S.M. Abedin, L.K. Thompson and J. Passmore, *Dalton Trans.,* 2008, 4029. b) A. Decken, T.S. Cameron, J. Passmore, J.M. Rautiainen, R.W. Reed, K.V. Shuvaev and L.K. Thompson, *Inorg. Chem.,*2007, **46**, 7436. c) A. Decken, M. Ebdah, R.M. Kowalczyk, C.P. Landee, E.J. McInnes, J. Passmore, K.V. Shuvaev and L.K. Thompson, *Inorg. Chem.,* 2007, **46**, 7756.

[17] D.J. Tozer and F. DeProft, *J. Phys. Chem.*, 2005, **109**, 8923.

[18] a) N. Burford, J. Passmore, and M.J. Schriver, *Chem.Commun.*, 1986, 140; b) J. Passmore and X. Sun, *Inorg.Chem.* 1996, **35**, 1313.

[19] C. Aherne, A.J. Banister, A.W. Luke, J. M. Rawson and R.J. Whitehead, *Dalton Trans.*, 1992, 1277.

[20] a) A.F. Bedford, P.B. Edmondson and C.T. Mortimer, *J.Chem. Soc.,* 1962, 2927; b) T. Grelbig, B. Potter and K. Seppelt, *Chem. Ber.,* 1987, **120** 815.

---

[21] a) M. Murchie and J. Passmore, *Inorg. Synth.,* 1988, **27**, 76; b) M.P. Murchie, R. Kapoor, J. Passmore, G. Schatte and T. Way, *Inorg. Synth.,* 1997, **31**, 102.

[22] J.Young o-ringette valves and Pyrex adaptor were obtained from Wilmab Lab Glass (www.wilmad-labglass.com).

[23] A. Decken, A. Mailman, S.M. Mattar and J. Passmore, *Chem. Commun.,* 2005, 2366.

[24] The FT-IR was obtained on a Bruker IFS-25 spectrometer (4000-600 cm^{-1}; 32 scans at 2 cm^{-1} resolution) as a Nujol mull between KBr plates.

[25] The reaction corresponds to that given in: A. Decken, A. Mailman, S.M. Mattar and J. Passmore, *Chem. Commun.,* 2005, 2366.